Ph.D. Program in Civil, Chemical and Environmental Engineering

Curriculum in Fluid Dynamics and Environmental Engineering

Department of Civil, Chemical and Environmental Engineering

Polytechnic School, University of Genoa, Italy

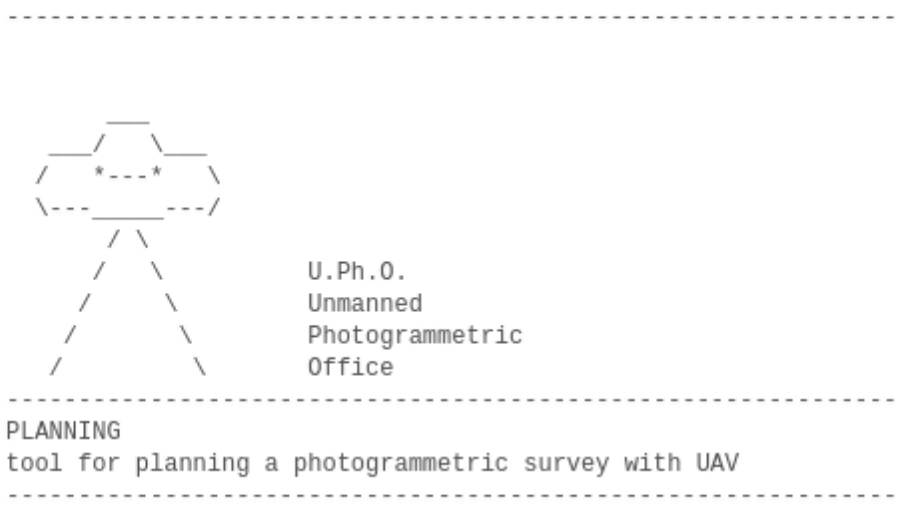

Innovative Tools For Planning, Analysis, and Management of UAV Photogrammetric Surveys

Daniele Passoni

INNOVATIVE TOOLS FOR PLANNING, ANALYSIS, AND MANAGEMENT OF UAV PHOTOGRAMMETRIC SURVEYS

BY

DANIELE PASSONI

Dissertation discussed in partial fulfillment of
the requirements for the Degree of

DOCTOR OF PHILOSOPHY

Civil, Chemical and Environmental Engineering
curriculum in Fluid Dynamics and Environmental Engineering,
Department of Civil, Chemical and Environmental Engineering, University of Genoa, Italy

September, 2019

Adviser(s):
Prof. Domenico Sguerso
Department of Civil, Chemical and Environmental Engineering , University of Genoa

External Reviewers:
Prof. Antonio M. G. Tommaselli
Departamento de Cartografia, Universidade Estadual Paulista Júlio de Mesquita Filho

Prof. Gianfranco Forlani – Department of Civil and Environmental Engineering and Architecture, University of Parma

Examination Committee:

Prof. Gianfranco Forlani – Department of Engineering and Architecture, University of Parma

Prof. Vittorio Casella – Department of Civil Engineering and Architecture, University of Pavia

Prof. Andrea Mazzino – Department of Civil, Chemical and Environmental Engineering, University of Genoa

Ph.D. program in Civil, Chemical and Environmental Engineering

Curriculum in Fluid Dynamics and Environmental Engineering

Cycle XXIX

Acknowledgements

Acknowledgement for fellowships sponsored by external institutions (only)

ABSTRACT

The Unmanned Aerial System (UAV) is widely used in the photogrammetric surveys both for structures and small areas. The geomatics approach, for the several applications where the 3D modeling is required, focuses the attention on the metric quality of the final products of the survey. As widely known, the quality of results derives from the quality of images acquisition phase, which needs an accurate planning phase. Actually, the planning phase is typically managed using dedicated tools, adapted from the traditional aerial-photogrammetric flight plan. Unfortunately, UAV flight has features completely different from the traditional one, hence the use of UAV for photogrammetric applications today requires a growth in the planning knowledge.

The basic idea of the present research work is to provide a tool for planning a photogrammetric survey with UAV, called "Unmanned Photogrammetric Office" (U.Ph.O.), that considers the morphology of the object, the effective visibility of its surface, in the respect of the metric precisions. The usual planning tools require the classical parameters of a photogrammetric planning: flight distance from the surface, images overlaps and geometric parameters of the camera. The created "Office suite" U.Ph.O. allows a realistic planning of a photogrammetric survey, requiring additionally an approximate knowledge of the Digital Surface Model (DSM) and the attitude parameters, potentially changing along the route. The planning products will be the realistic overlapping of the images, the Ground Sample Distance (GSD) and the precision on each pixel taking into account the real geometry.

The different tested procedures, the solution proposed to estimates the realistic precisions in the particular case of UAV surveys and the obtained results, are described in this thesis work, with an overview on the recently development of UAV surveys and technologies related to them.

INDEX

INDEX OF FIGURES

INDEX OF TABLES

INTRODUCTION

In the last years the use of UAV (Unmanned Aerial Vehicles) is increasingly catching on in the field of photogrammetry. According to the definition of UVS International (Unmanned Vehicle System), a UAV is a generic aircraft planned to operate without any human pilot on board (http://www.uvs-international.org). The terms "UAV" and "drone" are the most used ones in the geomatic applications, but there are also other terms, like "RPV (Remotely Piloted Vehicle)" or in Italian APR (Aeromobili a Pilotaggio Remoto), which are used according to the kind of aircraft, the propulsion system, the altitude and automation level of the vehicle. The term UAS (Unmanned Aerial System) defines the totality of aerial aircraft and the Ground Control Station (GCS). Ground control stations are hardware and software devices which have the task to monitor and command the aircraft. Therefore, the GCS is a key system component, as it provides the interface to the pilot: any change in the itinerary, any possible mistake of the aircraft and, in general, any output of the on-board sensors is sent to the station and displayed through the station itself. Furthermore, GCS is an essential tool not only for the autonomous guide of drones, but also because it often provides the software needed for the planning of a survey flight.

UAV technology was originally developed for military purposes and applications and it is still widely used in this field. Its first use in the geomatic area dates back some decades ago, but only in the last 10-15 years UAV systems have become a common tool in the acquisition of territorial data. In particular, photogrammetry by drone has opened new opportunities in this field, introducing a low-cost alternative to the classical photogrammetry. The fast spread of UAV systems is due to the birth of new kinds of low-cost aircrafts, digital cameras and other sensors in combination with GNSS/INS systems (Global Navigation Satellite Systems / Internal Navigation System), which are essential for the georeferencing of surveys.

The currently available UAVs are different in dimension, shape, flight duration and altitude and load capacity. The attention of most operators is, for photogrammetric survey purposes, paid to mini and macro UAV, i.e. those with a weight lower than 25 kg. According to the Italian law (ENAC, 2018), these categories are further divided into three types: the harmless Remotely Piloted Aircraft System (RPAS), with a take-off weight lower than 300 g and have to be declared as RPAS by ENAC; RPAS Very Light (VL) with a take-off weight between 300 g and 4 kg and RPAS Light (L) with a take-off weight between 4 kg and 25 kg.

These RPAS have a flight duration between some minutes and just over 1 hour, but, in any case, the legislation allows only a limited operating distance and flight altitude.

There are two specific categories of aircrafts: fixed-wing and multirotor aircrafts, and any of them has different features, advantages and uses (Colomina, I., and Molina, P. 2014; Padua, L., et al. 2017). The dimension and orography characteristics of the covered area, the ground resolution of images (expressed by the so called Ground Sample Distance or GSD, directly connected to the flight altitude and the camera focal length) and the features of the take-off and landing area are the elements to take into account in order to choose between these two categories of aircraft. Fixed-wing RPAS are used for areas with a size between 1 and 10 km^2, for Ground Sample Distance (GSD) higher than 3-5 cm and need a flat take-off and landing area of some tens of square meters. Multirotor aircrafts are employed in areas with a dimension between 10000 m^2 and 1 km^2, for Ground Sample Distance (GSD) between some millimeters and 3 cm and have no particular requirements about the take-off and landing area.

In both cases the flight planning is guaranteed by the on-board presence of the Global Navigation Satellite System (GNSS) receiver, able to keep the pre-planned route. A more or less sophisticated self-piloting system allows different autonomy levels of flight in the most delicate take-off and landing phases and some RPAS of the latest generation are finally equipped with anti-collision telemetric systems in order to secure a minimum distance from obstacles during the shooting phase (Accardo, D., et al. 2013).

The low-cost and light-weight sensors, suitable to be carried by a VL-RPAS or L-RPAS, has considerably developed in the recent years and the market is now offering a lot of solutions for several passive and active sensors. Among passive sensors it is possible to distinguish the so called RGB cameras, sensitive to the visual part of the electromagnetic spectrum (from about 400 to 700 nm), NIR or CIR cameras, sensitive to the infrared part of the spectrum (from 700 to 1000 nm for NIR sensors, from 400 to 1000 nm for CIR sensors), thermal cameras (whose sensors are sensitive to the spectrum components between about 5000 and 14000 nm) and, finally, multispectral and hyperspectral cameras, that generally assure the acquisition of a variable amount of spectrum components that depends on the amount of registration channels. Among active sensors, a particular case is represented by LIDAR that determines georeferenced point clouds, which the reflectance of the surface hit by the laser pulse is associated to. These systems are used in several applications like i.e. the restoration of the cultural heritage, the evaluation of the growth of arboreal vegetation, the assessment of the biomass and to acquire the morphology of the terrain for hydraulic studies (Wallace, L., et al. 2014; Malinowski, R., 2016; Bareth, G., et al. 2016). Because of their high costs, these products are not yet widely used.

All sensors have a weight between few grams (Action Cam) and some kilograms (Lidar) and are suitable to be carried by most types of RPAS. Costs are also considerably variable: except for LIDARs, which are still very expensive, with costs in excess of some tens of thousands of euro, the cameras equipped optic sensor can have a cost between few tens of euro (RGB Action Cam cameras) and about 10,000 euro for multispectral cameras (Nebiker, S., et al. 2016).

UAV have found their space in several application fields. Video and photo documentation, security and monitoring, precision agriculture and territory survey, intelligence, surveillance and reconnaissance, inspection, cultural heritage and archaeological survey, traditional surveying and cadastral applications, are only some of the numerous fields, in which this tool is widely used. The scientific community has enthusiastically embraced the potentialities expressed by UAV and has worked hard to develop them as tools of metric measurement.

A great commitment has been taken in the technological development of both on-board sensors for navigation and for survey sensors.

As it always happens when a new technology is incoming, it is necessary to adapt old and consolidated operating methods to the new instruments. For this reason, photogrammetry software had to take on this new challenge abandoning consolidated procedures and beginning to interact with new processes particularly oriented on quick and automatic elaborations phase, strongly connected with the technology of the Computer Vision.

The aeronautic industry has spent a lot of energy in the last decade in the production of more and more performing drones, easy to be piloted even by less expert users. The technological development has

increased the ease and the security in their usage. The avionic research has produced models able to fly higher and higher and more and more faraway. The task of the scientific research in geomatics field, and of this thesis work in particular, is instead to help the drone users to deepen the knowledge and competences, so that they could better understand the applicative potentialities of drones in several fields, with particular attention to the metric aspects.

The present work is organized starting from the history and development of the Unmanned Aerial Vehicles, together with the essential characteristics and Italian and European norms and regulations that influence their functioning and governability respectively (chapter 1). In chapter 2, different fields of applications of UAV will be described (like i.e. intelligence, surveillance and reconnaissance, inspection, cultural heritage and archaeological survey, traditional surveying and cadastral applications, but also precision farming, forestry and environmental applications) in order to identify their strong points and critical issues. In chapter 3 the basic principles of photogrammetry and of the use of UAV in this field, to obtain metric information about the survey object, will be discussed. However, the concept of "metric information" of a survey will be defined and deepened in the following chapter (chapter 4), whose goal is not only to recognize its capacity of recovering the dimensions of the observed objects, but also the ability to determine the precision of the registered metric information, both a priori and a posteriori. Following this perspective, after presenting the current situation of the survey by drone giving basic technical information to understand its complexity and potentialities, in chapter 5 an a priori precision estimate method will be provided. It will be proposed like a useful practice to apply to surveys by means of real and concrete tools. Before dealing with this topic, it is important to know the interface between man and machine in the surveys by UAV and to learn how the planning of a survey takes place in practice. The tools presented, starting from chapter 5, are collected in an "office suite", called U.Ph.O. (Unmanned Photogrammetric Office), realized in Matlab environment. The proposed solutions are the result of an accurate study of estimation methods of the expected precisions for a survey by drone, starting from the consolidated basis of aerial and close-range terrestrial survey. The "Office suite" proposed permits to design a "realistic" survey planning of the navigation route in respect of the a priori DSM, both providing standard solutions and predicting the expected precisions. The starting points are: the a priori information about required precisions and/or the so called Ground Pixel Dimensions (GSD), the overlap of the projected images on the ground/object (in the two directions, longitudinal and transversal on the UAV navigation route), an approximate knowledge of the DSM and the desired attitude parameters, potentially changing along the route. The basic idea of the present research work is to considers the morphology of the object, the effective visibility of its surface, in the respect of the metric precisions rigorously evaluated with a least square simulation. Thus, the created "Office suite" U.Ph.O. allows a realistic planning of a photogrammetric survey with overlapping of the projection of the images covering the DSM, their Ground Sample Distances (GSD) and the expected precision on each object pixel, taking into account the real visibility by the images. This work is aimed to provide both the theoretical instruments to make a good planning of a survey with an evaluation of the expected precisions and the practical tools to support the everyday practice of metric survey by UAV.

The U.Ph.O. tool is made up with a second module for the analysis phase of the survey campaigns, useful to verify the obtained coverings on DSM coming from the frames, checks the absence of holes and estimates the accuracy of the survey. The analysis tool uses the telemetry recorded by the drone during the flight or the External Orientation parameters obtained from expeditious processing of the images as its starting data.

In chapter 6, the U.Ph.O. Office suite will be applied to two case studies. The case study of the Belvedere glacier will show the possibility to design different scenarios to better choose the best solution for each specific case, the case study of the Castle of Casalbagliano (Fagandini, R., et al. 2017) will be shown how this survey has been planned before the realization and analysed after the performance of the flight. Considering that the case study is rich of information coming from additional data set, it can be used to show the use of U.Ph.O. and also to validate its reliability.

The different tested procedures, the solution proposed to estimates the realistic precisions in the particular case of UAV surveys and the obtained results, are described in this thesis work and resumed in the conclusions and perspectives, with an overview on the recently development of UAV surveys and technologies related to them. Some operative good practice criteria has been suggested, coming from the analysis of different configurations simulated in two real scenarios. Finally main steps to optimize the Office suite tools U.Ph.O. and which future developments are proposed.

1. UNMANNED AERIAL VEHICLES

The acronimous UAV (Unmanned Aerial Vehicle) represent the much more popular word “drone”. In order to better understand the potentialities and the problems related to a survey performed through Unmanned Aerial Vehicles, in this first chapter the history of their development and the features of the UAVs available on the market, together with the essential characteristics that influence their functioning will be described. Finally, the regulations governing their use on the legislative front both in Italy and in Europe will be introduced.

The diffusion of UAVs has been incredibly fast in the last years and they are becoming part not only of everyday language, but also of collective imagination. This technology, created for military purposes, has rapidly found its place in the recreational and professional fields for video recording, photography and photogrammetric surveys; this last one field is particularly treated in this thesis. It is not uncommon that a technology originally invented for military purposes becomes so useful in the civil society. The Global Navigation Satellite System (GNSS), the optical satellites and the Synthetic Aperture Radar (SAR) are known examples of the Geomatics’field and the so-called UAVs are not an exception.

Due to its diffusion and numerous fields of application, we do not have a “unique” and shared definition of this technology yet. In the 1990s, the term was changed to UAV and, a decade later, the Federal Aviation Administration (FAA) of the US Department of Transportation has introduced the generic term UAS (Unmanned Aircraft System): it underlines that the whole system is composed by an Unmanned Aircraft (UA) plus a Control System (CS) -usually a Ground Control Station (GCS)- and a communication data link between the UA and the GCS (Eisenbeiss, 2009).

Its definition is now well known: a UAV is a powered aerial vehicle, which does not need a human operator physically onboard; it can fly autonomously or be remotely piloted and it uses aerodynamic forces to provide vehicle lift. In particular, UAVs can be remotely controlled, semi–autonomous, autonomous or have a combination of these capabilities. In many cases, the crew responsible for a UAV is larger than that of a conventional aircraft (Everaerts, 2008).

The recent terminology "UAV Photogrammetry” (Everaerts, 2008) describes a photogrammetric platform, equipped with a photogrammetric measurement system with RGB (Red, Green, Blue) camera, airborne LiDAR system (Light Detection and Ranging), thermal and multispectral systems or a combination thereof. The definition of a “UAV Photogrammetry” opens new scenarios and developments both for the aerial and for the close-range photogrammetry. It’s in this perspective, as it will be shown in the following chapters, that the development of new shooting sensors and software for image processing related to Computer Vision (CV) is to be found. In Table 1.1 Eisenbeiss (2009) has resumed the main characteristics for different photogrammetric phases, for the different kind of acquisition: aerial, close range and UAV.

Table -1 Features of aerial, close range and UAV Photogrammetry (Eisenbeiss, 2009)

	Aerial	Close Range	UAV
Planning	(semi) automatic	Manual	Automatic/manual
Data acquisition/Flight	Assisted/manual	Autonomous/assisted/manual	Autonomous/assisted/manual
Size of the area	km^2	$mm^2 – m^2$	$m^2 – km^2$
Image resolution/GSD	cm – m	mm – dm	mm – m
Distance to the object	100 m – 10 km	cm – 300 m	m – km
Orientation	Normal case, recently also oblique	Normal/oblique	Normal/oblique
Absolute accuracy of the initial orientation values	cm – dm	mm – m	cm – 10 m
Image block size/number of scan	10 – 1000	1 – 500	1 – 1000
Special applications (examples) and features	Aerial view large scale area (mapping, forestry, glaciology, 3D-ciry, modelling, etc.)	Terrestrial view small-scale areas and objects (archaeological documentation, 3D modelling of buildings and objects), architectural and industrial Photogrammetry	Aerial view small and large-scale areas (archaeological documentation, 3D modelling of buildings and objects), applications in inaccessible areas and dangerous objects, real-rime applications (monitoring)

The Table 1.1 shows the comparison between UAV photogrammetry, traditional aerial photogrammetry (for example from an airplane) and Close Range Photogrammetry (CRP), where images are collected from ground. UAV photogrammetry offers the possibility to perform aerial surveys in close range, it is a low-cost alternative to the traditional manned aerial photogrammetry and can be used for real-time applications (e.g. monitoring).

1.1 UAV Classification

The classification of UAV includes a wide range of aircrafts with different features and technologies: according to these and other parameters a UAV can be suitable to an application and unsuitable for the other ones. There are several possible classifications of UAV:

- powered or unpowered;
- flexible, fixed or rotating wing;
- single, coaxial, quad-rotor or multi-rotor;
- lighter than air (balloons) or heavier than air (kites, drones, etc.).

Among all these possible classifications, the most obvious one, mostly influencing the usage modality and fields applications, is the distinction between “Fixed-wing” and “Rotary-wing”.

Fixed-Wing UAV

Fixed-wing UAVs (Figure 1-1) are capable of flight thanks to the wings that generate lift, produced by the vehicle’s forward airspeed and the shape of the wings themselves. These drones are ideal for longer missions, generally when the area to be mapped is very large. Moreover, some models with wingspans greater than 2m may also be suitable for carrying large payloads, such as high resolution DSLR (Digital Single Lens Reflex) cameras, LiDAR (Light Imaging Detection and Ranging), gas and thermal sensors. On the other hand, fixed-wing drones require a flat take-off and landing strip of some tens of square meters.

Figure 1-1 Fixed-wing UAV

Rotary-Wing UAV

Rotary-wing UAVs, commonly drones (Figure 1-2), use lift generated by wings, called rotary wings or rotor blades, that revolve around a mast. These devices differ from the previous ones, because generally they have less autonomy. Their dimensions should be significantly increased in order to be able to support such a payload. On the other hand, they are cheaper than fixed-wing drones, because they have a huge spread into the hobby market that brings a dramatic cost reduction of their components. In addition, they are more agile than fixed-wing drones and can perform vertical take-off, which is a great advantage in harsh environments.

Figure 1-2 Rotary-wing drone

According to dimensions, Maximum Take-Off Weight (MTOW), engine, payload, maximum reachable distance and flight height, UAS can be classified as follows:

- micro or mini;
- close, short, medium or long range;
- low, medium or high altitude.

A classification based on the above features is adopted by the UVS International (Unmanned Vehicle System International). Born in 1995 with the name EURO UVS, UVS International is since year 2000 «a non-profit association [...] which represents manufacturers of Remotely Piloted Systems (RPS), related subsystems and critical components and associated equipment, as well as companies supplying services with or for RPS, research organizations and academia» (www.uvs-international.org). In particular, UVS International subdivides UAS into three main groups, namely tactical, strategic and special purpose, shown in Table 1.2.

Table 1-2 UAS categories (van Blyenburgh, 2011)

UAS Categories	Acronym	Range (km)	Flight Altitude (m)	Endurance (hours)	MTOW (kg)	Currently Flying
Tactical						
Nano	η	< 1	100	< 1	< 0,025	yes
Micro	μ (Micro)	< 10	250	1	< 5	yes
Mini	Mini	< 10	150 [b] to 300 [a]	< 2	< 30 (150 [b])	yes
Close Range	CR	10 to 30	3.000	2 to 4	150	yes
Short Range	SR	30 to 70	3.000	3 to 6	200	yes
Medium Range	MR	70 to 200	5.000	6 to 10	1.250	yes
Medium Range Endurance	MRE	> 500	8.000	10 to 18	1.250	yes
Low Altitude Deep Penetration	LADP	> 250	50 to 9.000	0,5 to 1	350	yes
Low Altitude Long Endurance	LALE	> 500	3.000	> 24	< 30	yes
Medium Altitude Long Endurance	MALE	> 500	14.000	24 to 48	1.500	yes
Strategic						
High Altitude Long Endurance	HALE	> 2000	20.000	24 to 48	(4.500 [c])12.000	yes
Special Purpose						
Unmanned Combat Aerial Vehicle	UCAV	approx. 1500	10.000	approx. 2	10.000	yes
Lethal	LETH	300	4.000	3 to 4	250	yes
Decoy	DEC	0 to 500	5.000	< 4	250	yes
Stratospheric	STRATO	> 2000	>20.000 & <30.000	> 48	TBD	no
Exo-stratospheric	EXO	TBD	> 30.000	TBD	TBD	no
Space	SPACE	TBD	TBD	TBD	TBD	no

TBD = To Be Defined [a] = according to national legislation [b] = in Japan [c] = Predator B

1.2 UAV Components and Sensors

Even if UAVs belong to different classes, they have all similar components and tools, which are indispensable for the flight and the autonomous navigation.

In the following section, we will analyze each component of the drone explaining its role inside the system.

- Frame

The frame is the skeleton of the UAV. The essential characteristics of a frame are lightness and robustness. The frame shall have all the aeronautical features for the flight and be able to contain the navigation tools and the survey sensors.

- Motors and propellers

The motors and propellers provide thrust to the fixed-wing, and lift and direction to the multicopter; they are very delicate parts of the drone to be dimensioned, since they must act accordingly to the payloads and the battery capacity. All the latest drones use electric brushless motors which are more efficient, more reliable and quieter than brushed ones. There are also drones with combustion or turbine engines, but they are not suitable to survey and, for this reason, they will be not mentioned in the present work.

- Electronic Speed Control (ESCs)

The ESC is an electronic circuit with the purpose of varying the motor's speed, its direction and, possibly, to act as a dynamic brake. Its main function is to convert DC battery power into 3-phase AC for driving brushless motors. The control of the speed of rotation of the propellers is an important factor for the flight, being able to manage this parameter with high precision allows stable flights and high manoeuvrability of the aircraft.

- Flight controller

The flight controller is the computational centre of the drone, it elaborates inputs from the receiver, GNSS module, battery monitor, IMU and other on-board sensors. Using this information, it controls motor speeds through the ESCs, it triggers the camera and monitors autopilots and waypoints.

- Battery

LiPo batteries provide power, they can vary both in number of cells (2S-6S) and in capacity (mAh). In all cases, we need to pay a lot of attention to the battery choice, because the drone must be able to work in different regions and places, where the temperature can be very high or reach negative values. The high or low temperatures affect negatively the battery capacity by decreasing it up to 50% of its initial value.

- Radio controller

The radio receiver allows the drone to communicate with the ground controller, that can be both a ground station and a human pilot. In most cases, the drone can be controlled also by a dedicated software using the given waypoints, elaborate the drone's trajectory, optimizing the chosen parameters. Radio frequencies, traditionally used in the model aircraft building field, have been recently substituted by the common frequencies of Wi-Fi transmissions (2.4GHz in Europe and 5GHz in the USA).

- GNSS receiver

The GNSS receiver is a key module to provide some fundamental localization parameters, such as latitude, longitude, elevation. Position data are necessary to execute all the autonomous flight modes and for the waypoint navigation.

- Ground station

In general, a ground station is a computer or a dedicated hardware that runs some software able to communicate with the drone by means of radio waves. It is able to control the drone navigation following a specific algorithm, like the waypoint navigation. In recent years some applications performing this same task from tablet or smartphone have been developed too.

- Gimbal

The gimbal is a motor-powered camera support that is usually placed under the frame. It contains the camera and, through the servo-motors, it guarantees to maintain pointing according to plan. It is usually realized through physical mechanisms and can be replaced to some extent by the image electronic stabilization.

- IMU

The Inertial Measurement Unit (IMU) uses a combination of sensors, usually a gyroscope, an accelerometer and a magnetometer, to keep tracks of the drone's specific force, angular rate and magnetic field surrounding the body.

- Cameras and sensors

Drones can be equipped with a photogrammetric measurement system, including thermal, infrared or RGB (Red, Green, Blue) camera systems, airborne LiDAR systems or a combination thereof.

1.3 Current International and Italian Regulations

The number of UAV users for "specialized operations" is constantly increasing. Its users are professionals dealing with architectonic, artistic or technical cadastral survey, but also governmental authorities involved with internal security matters (e.g. municipal and national police, anti-terrorist squads, fire brigades, forest fire fighters, coast guards, civil defense, environmental protection agencies) have shown great interest in the use of UAS. Large corporate entities (e.g. electric grid operators, pipeline network operators, railway operators, oil companies) have also started to realize how much UAS can benefit

their corporate operations (van Blyenburgh, 2014). If on the one hand the increasing number of users has encouraged the technological development of more and more performing drones and highly automated software, on the other it has stressed the need of a legislative regulation able to guarantee public safety and security. It is important to remember that the drones, the more so if equipped with heavy payloads, are real aircrafts that can fly over “critical areas”, such as residential areas, crowded places or “sensitive” infrastructures (highways, rail system…).

The first example of operating regulation in the world was approved by the Australian Civil Aviation Safety Authority (CASA) in 2002. This document sanctions that anyone who is interested in letting UAS fly for professional purposes needs to have an operator certificate guaranteeing the proper education of the pilot and the suitability of his drones. The Federal Aviation Administration (FAA) of the United States also developed a complete plan to insert UAS in the National Airspace System.

Currently (epoch when the present thesis has been written i.e. 2018), in the European Union (EU) the regulatory responsibility for civil UAS with a Maximum Take-Off Weight (MTOW) of more than 150 kg lays with the European Aviation Safety Agency (EASA) and for those with a MTOW of less than 150 kg with the National Aviation Authorities (NAAs). Various initial national regulations related to the operation of civil UAS are now in place (Austria, Czech Republic, Denmark, France, Germany, Ireland, Italy, Sweden, United Kingdom), are about to enter into force (Belgium, Finland, Lithuania, Norway, Switzerland), or are in progress (Malta, The Netherlands, Spain). In practically all cases, at the moment flight operations are taking place within visual line-of-sight, at a flight altitude of less than 150 m above ground level with UAS characterized by a MTOW of less than 25 kg. A significant amount of European NAAs facilitate UAS operations by granting Permits-To-Fly on a case-by-case basis (van Blyenburgh, 2014). These regulations principally concern light UAS and they are not harmonized on a pan-European level, even if efforts towards this direction are in place: indeed, in June 2013, the European RPAS Steering Group (ERSG) released the "Roadmap for the integration of civil Remotely-Piloted Aircraft Systems into the European Aviation System". This report comprehends detailed proposals and a schedule for a regulatory approach, a strategic research plan and a study on the societal impact of UAS (ERSG, 2013). Furthermore, the Joint Authorities for Rulemaking on Unmanned Systems (JARUS), which federates the NAAs of 22 countries, as well as EASA and EUROCONTROL, published its first certification specification (CS-LURS) in November 2013 (JARUS, 2013). JARUS intent is to eliminate the need for each country to write their own requirements and to promote the reciprocal acceptance of UAS-related certificates, approvals and licenses.

The main challenge still remains the creation of rules proportionate to risk, by taking into account characteristics like MTOW, speed, system complexity, airspace class, population density in the overflow area, as well as the specificity of operations. A more comprehensive description of the most recent work and developments is presented in the work of van Blyenburgh (2013 and 2014).

The use of UAVs in the Italian National Air Space is regulated by the national agency for civil aviation ENAC (Ente Nazionale per l’Aviazione Civile). The reference regulation is the “Regolamento Mezzi Aerei a Pilotaggio Remoto” (ENAC, 2018). The regulation refers to the UAVs as Remotely Piloted Aerial Vehicles (RPAV). The notion of remotely piloted aerial vehicle is introduced by the article 743 of the Italian Navigation Code: "Aircraft shall mean any machine designed for the transportation by air of persons or

property. Remotely piloted aerial vehicles are also considered aircraft, as defined by special laws, ENAC regulations and, for the military, by decrees of the Ministry of Defence. The distinctions of the aircraft, according to their technical specifications and use shall be established by ENAC with its regulations and, in any case, by special legislation in this field".

The ENAC regulation splits the remotely piloted aerial vehicles into two categories: Remotely Piloted Aircraft Systems (RPAS) and Model Aircrafts. The RPAS are intended to be operated for specialized operations or for experimental, scientific and research activities and the provisions of the Italian Navigation Code apply, in accordance with the ENAC regulation.

The main characteristic for which RPAS is classified and which determines the applied regulations is the take-off mass of the vehicle. RPAS are classified as follows:

- RPAS with operating take-off mass of less than 25 kg (with the particular cases of mass less than or equal to 2 kg and to 0,3 kg);

- RPAS with operating take-off mass equal to or more than 25 kg and less than 150 kg.

Different classes of the RPAS are subject to various provisions concerning the identification of the vehicle and the on-board equipment. Furthermore, the regulation establishes when it is necessary to make a declaration or to request an authorization to operate with RPAS depending also on the visual contact with the vehicle. The regulation defines three types of operations for RPAS:

- Visual Line of Sight (VLOS), that are operations at distances, both horizontal and vertical, in which the remote pilot maintains continuous visual contact with the vehicle, in order to be able to directly control it with the aim to conduct the flight and to meet separation and collision avoidance responsibilities;

- Extended Visual Line of Sight (EVLOS), that are operations at a distance exceeding the limits of the VLOS operations, for which the VLOS conditions are complied with by the use of alternative means, such as the presence of additional pilots or observers;

- Beyond Visual Line of Sight (BVLOS), that are operations at a distance that does not allow the remote pilot to continuously remain in direct visual contact with the vehicle.

One of the main requirements concerns the need for the pilot to have a "RPAS Pilot Certificate" or a "RPAS Pilot License": the certificate is required to use RPAS with operating take-off mass less than 25 kg in VLOS operations, while the license in needed to use RPAS in BVLOS operations or RPAS with operating take-off mass equal to or more than 25 kg; the only case in which no certificate or license is required is the use of RPAS with operating take-off mass less than or equal to 0.3 kg, with rotating parts safeguarded against impacts and having maximum speed less than or equal to 60 km/h. These requirements are synthesized in Table 1-3.

Table -3 ENAC requirements for the use of RPAS

RPAS Category	Operations	Authorization	Certificate
Take-off mass ≤ 0.3 kg and maximum speed ≤ 60 km/h	always considered non-critical	declaration	no certificate is needed
Take-off mass ≤ 2 kg	always considered non-critical	declaration	RPAS pilot certificate
Take-off mass < 25 kg	non-critical	declaration	RPAS pilot certificate

Furthermore, the operations are divided into:

- non-critical operations, that are VLOS operation which do not overfly, even in case of failures, congested areas (i.e. residential, industrial, commercial, sporting areas and where gathering of people are possible), crowd of people, urban areas or critical infrastructures;

- critical operations (all operations that do not fall into the "non-critical" category).

However, the regulatory debate is still lively and the rules, defined since 2013, have been modified and reviewed almost every year. What has been synthesized in the present paragraph, as written before, is referring to the epoch when the present thesis has been written, i.e. 2018. Anyway, for Italian regulation, it is possible to refer to the official regulation published by ENAC on its official spaces (https://www.enac.gov.it/). The first edition of the “REGOLAMENTO dei mezzi a pilotaggio remoto” (REGULATION of remote-controlled vehicles) has been published in December 2013 and replaced in July 2015 by a second edition, which has been amended 4 times up to the last version published in May 2018 (ENAC, 2018). All this activity in the regulatory field confirms the strong interest on the survey by drone and highlights its fast development, which is still in progress.

2. THE SURVEYS FROM UAV

In this chapter, the main applications of UAV in the field of survey will be described, in order to identify their strong points and critical issues. This analysis allows a better reading and understanding of the innovations proposed in chapter 4 and 5.

The use of UAS (including the military ones) is certainly connected to their ability to perform the so-called "dull, dirty and/or dangerous" tasks: UAS substitute manned vehicles in all the situations where a pilot and a crew may be significantly at risk of losing their lives or “dying of boredom” (Eisenbeiss, 2004). Moreover, thanks to the decreasing cost of UAV and GNSS/INS systems, as well as the range of available sensors, UAS can be employed in all the situations where a traditional platform (i.e. airplane) would be too expensive to justify its use. The high flexibility and the total low cost per acquired information compared to classical systems – terrestrial or aerial – offer really a high variety of different applications. A widespread use of UAS is aimed to the acquisition of videos and photos for purely commercial and documentation purposes (advertisements, movies, landscapes, real estate and so on). The other applications can be summarized as "observation, maintenance, surveillance, monitoring, Remote Sensing and security tasks” (Eisenbeiss, 2004). In 2007 the European Commission carried out a comprehensive study to monitor the uses of UAS in Europe: the provided list of potential applications for civil and commercial purposes is illustrated in Figure 2-1 (European Commission, 2007). An overview of the survey tasks currently carried out by drones will be proposed below, according to the classifications stressed by this research. The applications privileging the metric aspect to the qualitative one will be preferred.

2.1 Different Fields of Applications

The following picture (Figure 2-1) shows the classification made by the European Commission in 2007.

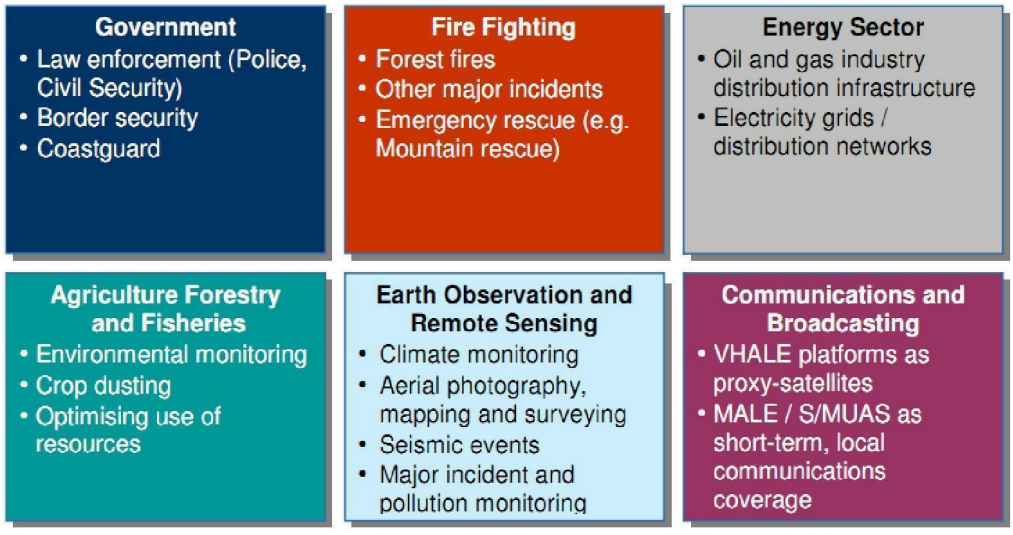

Figure 2-1 List of UAS civil and commercial applications (European Commission, 2007)

This research confirms the importance of the survey by drone in several situations and different public and private fields. However, this work prefers a classification based on the task given to the drone regardless of the application field, in order to be able to ponder the importance of the metric quality of results in every category.

2.1.1 Intelligence, Surveillance, Search-and-rescue

The capacity of UAV to travel repeatedly along a defined route at regular intervals in autonomous flight mode and to give updated images of the same scenario at every passage makes them an example of perfect surveillance tools. In fact, drones are commonly used in the control of borders and as support to the coast guard. In the role of surveillance, positioning accuracy is normally not the main issue. In fact, the required metric precisions in the localization of the surveyed object are in the order of magnitude of one meter or more. Therefore, more attention is paid to camera optic characteristics and the high quality of the images.

UAS can be useful also in the prevention and early detection of forest fires, thanks to their "above-the-head" privileged point of view. Indeed, UAS permit to supply real-time videos and information about fire's location, as well as wind speed, temperature, humidity and other parameters depending on the on-board sensors (Merino et al., 2010; Roberts, 2014). In this case the positioning of the observed scene requires a better metric quality, but the dynamic of the scene and the size of calamitous phenomena require metric precisions too.

The flexibility, safety, ease of operation and relatively low cost of ownership and operation facilitate UAS implementation also in disaster situations, such as floods, earthquakes, hurricanes, fires, volcanoes eruptions and so on (Pratt et al., 2006). Unfortunately, there have been several application cases of this kind in the last years and also in the national area like during Central Italy earthquake (August – October 2016). An example of a survey damaged or collapsed buildings in Norcia and Amatrice is described by Gagliolo et al. (2017, 2018).

An overview of UAS usage for disaster monitoring and management can be found in Adams and Friedland (2011). The drones have been used for the first time in calamitous events on an experimental basis in 2005, for the catastrophe of the hurricane Katrina. In 2011, after a devastating earthquake and subsequent tsunami, the Japanese Fukushima Daiichi nuclear facility was significantly damaged and began to emit radiation. This hazard complicated repair and traditional reconnaissance efforts as humans were advised to avoid the area. Thus, remotely operated UAS were deployed: for instance, a T-Hawk Micro Aerial Vehicle with special radiation sensors completed five reconnaissance missions and acquired hours of video and valuable imagery data of the nuclear reactor (Reavis and Hem, 2011). In the nuclear site of Chernobyl, 30 years after the tragedy, the danger for human lives is still high and the present reconnaissance in the Chernobyl Exclusion Zone (ChEZ) are performed by drones. The most recent studies reveal an accurate and reliable UAV-based detection of unknown radioactive biomass deposits in the ChEZ (Briechle et al).

2.1.2 Inspection

Another field of application for drones, which is now developing, is that of inspections. With inspection it is usually meant the visual control of the conservation state of an artifact, like bridges and dams or the check of the functionality of infrastructures, like high or medium voltage overhead power lines. In these cases, the use of drones makes logistics much easier, as it is possible to go near the artifact without the need of mobile lift trucks or harnesses and it makes the work of the inspector safer. Further examples of inspectable infrastructures are roads, railways, oil and gas pipes, photovoltaic installations, historical buildings and monuments.

2.1.3 Cultural Heritage and Archeological Surveys

Cultural heritage 3D models could help in securing, planning and performing the restoration of damaged buildings. Considering this last task, UAS photogrammetry can guarantee the metrical precision of the results, facilitating at the same time the access in areas where otherwise it would be impossible to enter. Furthermore, the instrumentation used by this technique is cheap and the survey operations are performed quickly. Hence, its use is very common and there is a plenty of applications spacing in different fields. The UAS photogrammetric capabilities could be very helpful in emergency situations (e.g. earthquakes), when a high level of precision and accuracy is required to ensure building conservation, as well as to preserve their cultural value.

The use of UAS for post-emergencies events and their integration with different surveying methods has been documented by a number of authors (see for instance Wang, 2014; Achille et al., 2015; Meyer et al., 2015; Ballarin et al., 2013; Gagliolo et al., 2017, 2018).

UAV have become very common also in the survey of archeological sites: the maneuverability of UAV, the fast and easy operation and the possible frequent repetitions of flights have played a key role in the choice of this tool again. In the case of archeological excavations, in fact, it is very important to monitor day by day both the new areas and the results, in order to schedule the following activity. In this context a UAS represents a cheap and efficient solution to create high resolution 3D models and orthophotos, keeping low costs and guaranteeing a good quality.

2.1.4 Traditional Surveying and Cadastral Applications

The use of UAV in surveys is not limited any more to new and particular operating fields, but it is substituting consolidated aerial survey techniques in several situations.

Thanks to the use of gimbals, it is possible to vary the inclination of the optic sensor, allowing to control in a better way the acquisition geometry and having configurations similar to those of close-range photogrammetry. Nocerino, Menna, et al. (2013) show how it is possible to improve the final accuracy by adding oblique images to the nadir ones. In UAS acquisitions it is frequent to have strong variation in the number of overlap images, because of the poor stability of the platform itself and, for this reason, it is necessary to increase the longitudinal and transversal overlap. The along-track overlap is usually about 70 − 90%, while the one along the across-track direction is about 60 − 90% (Skarlatos et al., 2015). The limit of UAV, in comparison to an aerial survey, is the short duration of batteries (less than an hour flight, depending on hardware characteristics, but it may be only 20 minutes) and the need to operate in the area

of visibility of the pilot on the ground, that are the reason why UAV are suitable for surveys of areas not wider than 100 hectares with cartographic or cadastral purposes.

2.1.5 Precision Farming, Forestry and Environmental Applications

New sensors mounted on UAV and optimal procedures for survey, data acquisition and analysis are continuously developed and tested for applications in precision farming. Procedures to integrate multispectral aerial data about soil and crop and ground-based proximal geophysical data are a recent research topic aimed to delineate homogeneous zones for the management of agricultural inputs (i.e., water, nutrients). Thanks to these tools it is possible to realize multispectral and multitemporal orthomosaics and to map vegetation and soil indices. The versatility of UAV allows to perform flights in two moments during the crop season, before sowing on bare soil and just before flowering. During the flights two cameras, for color (RGB) and false color (NIR-RG, Near Infrared-Red Green) images, can be used simultaneously. In addition to this, there are low cost thermal cameras, that can be mounted on lightweight UAV. UAVs have already given evidence of being an appropriate platform for mapping forests and agricultural crops, where aerial or satellite images have poor spatial or temporal resolution (Laliberte et al., 2011; Gini et al., 2014, Dunford et al., 2009, Berni et al., 2009, Nebiker et al., 2008, Hunt et al., 2005). On the other hand, the so-called "precision agriculture" requires information on the inherent spatial variability of soil and crop properties and uses this information to prescribe appropriate management strategy on a site-specific basis (Agüera et al., 2011). UAVs are always used in precision agriculture, in addition to ground observations. In recent years, extensive and accurate studies were done to enhance and speed up the spatial co-registration and the processing of images, in order to generate different kinds of thematic maps for agricultural crop monitoring. Nevertheless, the production of soil or vegetation maps from UAV imagery still presents challenges. Although the spatial resolution is very high, the spectral and radiometric resolutions obtained by the low-cost compact cameras are relatively low. Moreover, poor radiometric and geometric calibrations are often obtained when using common digital cameras. On the other hand, lightweight multispectral and hyperspectral sensors of high quality, which can be mounted on mini-UAV, are available only since few years and are not so widespread due to their high costs. Therefore, it can be said that several efforts have been done to optimize the procedures for acquisition and processing of images taken from UAV, mounting low cost cameras with low spectral resolution.

2.2 Survey Sensors

The overview of the discussed applications is not surely thorough, but it is relevant enough to show how the drone acts as a vector able to carry a specific sensor according to an a priori planned specific flight path in the survey functions. The difference among applications is given by the sensor and the geometry of data acquisition.

In the last years, a huge growth of low-cost and low-weight sensors, suitable to be mounted on very light and light RPAS has been registered. Different solutions are available on the market, both active and passive sensors, that can be employed in agroforestry field with many purposes. Among passive sensors, several types of cameras can be distinguished: RGB cameras, sensitive to the visible part of the electromagnetic spectrum (about in the range between 400 and 700 nm), Near Infrared (NIR) or Color Infrared (CIR)

cameras, which can detect also near infrared wavelengths (from 700 to 1200 nm), thermal cameras, sensitive to the thermal infrared wavelengths (about 8000 – 14000 nm) and, finally, multispectral and hyperspectral cameras, that allow to acquire a varying number of bands, equal to the number of optics or registration channels (in case that electromagnetic radiation is divided after its entrance in the sensor lens). A particular type of sensor is LIDAR. It is an active sensor able to generate georeferenced point clouds, which include also information about surface reflectance of the laser beam sent from the LIDAR itself. Whereas for passive sensors the data processing involves analysis and combination of different spectral bands, for LIDAR the geometric information is especially examined: in agroforestry applications LIDAR are employed for evaluating vegetation growth, for estimating biomass or for acquiring terrain morphology for hydraulic studies (Wallace et al., 2014; Malinowski et al., 2016; Bareth et al., 2016).

All sensors have weight varying between few tens grams (i.e. Action Cam) and some kilograms (i.e. LIDAR), hence suitable to be mounted on the most of RPAS. Even their costs are very variable: optical cameras prices start from a few tens euro for the RGB Action Cams up to around 10,000 euro for multispectral cameras (Nebiker et al., 2016), while LIDAR are expensive (more than ten thousand euro) and for this reason not diffusely used.

The Table 2-1 shows the scenario of the different sensors that can be used and their field of application.

Table 2-1 Sensors and field of application

Camera type	Spectral band	Applications	Image
RGB	Blue, Green, Red 400 nm – 700 nm	Whenever "true colours" images (orthoimages, 3D modelling) are requested	
NIR	Near Infrared 700nm – 1500 nm	Forest and agriculture applications, surveillance, inspections	
Multi-Spectral or Hyper-Spectral	Different bands	Remote Sensing, precision farming	
Thermal	Infrared 700 nm – 10^6 nm	Surveillance, traffic monitoring, building inspections, precision farming	
LIDAR	~1064 nm	Whenever geometric information only is requested	

3. UAV PHOTOGRAMMETRY

According to Kraus' definition, "Photogrammetry is the art and science of determining the position and shape of objects from photographs", in particular, it is the process of extracting metric information from an object through measurements made on photographs (Kraus, 1993).

In this chapter the basic principles of photogrammetry and the use of Unmanned Aerial Vehicles (UAV) in this field will be discussed. After defining the concept of photogrammetry, its theoretical principles will be presented: the central projection model, on which photography is based, and the different phases of the photogrammetric campaign. Finally, it will be briefly presented how, thanks to the development of UAVs, the relationship between photogrammetry and Computer Vision has changed in recent years.

This introduction to photogrammetry is not intended to be exhaustive. Its purpose is just to introduce the reader to concepts that will be treated in more detail later.

3.1 Characteristics of UAV Photogrammetry

In the last years the definition "UAV Photogrammetry" has been introduced in the scientific literature. The first use of the term is thought to be in the Eisenbeiβ (2009) PhD thesis, where it was used to identify a photogrammetric measurement platform that could be remotely controlled or could fly completely autonomously. The platform could be equipped with a photogrammetric measuring system that included tools, such as small or medium size cameras, video cameras or action cams, or other sensors. In this regard, the photogrammetry from UAV opens new possible applications, especially in the short-range field, since it is a good compromise between aerial and terrestrial photogrammetry.

The use of drones in photogrammetry has several advantages over aerial photogrammetry platforms, such as airplanes, helicopters and satellites. The advantages can be summarized as follows:

- lower initial and maintenance costs;
- it is not necessary to have a qualified pilot on board;
- the drone is easily maneuverable;
- the drone can fly autonomously following a pre-established flight plan;
- the survey is fast and, in general, repeatable several times in a short period of time;
- generally, there is the possibility to see in real time what the camera is acquiring;
- it is possible to carry out surveys in areas not accessible to other aircrafts and there are no limitations given by the presence of high-altitude clouds;
- UAVs can be used in high risk situations and inaccessible areas (e.g. natural disaster sites, accident scenes, mountainous areas);
- if using multirotor UAVs, it is possible to take-off and land vertically in narrow spaces and to acquire images on a hovering point;
- the flight height is lower and therefore the resolution is higher.

However, there are also some limitations in the use of drones:

- the need to reduce the weight of the aircraft as much as possible to increase flight endurance; this, together with the limits on the dimensions, leads to equip the drone with compact instrumentation, generally of lower quality compared to that used with larger aircrafts;
- the need for systematic calibration of the camera on board, because it's not usually a metric camera;
- the difficulty of flying in the event of wind on the ground or at altitude;
- there is a strict ENAC regulation for their use.

3.2 Theoretical bases of photogrammetry

Photogrammetry is a survey technique that allows to recreate the shape, dimensions and position of a three-dimensional object starting from two-dimensional images of it. The basic principle consists in the partial overlap of consecutive stereometric frames taken from different points. These frames are taken while the camera is moving, so that they show the object from different positions. To determine the three-dimensional coordinates of the object, it is necessary to identify the same point on at least two images and draw the projection rays: the three-dimensional position of the point is identified by the intersection of the rays.

A photogrammetric campaign consists of the following phases (Cannarozzo et al., 2012):

- *acquisition phase*: the object is photographed from several positions, ensuring that each frame partially overlaps with those that follow it and precede it;
- *orientation phase*: according to mathematical principles, the position and orientation of images at the time of acquisition are reconstructed;
- *restitution phase*: a 3D object model or a point cloud is generated in three-dimensional space starting from the two-dimensional images.

The photogrammetric technique is typically used in the field of architecture, construction and civil engineering for surveys of buildings or entire areas of the territory. It can be performed from the ground or from an aircraft (e.g. drone, airplane, helicopter or satellite).

3.2.1 The basic principle of photogrammetry

The *central projection model* is the model behind the photographic technique: each point on the image plane is the central projection of the corresponding point on the object in the three-dimensional space. The model is shown in Figure 3-1 in which:

- P is a generic point in the space;
- P’ is the image of P and belongs to the *image plane*;
- O is the *projection center*, it coincides with the ideal point where every ray light pass to impress the sensor creating the image;
- PP is the *principal point*, it is the projection of O on the image plane;

- c is the *focal distance* or, more exactly, the *principal distance*, that is the distance between O and the camera image plane; it isa characteristic of the objective.

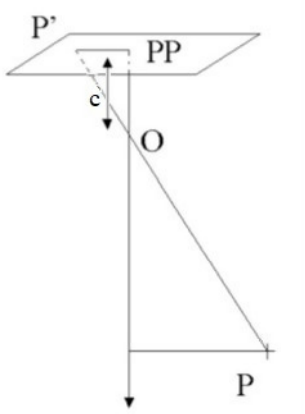

Figure 3-1 Central projection model

To describe appropriately a three-dimensional object in space, at least two frames from two different projection centers are required. One single frame is not sufficient because, as shown in Figure 3-2, a generic point P' belonging to the image plane having as center of projection O_1 can be the projection of infinite points P_1, P_2, P_3... along the projection ray. Therefore, it is not possible to uniquely determine the point P belonging to the real object. Instead, if two different frames are used with different centers of projection O_1 and O_2, it is possible to univocally determine the position of point P at the intersection of the projection lines coming from P' and P'' respectively on the frame 1 and 2, image points of the object point P. This principle is at the base of photogrammetry and is shown in Figure 3-2.

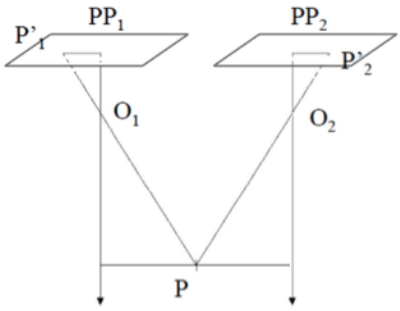

Figure 3-2 Basic principle of stereo-photogrammetry

This projection connects the points of the object with the projection centre and, intersecting the projection plane, generate the image points that are the point projections. The consolidated photogrammetric approach, reasumed for instance by Kraus (1993) and other authors, explain that, when we acquire a frame, the object point P, the projection centre O and the image point P' lie on the same straight line. The mathematical representation that indicates the collinearity conditions, representing the alignment between the points in the image and in the object system, in the simplest case when the image and the object frames are aligned can be expressed in the following way:

$$\frac{\xi-\xi_0}{c}=\frac{X'-X'_0}{Z'_0-Z'} \qquad \frac{\eta-\eta_0}{c}=\frac{Y'-Y'_0}{Z'_0-Z'} \tag{3.01}$$

where ξ and η represent the image coordinates, ξ_0 and η_0 represent the principal point coordinates, c is the principal distance, X', Y', Z' the coordinates of the object point P and X'$_0$, Y'$_0$, Z'$_0$ the coordinates of the projection centre that may be processed in the system X, Y, Z by the spatial rotation matrix R:

$$\begin{pmatrix} X-X_0 \\ Y-Y_0 \\ Z-Z_0 \end{pmatrix}=\begin{pmatrix} r_{11} & r_{12} & r_{13} \\ r_{21} & r_{22} & r_{23} \\ r_{31} & r_{32} & r_{33} \end{pmatrix}\cdot\begin{pmatrix} X'-X'_0 \\ Y'-Y'_0 \\ Z'-Z'_0 \end{pmatrix} \tag{3.02}$$

So, if we multiply the matrix above for the matrix $R^T = R^{-1}$ and replace the latter in the equations, making explicit the image coordinates, we will get the relationship between the image coordinates and the ground coordinates, called the collinearity equations:

$$\xi = \xi_0 - c\cdot\frac{r_{11}(X-X_0)+r_{21}(Y-Y_0)-r_{31}(Z-Z_0)}{r_{13}(X-X_0)+r_{23}(Y-Y_0)-r_{33}(Z-Z_0)} \tag{3.03}$$

$$\eta = \eta_0 - c\cdot\frac{r_{12}(X-X_0)+r_{22}(Y-Y_0)-r_{32}(Z-Z_0)}{r_{13}(X-X_0)+r_{23}(Y-Y_0)-r_{33}(Z-Z_0)} \tag{3.04}$$

The collinearity condition is expressed by non-linear equations and the estimation of the coordinate X, Y, Z of point P, at the intersection of the straight lines of each frames, is computed with a least squares estimation. For this reason, the expressions can be rewritten in terms of differential relations, and approximate initial parameters must be recovered to solve the system.

3.2.2 Image Acquisition Phase

In all the photogrammetric approaches (aerial, terrestrial, close-range or UAV) planning data acquisition is a fundamental step.

Especially in the case of UAVs, drawing a flight plan allows a reduction of the number of images and of flight time. This is essential to optimize battery consumption and to reduce the processing time of the acquired images. A flight plan also allows us to define the expected resolution of the final product and to define other flight parameters. Flight planning should also take into account the weather and light conditions (which can interfere with the flight and the image quality), wind speed (that is significant in the case of lightweight systems) and system vibrations (that have to be avoided or compensated during the flight).

In relation to the specific case study, a flight plan needs to be designed taking into account operative variables, as well as the area and the expected result.

First, the UAS type best suited according to the size of the area: fixed wings are preferable for big areas and multi-rotors for smaller ones. Then it is important to a priori define the objectives to be achieved in

terms of the resolution and accuracy in terms of GSD (Ground Sample Distance) and the block orientation precision. These parameters have to be considered in the flight planning (Figure 3-3).

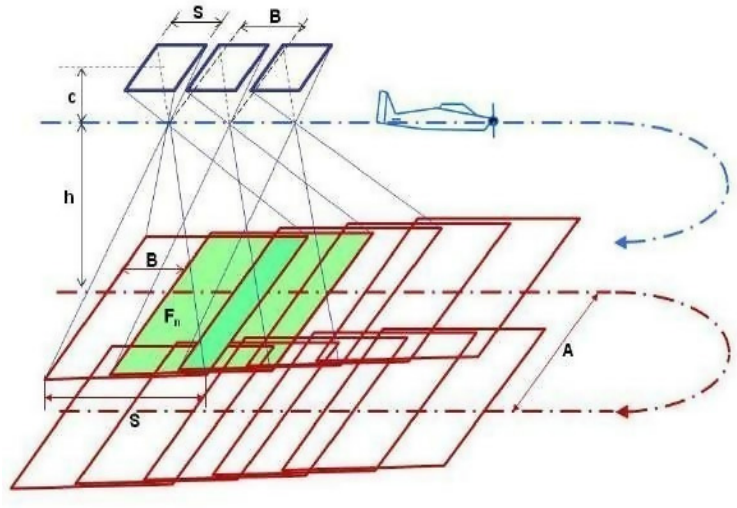

Figure 3-3 Flight plan schema for flat ground

Starting from well-known formulas, the main parameters to be considered for an aerial flight (in the *normal case*: camera axes are perpendicular to the base B and parallel to each other) are:

Image scale factor:

$$mb = h/c \tag{3.05}$$

where c is the principal distance and h is the relative flight height;

Image size on the ground:

$$Sx = sx \cdot mb;\ Sy = sy \cdot mb\ ;\ GSD = dpixel \cdot mb \tag{3.06}$$

where sx and sy are the sensor sizes and dpixel is the pixel size (in the same units of the principal distance c, generally in millimeters); base length (distance between consecutive images) for a given forward overlap percentage l:

$$B = Sx \cdot (1 - l/100) \tag{3.07}$$

distance between strips for a sidelap percentage q:

$$A = Sy \cdot (1 - q/100) \tag{3.08}$$

area covered by the stereoscopic model:

$$Fn = (Sx - B) \cdot Sy \tag{3.09}$$

From equations (3.03) and (3.04) we obtain the coordinates of the object point P

$$\begin{aligned} X &= -Z\,\frac{\xi_1}{c} \\ Y &= -Z\,\frac{\eta_1}{c} = -Z\,\frac{\eta_2}{c} \\ -Z &= \frac{c*B}{\xi_1 - \xi_2} \end{aligned} \tag{3.10}$$

Where ξ_1, η_1, ξ_2, η_2, are the image coordinates of the object point P

And the propagation of variance, the theoretical accuracy is:

$$\sigma_x = \sqrt{\left(\frac{\xi}{c}\sigma_z\right)^2 + \left(m_b\,\sigma_\xi\right)^2} \tag{3.11}$$

$$\sigma_y = \sqrt{\left(\frac{\eta}{c}\sigma_z\right)^2 + \left(m_b\,\sigma_\eta\right)^2} \tag{3.12}$$

$$\sigma_z = \left(m_b\,\frac{h}{B}\,\sigma_{p_x}\right) \tag{3.13}$$

However, the problem of estimating the expected accuracies requires further investigation, which will be addressed in chapter 4.

So, the parameters that have to be previously defined are the relative flight height (h) and the overlaps in the two directions, since the flight is performed following parallel strips. In the case of UAV photogrammetry, it is an established practice to use between 60% and 90% of forward overlap (usually 80%) and between 20% and 60% of side overlap (usually 60%). These values tend to be higher than classical aerial photogrammetry due to different issues: UAVs are quite sensitive to wind and the waypoint position is reached through the internal navigation system that usually has an accuracy of a few meters. For these reasons, real flight can be quite different from the planned one.

These concepts will be examined in depth in the next chapter, showing how they have been dealt with in this research work.

At the moment there are several software packages for flight planning integrated within the Ground Control Station (GCS). The software allows to draw the flight path on maps or, via internet connection, on web resources such as Google map, and can directly communicate with the navigation system of the UAV in order to perform the (semi) autonomous flight. One of the most used open-source software is the Mission Planner ArduPilot, while a commercial one is the pix4dcapture developed by pix4d that is directly connected, for example, with the Parrot or DJI drones (Figure 3-4).

Figure 3-4 GCS software for photogrammetric flight plans: Mission Planner on the left and pix4dcapture on the right

As shown in the figure, once the area of interest, the desired GSD and the strip overlap have been specified, the program generates the waypoint positions according to the expected result. The latest versions of Mission Planner allow to perform a fully automatic flight, since take-off and landing can also be programmed and directly managed by the UAV. With fixed-wings drones, the take-off is usually assisted by the pilot and the landing is automatic.

These GCS software are also relevant to the dynamic control of the flight and the management of mission information logs. In fact, they can be used to:

-plan, save and load the mission directly in the autopilot board using a base map to easily detect the waypoints;

-simulate the flight before performing it, in order to let the pilot identify possible issues;

-verify the flight height according to the terrain information of the software that can result from Google Earth (GE) or Shuttle Radar Topography Mission (SRTM) data, respectively by Google Inc. and by NASA;

-monitor the system status during the flight thanks to telemetry;

-download and analyze the log files to have complete information.

However, it will be shown in chapter 5 how this kind of software simplifies a lot the issues of planning and sometimes it is unsuitable to the use with applications where the metric element is essential.

3.2.3 Image Orientation

It is possible to distinguish between internal orientation and external orientation parameters. Internal orientation parameters define the position of the projection center O with respect to the camera image plane. This information, reported in the calibration certificate provided by the camera manufacturer with metric cameras, is today in most cases obtained by strict calibration procedures as digital non-metric cameras are commonly used in close-range and UAV photogrammetry.

The external orientation parameters define the position and the attitude angles of each frame in the object system at the time of acquisition.

For a single image, the image orientation phase depends, therefore, on 6 parameters for the external orientation (3 for the position and 3 for the attitude angles) and others for internal orientation parameters

(I.O.) that are specific to each camera (usually the principal distance, the image coordinates of the principal point and the coefficients of the lens distortion). They define an ideal geometric model that does not correspond exactly to reality because of lens distortion, so it is necessary to calibrate the instrument to create a correspondence between real and ideal parameters. These parameters are:

- **c**: *principal distance*, that is the distance between the projection center O and the image plane;
- ξ_0, η_0: coordinates in the image system of the principal point PP.

The I.O. parameters are considered known and the same for all images taken with the same camera in a given flight, at least for calibrated metric cameras. The 6 external orientation parameters describe camera position and attitude by 3 translations and 3 rotations:

- X_0, Y_0, Z_0: parameters of translation, they are the coordinates of the projection center O and define the position in space of the frame;
- **ω**, **φ**, **κ**: parameters of rotation around axis X, Y, and Z, defined with respect to the object system.

A single stereo pair is enough to reconstruct the surveyed object about a stereo model, generated by the overlap of the two frames; for the external orientation of the model (or, equivalently, of the image pair) a total of 12 unknown parameters (6 for each frame, as shown in Figure 3-5) must be determined.

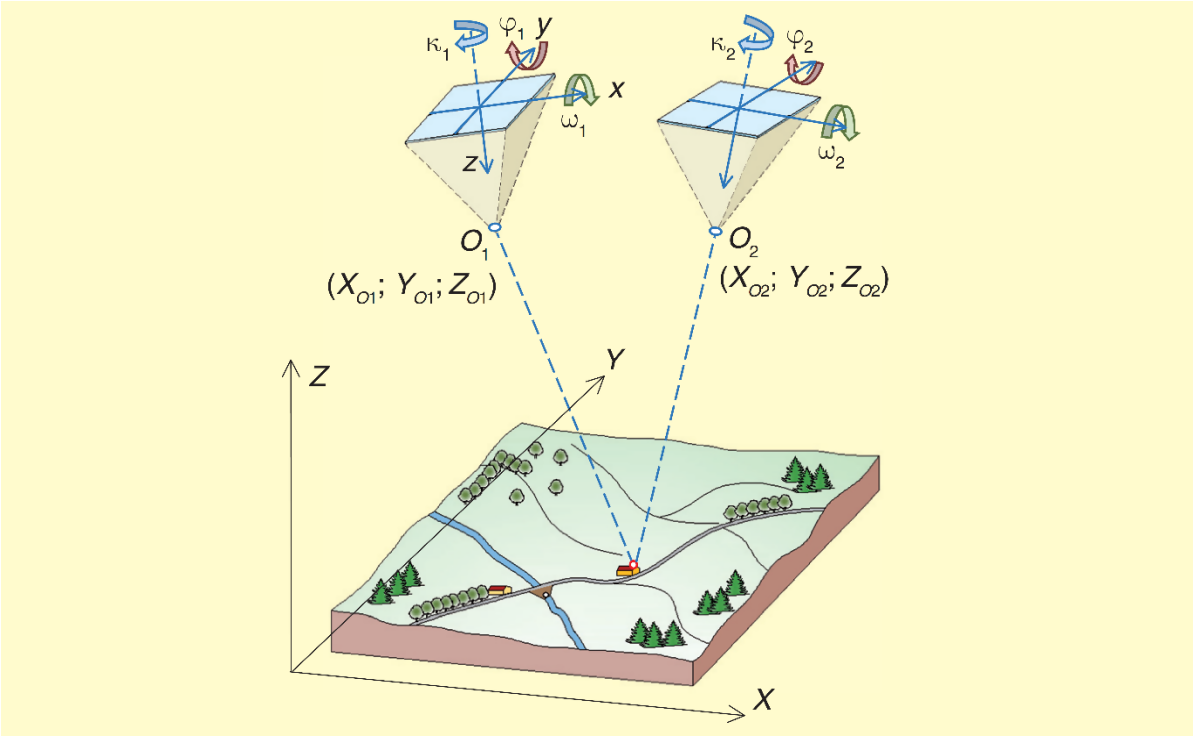

Figure 3-5 Parameters needed for the external orientation of a model composed by two frames (Cannarozzo et al., 2012)

The external orientation procedure, by independent models, involves two distinct phases:

- the *relative orientation*, that is the determination of the relative position and attitude of the camera in space at the moment of acquisition of the first frame, with respect to the reference system of the first camera when the second frame is taken. In this phase a model of the surveyed object is obtained, similar to the real one but in a generic position of the space and on an arbitrary scale;
- the *absolute orientation*, that is the determination of the correct position, orientation and scale in the space of the object in the external reference system. The model obtained in the previous phase is transformed infact by converting it to the desired position, imposing the same orientation of the surveyed object and its scale.

In order to complete the absolute orientation phase, it is necessary to know the position of a certain number of object points called *control points*, which must be clearly identifiable on the frames. In the case of aerial photogrammetry, they are points of the territory or artificial targets called *Ground Control Points* (GCPs) of which the coordinates are known (previously surveyed with other technologies like for instance the GNSS). At least three GCPs non-aligned-and well distributed on the object are required to perform the absolute orientation, a major number of GCPs increase the redundancy to the orientation permitting the control of the process. There are different possibilities in the selection of GCPs: it is possible to use high-contrast targets positioned on the ground or it is possible to use points belonging to the territory or to the objects to be detected, in any case these points must be easily recognizable on the frames.

As known the external orientation procedure may have another approach, where the orientation of all the frames are obtained in a unique step. The previous approach belongs to the past technique of analogue photogrammetry. while this one it is actually used by the software with the so-called Structure From Motion (SFM) approach. This mode of orientation will be the privileged one in the development of this work.

The procedure of orientation of all the frames in a unique step is called compensation of the block with Bundle adjustment technique. The Figure 3-6 shows the principle of the compensation of a block when a sufficient number of “tie points” is introduced. The tie points are object points observed in at least 3 images (that means in at least 2 stereoscopic models); in this way these points connect all the images in a unique group called block and it is possible to estimate all the unknown parameters (object coordinates, external orientation of the images, ...) introducing the GCPs necessary for a single block (theoretically the minimum of three points). It is important to highlight that the object coordinate of the tie points are unknown like the other parameters.

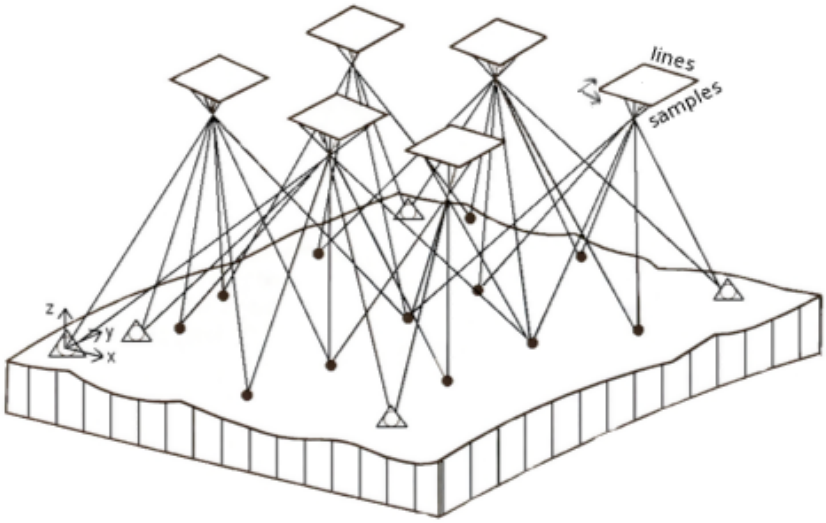

Figure 3-6 Principle of Bundle Adjustment method (from Kraus, 1993)

For a better comprehension we will start with the transformation of an image with central perspective between the image space and the object space (Schwidefsky and Ackermann, 1976):

$$\begin{vmatrix} \xi_i - \xi_0 \\ \eta_i - \eta_0 \\ -c \end{vmatrix} = sR \begin{vmatrix} X_i - X_0 \\ Y_i - Y_0 \\ Z_i - Z_0 \end{vmatrix} \tag{3.14}$$

where x_i , y_i are the coordinates of the point P_i, c is the focal length or principal distance and x_0 , y_0 are the coordinates of the principal point in the image system; s is a scale factor, R the rotation matrix applied to the object coordinates X_i , Y_i , Z_i of P_i, shifted on the projection centre with coordinates X_0 , Y_0 , Z_0. From this relation we get the well-known observation equations, called collinearity equations, previously introduced with the (3.03) and (3.04).

$$\frac{\xi_i - \xi_0}{c} = -\frac{r_{11}(X_i - X_0) + r_{21}(Y_i - Y_0) + r_{31}(Z_i - Z_0)}{r_{13}(X_i - X_0) + r_{23}(Y_i - Y_0) + r_{33}(Z_i - Z_0)} \tag{3.15}$$

$$\frac{\eta_i - \eta_0}{c} = -\frac{r_{12}(X_i - X_0) + r_{22}(Y_i - Y_0) + r_{32}(Z_i - Z_0)}{r_{13}(X_i - X_0) + r_{23}(Y_i - Y_0) + r_{33}(Z_i - Z_0)} \tag{3.16}$$

For a fixed internal orientation of the camera (known coordinates x_0 , y_0 and focal length c), the left part of equations can be interpreted as directions in space to be measured. Using as matrix rotation R the traditional one employed with Cardano sequential rotations ω, φ, κ respectively around X, Y and Z axes:

$$R: = \begin{vmatrix} r_{11} & r_{12} & r_{13} \\ r_{21} & r_{22} & r_{23} \\ r_{31} & r_{32} & r_{33} \end{vmatrix} = R(\omega)R(\varphi)R(\kappa) \tag{3.17}$$

$$R(\omega) := \begin{vmatrix} 1 & 0 & 0 \\ 0 & \cos(\omega) & -\sin(\omega) \\ 0 & sin(\omega) & \cos(\omega) \end{vmatrix} \quad (3.18)$$

$$R(\varphi) := \begin{vmatrix} \cos(\varphi) & 0 & \sin(\varphi) \\ 0 & 1 & 0 \\ -sin(\varphi) & 0 & \cos(\varphi) \end{vmatrix} \quad (3.19)$$

$$R(\kappa) := \begin{vmatrix} \cos(\kappa) & -\sin(\kappa) & 0 \\ \sin(\kappa) & cos(\kappa) & 0 \\ 0 & 0 & 1 \end{vmatrix} \quad (3.20)$$

All these considerations explain the fact that the determination of points by means of photogrammetry is just a spatial triangulation. This means that the photogrammetric network, measured from angles, is invariable under a 3D rigid transformation, i.e. can be translated, rotated and scaled without any variation in the observations. Thus the number of invariant parameters is 7: 3 translations, 3 rotations and the scale factor. This rank deficiency can be overcome applying the information coming from the Ground Control Points, in order to estimate the external orientation parameters X_0 , Y_0 , Z_0 , ω, φ, k, as well as the object coordinates X_i , Y_i , Z_i. The unknown parameters are estimated in the "Bundle Adjustment" where the rank deficiency it is the same of a unique block, due to the introduction of the tie points above introduced in chapter 4 we will start from this notions in order to evaluate how it can be possible, not only to know the value of unknown parameters, but also to estimate their precision and, therefore, to indicate the possible expected precisions of a photogrammetric survey.

3.2.4 Outputs of the Photogrammetric Survey

Following the orientation of the images the processes of restitution and production of the final products occur.

With the restitution process we get the three-dimensional space of the rebuilt object from the two-dimensional space of the images, that is, from the image coordinates of a point (image space) to the object coordinates (object space).

This workflow allows to obtain the following products in the external reference frame (introduced by the GCPs coordinates):

- a list of coordinates of the relevant points of the surveyed object;
- a 3D vector restitution;
- a *point cloud*, that is a set of georeferenced and colored points.

Starting from these results, in particular from the point cloud, it is possible to obtain several outputs, including the *Digital Elevation Model* (DEM), the *orthophoto* (or orthomosaic photo) and the *3D mesh* of the surveyed area.

The DEM is a discrete representation of the elevation, often stored as raster data. It primarily contains elevation data concerning the terrain proper, but vegetation and buildings can be represented too. In particular, if the DEM represents only the elevation of the terrain surface, it is generally called *Digital Terrain Model* (DTM). If it contains, instead, information regarding the elevation of the external surface of the territory, including vegetation and man-made constructions, then it is called *Digital Surface Model* (DSM).

The orthophoto is an orthogonal projection of the image on the object surface. It has a uniform scale and is not affected, as the original image, by the perspective distortion: for these reasons it can be considered a photographic map on which it is possible to make measurements.

The 3D mesh is the three-dimensional reconstruction of the surveyed objects by means of surfaces. The surfaces are composed by vertices, edges and faces that define the shape of the objects and by the texture from the images that is projected on them. Thanks to the 3D mesh it is possible to easily visualize the reconstructed area.

3.3 Photogrammetry and Computer Vision

Besides the classical photogrammetric algorithms, some computer vision techniques have been applied in the last decade to solve the question of image orientation. They use digital images permitting the application of automatic algorithms for points and region detection.

The main feature is that both the techniques start from the analysis of 2D images to discover 3D shape information, even if the employed approach is sometimes different: originally, the goal of photogrammetry was the measurement of the position of a set of 3D points, while the computer vision aimed at the final appearance of the model. The main goal of Photogrammetry was mapping and the technique was linked to the achievement of the best possible metric accuracy.

Computer vision is born as a branch of artificial vision; its aim is the achievement of the so-called “vision for action”. On the one hand, dynamic 3D information about the environment is acquired, and on the other hand, vision algorithms are implemented to be used in real-time.

Several techniques, such as edge detection, image segmentation, object recognition, optic flow, and disparity, are suitable to interpret image visual features into real-world properties.

Localized features are called *key-point features* or *interest points*; edges and lines provide complementary information with respect to key-point and region-based descriptors.

Key-point features are used for:

- images alignment;
- 3D reconstruction;
- motion tracking (robots, drones, Augmented Reality - AR);
- indexing and database retrieval;

- object recognition.

Among these operations, images alignment and 3D reconstruction are common phases of computer vision and photogrammetric post-processing.

The principles of images alignment from the computer vision point of view are shortly resumed in the following.

First of all, key-points are detected, described concerning their qualities (e.g. intensity, RGB, etc.) and matched. Good features are characterized by repeatability, saliency, compactness, efficiency, and locality. The detected points are identified by invariant and distinctive descriptors. The best matching between two images is found defining a distance function that compares two descriptors, then testing the corresponding features in the second image; the match is confirmed for the one with minimum distance. An example of simple descriptor to illustrate the neighbourhood configuration around an interest point is the intensity vector, as shown in figure 3-7.

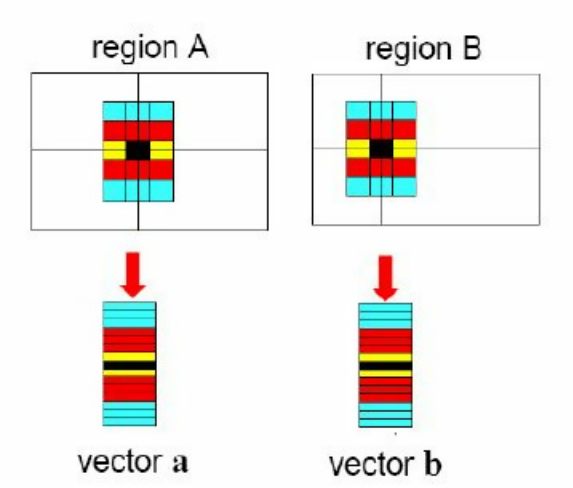

Figure 3-7 Descriptor vector in the matching.

Starting from the image matching, it is possible to perform the following step, i.e. the scene reconstruction. The ideal mathematical model can be expressed using a homographic transformation:

$$Z_c \begin{pmatrix} u \\ v \\ 1 \end{pmatrix} = \begin{pmatrix} f_x & s & u_0 & 0 \\ 0 & f_y & v_0 & 0 \\ 0 & 0 & 1 & 0 \end{pmatrix} \begin{pmatrix} R & t \\ 0^T & 1 \end{pmatrix} \begin{pmatrix} X \\ Y \\ Z \\ 1 \end{pmatrix} = M_1 M_2 \vec{X} = M\vec{X} \qquad (3.21)$$

Where:

(u, v, 1) are the homogeneous image coordinates;

Zc is the space point depth under the camera system;

$(\vec{X}) = (X,Y,Z,1)^T$ is the space point homogeneous coordinates in the object-space coordinate system;

$M = (M_1\ M_2)$ is a 3x4 projection matrix composed of:

M_1 -that represents the camera calibration matrix containing:

fx, fy the focal length along the two axes;

u0, v0 coordinates of the principal point in the image plane;

s the skew value between the x,y axes.

M_2 the exterior orientation matrix that contains: the R rotations; the t translation of the system.

The expression used in computer vision has a more compact mathematical form and it has no physical meaning as it describes the relationship between the space point coordinates and its image point coordinates.

The main advantage in this relation is that it can be expressed by a linear equation.

Computer vision has a wide variety of applications, e.g., mobile robot navigation, industrial inspection, military intelligence, human-computer interaction, image retrieval in digital libraries, medical image analysis, and the realistic rendering of synthetic scenes in computer graphics.

Currently, in the field of 3D model reconstruction, photogrammetry and computer vision have the same goal and purpose whilst approaching the problem from two different points of view. First of all, they start from the same mathematical model (the central projection), but the computer vision algorithms use a linear approach to solve the problem, while the photogrammetry theory generally considers a non-linear solution, that must be linearized according to the approximation of the initial parameters. In many cases of photogrammetric processing it is preferable to know the internal orientation parameters of the used camera, or they have to be at least stable, while the computer vision approach starts from the concept of non-calibrated cameras (unknown internal orientation parameters) to reconstruct the 3D shape of the area of interest.

However, even if they seem to be two very different approaches, today it is difficult, if not even impossible, to define the border line between the two applications in the definition of the used algorithms and the obtained results.

4. THE PRECISION IN PHOTOGRAMMETRIC SURVEYS

In the previous Chapters 1 and 2 an overview of drone surveying has been presented. It has been shown that drones can be applied in a wide number of different survey techniques with different purposes. This research work is interested in the photogrammetric survey by drone with metric purposes and in Chapter 3 the main principles of photogrammetry have been introduced. However, the concept of "metric purposes" of a survey is still to be defined and deepened and this chapter is aimed to dealing with this perspective.

To understand the metric potentialities of a photogrammetric survey means not only to recognize its capacity to build a numeric reconstruction of the observed objects, but also the ability to determine its precision, both a priori and a-posteriori.

To know the achieved precisions a-posteriori means to validate the survey and to provide the quality and the applicability limits of this information. To know the reachable precisions a-priori it is necessary to plan the survey and the conditions ensuring the precisions expected of the survey will be met.

In order to understand how it can be possible to plan and analyze a photogrammetric survey from this point of view, it is necessary to review some key concepts mentioned in Chapter 3.

4.1 Error Theory

Thanks to the redundancy of observations in comparison with the number of variables, bundle adjustment and similar adjustment computations are classically formulated as non-linear least-squares problems. This statistical approach, as known, permits to estimate the unknown parameters and at the same time to estimate the standard deviation with which they are being estimated. This approach has given relevance to photogrammetry since the '60s as a simple, fast and reliable survey technique.

In the logic of applying the least-squares theory to the bundle adjustment solution, the linear functional and stochastic model can be written as:

$$v = A\,x - l \tag{4.01}$$

$$C_{ll} = \sigma^2_0\, P^{-1} \tag{4.02}$$

where l, v, and x are the vectors of observations, residuals and unknown parameters, respectively; A is the design matrix; C_{ll} is the covariance matrix of observations; P is the weight matrix and σ_0 is the variance factor.

The parameters estimate:

$$\hat{x} = (A^T P A)^{-1} A^T P\, l = Q_x A^T P l \tag{4.03}$$

The covariance matrix of the unknown parameters C_{xx} can be written as:

$$C_{xx} = \sigma^2_0 (A^T P A)^{-1} \tag{4.04}$$

To better understand the theory of evaluation of precisions it is necessary to start from several works presented at the end of the '80s and at the beginning of the '90s. In particular, it is interesting to consider

what Fraser (1984) published in the article "Network design considerations for non-topographic photogrammetry". According to what the authors wrote, accuracy is influenced not only by the quality of the observations (measurement of the coordinates of the points on the images) but also by the geometry of the network, the so-called “network design”. Network design analysis in engineering surveying are well covered in Alberda (1980) and Niemeier (1982), while reliability of observations in close-range photogrammetric networks have been addressed by Grün (1978, 1980) and Torlegård (1980).

A classification of network design issues has been identified by Grafarend (1974):

Zero-Order Design (ZOD): the datum problem

First Order Design (FOD): the configuration problem

Second Order design (SOD): the weight problem

Third Order Design (TOD): the densification problem

ZOD – The Datum Problem

In photogrammetry the datum problem is ordinarily always solved, when a ground control network is already in place. The datum problem is indeed solved by the introduction of the coordinates of some control points, whose number is equal or greater than the rank deficiency to fix the reference system. The minimum request is satisfied by 2 control points with all 3D information (XC, YC, ZC) and one control point in height (ZC) opportunely located. In fact, the geometric position of the control points in the photogrammetric block is also relevant. In modern aerial surveys and UAV surveys you can also think of using the coordinates of the display stations. In addition, trim angles can also be used as observations. This introduces techniques of direct georeferencing and integrated orientation of sensors. The point must be made that the datum problem is not independent of the configuration problem. The extent to which a change in datum will influence object point precision is very much dependent on imaging geometry. Parameters of shapes are determined solely as a function of the system observations, and they are invariant with respect to changes in the datum, and thus when the minimal constraints changed, one can expect the solution vector x and the cofactor matrix Cxx to be altered. In situations where the datum is arbitrarily assigned, ZOD can be thought of as being the process of establishing a particular zero-variance computational base which, for a given network geometry, yields a cofactor matrix Cxx of the parameters (exterior orientation, object space, and additional parameters) which is "best" in some sense.

FOD – The Configuration Problem

First Order Design primarily involves the choice of an appropriate imaging geometry for a given array of object target points. As the central component of FOD, the selection of an appropriate imaging geometry deserves close examination.

When shooting the images, camera axes can be normal to object surface or convergent towards the object center, as shown in Figure 4-1:

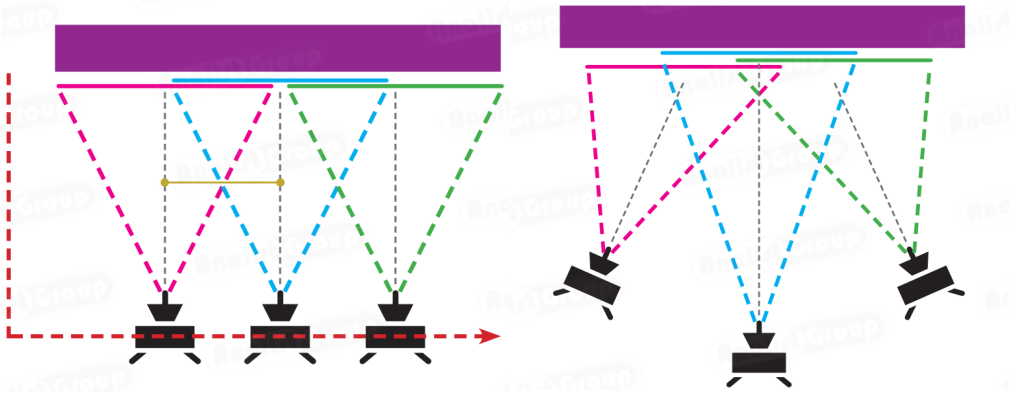

Figure 4-1 Imaging configuration normal (left image) and convergent (right image)

FOD problem, at least for the normal case, is mainly influenced by the base-to-distance ratio (B/D), i.e. the ratio of the distance between two consecutive overlapping images and their distance from the object, because a decrease in the B/D ratio leads to a less favorable ray intersection geometry. Several other parameters affect the camera network strength, like the number of camera stations, the number and multiplicity of tie points, the image scale, the sensor size and the focal length.

As already said, this issue deserves a detailed study because of the complexity and the number of parameters involved. The present research work will propose an approach to treat this problem.

SOD – The Weight Problem

In the photogrammetric case the observations are the images coordinate. If we suppose that the object point are with similar characteristics (for instance if we exclude the few targets and if we suppose that all the points comes from the same observations method) the covariance matrix is generally proportional to the identity matrix with the same accuracy σ. Thus, P-1 = σ02 I and the weight problem involves only an optimization of the scalar value σ.

TOD – The Densification Problem

In light of the fact that object point precision is largely independent of the target array density in photogrammetric survey with “strong” geometries, the densification problem does not seem to arise for the photogrammetric UAV survey.

4.2 The Estimation of a Priori Precision in UAV Photogrammetry

According to the considerations made up to now, when designing a photogrammetric survey with UAV, it is necessary not to neglect the possibility of estimating a posteriori the achieved precision and of estimating a priori the achievable precision.

As already said, the existing literature gives several interesting starting points to examine in depth the datum problem (ZOD). The problems of densification (TOD) and weight (SOD) are, instead, less

influencing in respect of the geometrical configuration (FOD). Therefore, it is essential to deepen the configuration problem FOD and provide practical instruments for the planning.

While the characteristics of aerial blocks with film cameras are well known, see Alberda (1980) and Niemeier (1982), digital aerial cameras are not yet assessed due to variety of camera formats and characteristics. Due also to the mixture of oblique and nadir imaging in the same block, high overlaps as well as camera and sensor characteristics, this is even more the case for UAV blocks.

4.2.1 The Model of Classical Photogrammetry

Kraus describes in its manuals an estimation of the expected accuracies in the traditional case of stereo restitution. This classical case supposes that the camera axes are parallel and normal to the base joining the cameras. This condition is always approximately met in aerial photogrammetry flights, where cameras are mounted on stabilized platforms; indeed, in case deviations from this ideal conditions (e.g. camera axis off nadir greater than 5°) are too large, the flight must be repeated.

Thus, it is possible to compute the object coordinates (X, Y, Z) from the quantities measured on the image and to evaluate the accuracy of these indirectly derived coordinates. These accuracies are shown in Figures 3.11, 3.12 and 3.13 in Chapter 3. Is here analyzedthe standard deviation only along the Z axis, because it is generally the most significant one.Supposing the principal distance c and base B error-free, the precision (standard deviation) of the elevation σ_z is as follows:

$$\sigma_Z = \frac{Z^2}{cB}\,\sigma_{p\xi} \tag{4.05}$$

where Z is the relative flight altitude and $\sigma p\xi$ is the precision of the measurements on the images. In the following Figure 4-2, the procedure to evaluate the expected precision in the stereo normal case is shown:

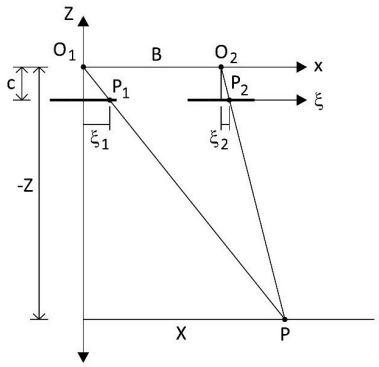

Figure 4-2 Stereo normal case, standard deviation evaluations

.

Historically, the production of cartography adopted the normal case of stereo restitution as the most practical and efficient; for this reason, it ignores the possibility of convergent imaging and of the visibility of an object point in more than two images. This was true for the classical analytical photogrammetry,

which used to fly with a 60% longitudinal and 30% transverse overlaps, such geometry has been then assumed as a boundary condition. With the use of digital cameras, UAVs and software derived from the Computer Vision, the methods of photogrammetric shooting have widely changed and the conditions of stereo normal case are almost never met.

4.2.2 The Terrestrial Close-Range Model

The relations used for terrestrial close-range photogrammetry significantly change due to the high level of overlap and the presence of oblique images. In fact, the number of images and their convergence are fundamental aspects to be taken into account for the computation of the final accuracy. According to Fraser (1992), the precision of an object point (X, Y, Z) can be expressed as:

$$\sigma_{XYZ} = \frac{qZ}{c\sqrt{k}}\,\sigma_{p\xi} \qquad (4.06)$$

where Z is the distance between the object and the camera, c is the focal length, k is the number of overlapping images, q is a form factor and $\sigma_{p\square}$ is the precision of the measurements on the images. The latter parameter ($\sigma_{p\square}$) strongly depends by the measurement principle used and by the quality of the image itself. In case of calibrated non-metric cameras, it can be assumed equal to the pixel size. The model of accuracy of the (4.13) conforms better to the conditions of a photogrammetric survey by UAV, because, thanks to the introduction of the parameters k" and "q", it takes into account the strong overlap of images and the shot geometry, which is rarely nadiral and often proves to be convergent.

However, while the number of overlapping images "k" is easily definable, the form factor "q" is a parameter that can be only estimated through the empirical analysis of several datasets from surveys by UAV. It is possible to find in literature indications for estimating "q" (Fraser, 1984 and Pagliari et al., 2017). These bibliographic sources say that the form coefficient q can be considered equal to 3.5 in case of nadiral acquisition with a standard overlapping equal to 60% of the image size. It decreases to 3 in case of acquisition with high cross overlapping and it reaches a value of 0.4 in case of high convergent geometry.

4.2.3 The Rigorous Approach

It is therefore obvious that the application of a priori expected precisions estimate methods, developed and used in aerial and close-range photogrammetry, gives approximate results, which are not always reliable. The estimate of expected accuracy used by Kraus simplifies too much the imaging geometry and does not take into account the redundancy of the observation of tie points. The evaluation method introduced by Fraser for close-range photogrammetry requires the knowledge of the factor "q", which is difficult to estimate in case of complex imaging geometry, like that of a survey by UAV.

Moreover, the methods described until now are based on the propagation of variance of the only operation of photogrammetric restitution, without taking into account the uncertainties due to the process of orientation of the photogrammetric block itself. These approaches can offer an initial and fast estimate of the excepted precisions from the restitution of a photogrammetric block. However, if we desire a rigorous estimate of the expected precisions, it is necessary to return to the general formulation of the problem by the Bundle adjustment i.e. about a generic 3D camera network.

Basically, the photogrammetric reconstruction of a points cloud describing an object or a territory is an optical triangulation technique. The fundamental observables are the measurement of the image coordinate pair (ξ, η) on the photograph. The (linearized) mathematical and stochastic model of an Aerial Triangulation (AT) can be written as shown in the formulae (4.01) and (4.02), where l, v, and x are the vectors of observations, residuals, and unknown parameters, respectively; A is the design matrix; C_l is the covariance matrix of observations; P is the weight matrix and σ_0 is the variance factor.

To eliminate the rank deficiency, it is possible to define the minimum number of not-estimable degrees of freedom. In this case we talk of a minimum constraint solution. In the compensation of local topographic and geodetic networks, even for considerations of statistic opportunity, more known (i.e. previously measured) points are introduced, belonging to networks of a superior order. In this case the solution is overconstraint and we talk of georeferencing of the local network in the network of superior order. Also, for "photogrammetric" networks more constraints than the strictly necessary ones are introduced. For this reason, we add constraint equations to the observation ones. For this approach a constraint on a variable number of ground known coordinates points (GCPs) and a constraint on the position of projection centers are selected. The constraint equations added to the system are reported in appendix to the observation equations with the effect of enlarging the matrix design A.

The Figure 4-3 shows an example of how the matrix design A is constructed and how the coefficients are distributed inside.

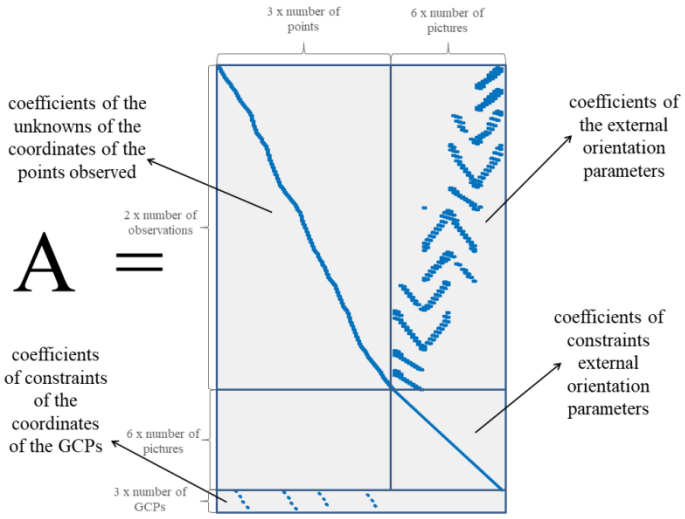

Figure 4-3 Representation of the sparse matrix A.

The stochastic model of observations, that is the matrix $C_{yy}= \sigma^2_0 P^{-1}$ is supposed to be known. The weights of the constraints are reported in the matrix C_{yy} (described in formula 4.07). The weights attributed to constraints can vary according to the conditions of the survey.

$$C_{yy}^{-1} = \begin{vmatrix} \frac{1}{\sigma^2_{observations}} & & & & \\ & \ddots & & & \\ & & \ddots & & \\ & & & \frac{1}{\sigma^2_{XYZ\ projection\ centres}} & \\ & & & & \ddots \\ & & & & & \ddots \\ & & & & & & \frac{1}{\sigma^2_{XYZ\ GCPs}} \end{vmatrix} \quad (4.07)$$

The constraints on the coordinates of the projection centers can usually have precisions of about 10 m, if these positions are achieved through a GPS on board of a UAV, which provides a GPS code solution. If we have, instead, a double-frequency or RTK on-board GPS, we can have precisions for the coordinates of the projection centers of about 3 cm. The constraints on slip angles are unknown at the moment, as the inertial sensors on board of UAV do not provide now optimal precisions for this purpose. However, it is possible to add this constraint too. In the same way the constraints on the coordinates of GCPs can vary according to the device used for their determination: for example, 5 mm in case of survey with total station or 3 cm in case of survey with GPS in RTK mode. Finally, the observations on photograms are considered with a sub-pixel equivalent precisions that is reasonable to fix in ½ pixel.

The main diagonal of the Cxx matrix in (4.11) provides the variances and, consequently, the precision for the (X, Y, Z) coordinates of the object points. Given the Internal Orientation (IO) parameters of the camera, the camera positions and attitudes of the flight plan as External Orientation (EO) parameters and an approximate DTM of the survey area, it is possible to simulate the photogrammetric network for AT and to know the standard deviation for each point inside the survey area, provided that its projection falls within the image format on at least a couple of images.

Such a system of equations can seem particularly complex from the computational point of view, because of the high number of observation and constraint equations. However, using a DSM of about 5 meters of resolution for territorial surveys limited to some hectares, we get the solution without computational problems and with a sufficient level of details.

5. THE U.Ph.O. PROJECT

The previous chapters have introduced the potentialities and the issues related to a survey by UAV from a strictly theoretical point of view. In particular, the methods developed so far for the a-priori precision estimate, both in classical aerial and close-range photogrammetry, have been introduced and discussed to get hints on a method for the a-priori precision estimate for photogrammetry by UAV.

In this chapter it will be shown how this a-priori precision estimate method can become a usual surveying practice applied by means of appropriate tools.

Before dealing with this topic, it is important to know the interface between man and machine in the surveys by UAV and to learn how the planning of a survey takes place in practice.

The software that allows this kind of connection is called Ground Control Station (GCS). A ground station is typically a software application, running on a ground-based computer that communicates with the UAV via wireless telemetry. It displays real-time data on the UAV's performance and position and can serve as a virtual cockpit, showing many of the same instruments that you would have if you were flying a real plane. A GCS can also be used to control a UAV in flight, uploading new mission commands and setting parameters and it is often employed to monitor live video streams from a UAV's camera. And last but not least, GCS hosts the software that allows the planning of a survey and manages its realization in case of a survey executed in autonomous mode.

5.1 A review of current UAV Flight Planning Software

To better understand what a GCS really does, it is worth presenting the most popular GCSs used today for the planning and the management of drone flights, also with survey purposes.

MISSION PLANNER

Mission Planner is a full-featured ground station application; it is a free, open-source, community-supported application developed by Michael Oborne for the open source autopilot project ArduPilot. Mission Planner is a ground control station for Plane, Copter and Rover. It is compatible with Windows only. Mission Planner can be used as a configuration utility or as a dynamic control supplement for your autonomous vehicle. Using an easy graphic interface (shown in Figure 5-1) with this software it is possible to:

- setup, configure a vehicle;
- plan, save and load autonomous missions into the autopilot with point-and-click way-point entry on Google or other maps;
- download and analyze mission logs created by autopilot;
- monitor the vehicle's status while in operation with appropriate telemetry hardware;
- record and view the telemetry logs.

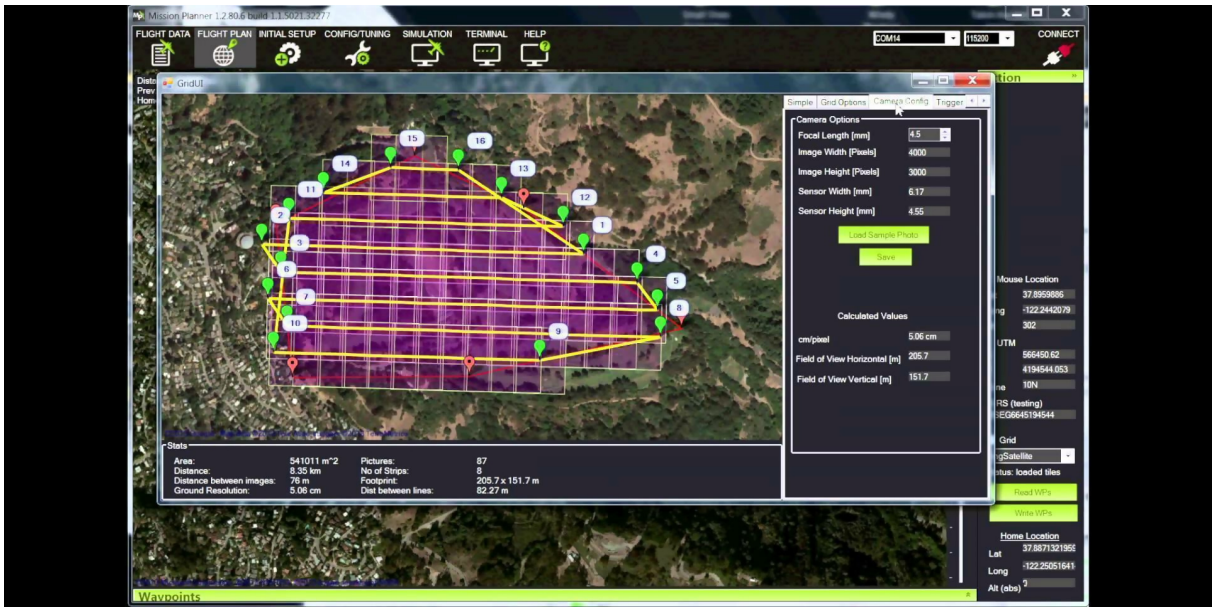

Figure 5-1 Graphical interface of Mission Planner

Mission Planner uses by default Google information, like maps and the relative DTM.

As said before Mission Planner is an open-source, community-supported application, for this reason has the advantage that an expert user programmer can change its functions.

Mission Planner allows the planning of a flight for photogrammetric survey setting up the desired overlaps, but it doesn't provide any information about the expected precisions, except for the ground pixel dimension GSD (Ground Simple Distance). Mission Planner allows the graphic visualization of the ground projection of photograms, but not the quantitative analysis of overlap percentage between images.

QGROUNDCONTROL

QGroundControl is an open-source "app" (application for mobile device) developed by a community of volunteers to configure and fly an autopilot based on the open source flight control software PX4. It is cross platform and supports all major operating systems:

- Mobile: Android and iOS (currently focused on tablet).
- Desktop: Windows, Linux, Mac OS.

It allows the planning of flights both for video documentation and photogrammetric surveys with waypoints navigation, as shown in Figure 5-2. This planning tool doesn't take into account the ground altitude variation and works considering the ground at a constant altitude. Furthermore, it is not able to provide the calculation of the expected precisions.

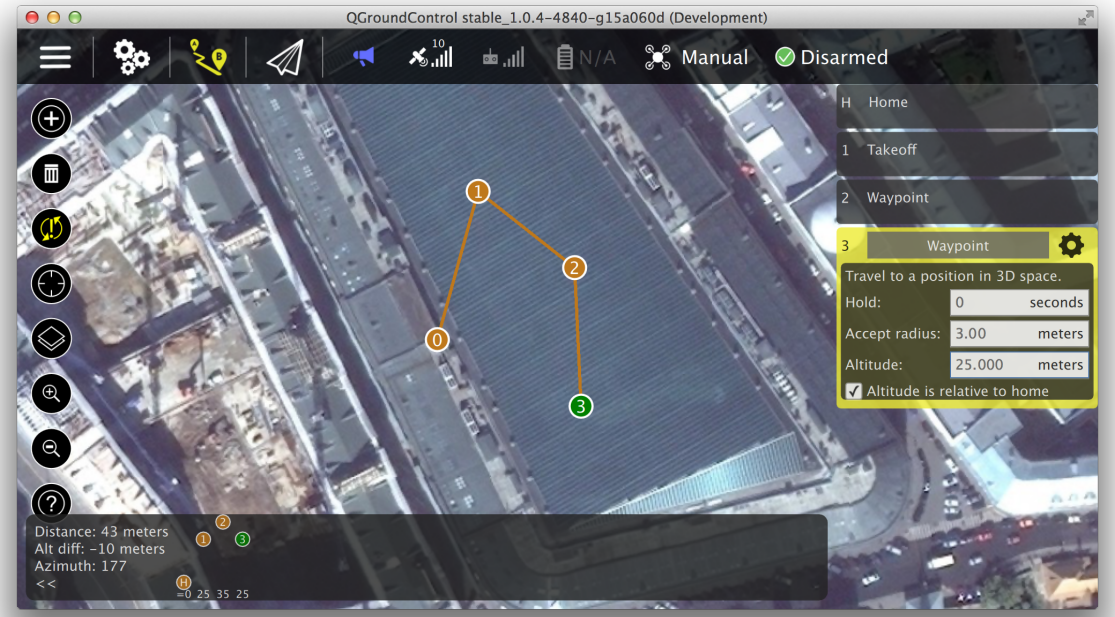

Figure 5-2 The planning tool of QGroundControl sw

However, it allows the management of flights and the real-time analysis of the telemetry that the vehicle transmits to the ground. As it is compatible with several platforms (IOS and Android), it can be installed on tablet and easily used on-site (Figure 5-3).

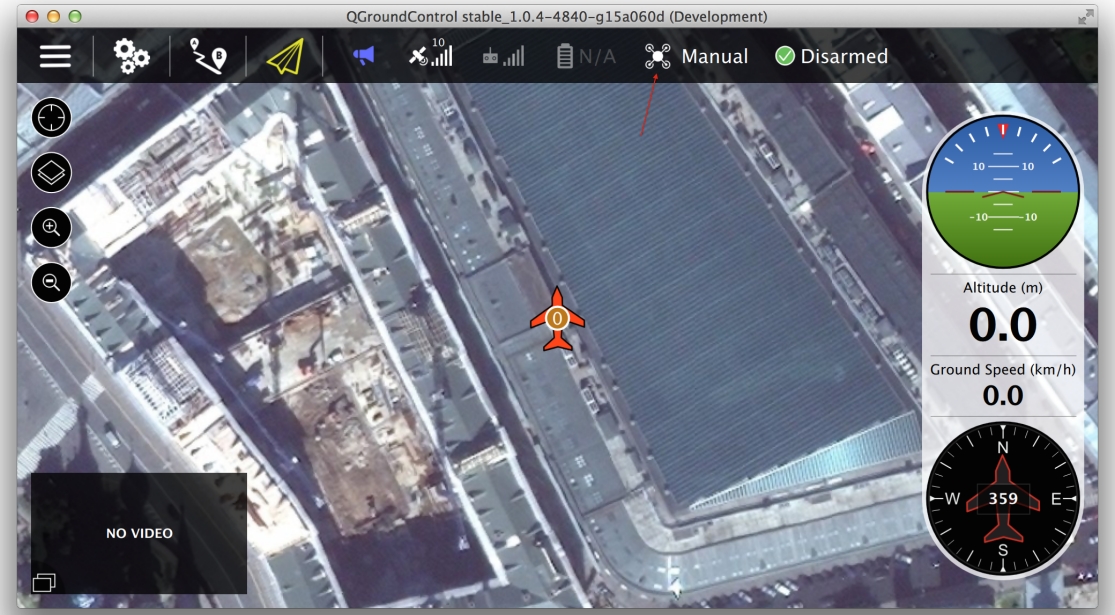

Figure 5-3 The navigation tool of QGroundControl sw

UgCS

The UgCS (Universal ground Control Software) is a software for central management of unmanned vehicles. It is a commercial software developed by SPH Engineering (Latvia) and requires the purchase of a user license. This software enables to control one or a fleet of drones on a single mission in multi-operator mode and multi-platform environments. The modular architecture of UgCS allows the integration and the addition of support for new vehicles or payloads. UgCS offers tools to make aerial surveys and mapping and gives the user the possibility to choose one of the pre-installed cameras pre-sets or to create a new one. The Area Scan and Photogrammetry tools can automatically calculate the flight path based on the camera settings. Alternatively, the Area Scan and Photogrammetry parameters can be manually adjusted, such as GSD, overlap or desired altitude. UgCS enables mission planning in "Terrain-following mode", as shown in Figure 5-4, i.e. this tool permits to automatically maintain a constant altitude above ground level.

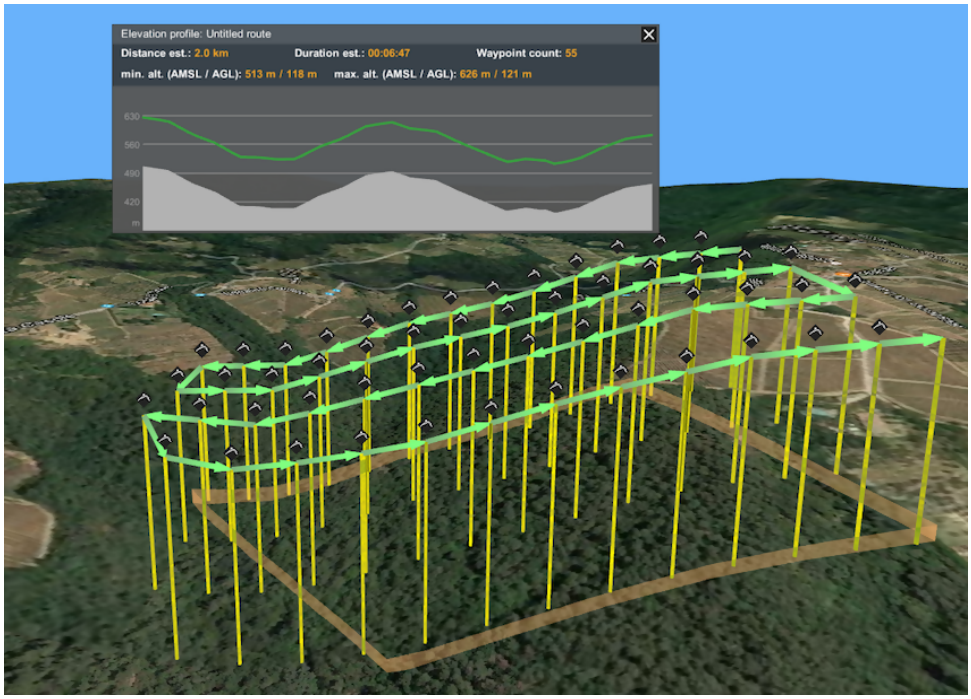

Figure 5-4 Photogrammetric flight path with Terrain-following mode

The accuracy of the default DTM SRTM (Shuttle Radar Topography Mission) by NASA database of UgCS is variable, therefore user supplied DTM data have to be imported in the survey area in order to get a precise and safe flight altitude. Through this tool it is possible to correctly calculate the achievable GSD and to keep it constant over the whole area of interest. However, also this software doesn't allows the calculation of the expected precisions for a survey.

PIX4DCAPTURE

A free application for flight planning and image acquisition from the drone with integration to the Pix4D photogrammetric processing software. Pix4Dcapture is developed by Pix4D and is available on Android and iOS. This "app" enables different imaging geometry (nadiral, nadiral sloped, circular, free flight). Pix4Dcapture supports drones from DJI, Parrot, and Yuneec, three of the biggest drone manufacturers on

the market. As shown in Figure 5-5, Pix4Dcapture allows the estimation of the expected precision of the survey on the base of the achievable GSD, but it doesn't allow the use of DTM and always considers the terrain to be flat.

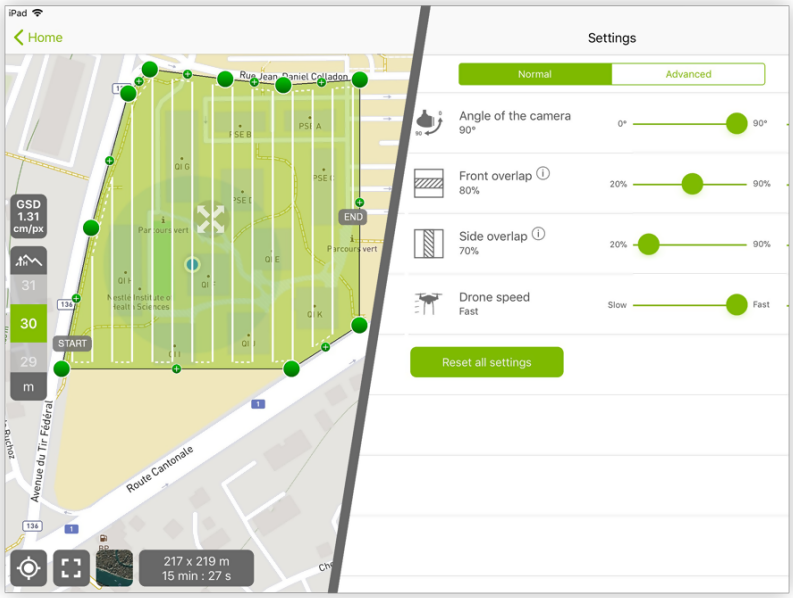

Figure 5-5 Photogrammetric flight plan in Pix4Dcapture

Pix4Dcapture is probably the most widely used application as GCS for UAV photogrammetric surveys.

DJI GO AND DJI GS PRO

DJI GO and DJ GS pro are software distributed by DJI, a Chinese company now the undisputed market leader. DJI GO is a software to plan recognition missions and video documentations, while DJ GS pro is the software to use as GCS for photogrammetric surveys. DJI GO is available multi-platform (Android and IOS), while DJI GS pro is available for IOS only. It allows the planning of photogrammetric missions defining the overlap parameters and taking into consideration the dimension of GSD, as Figure 5-6 shows.

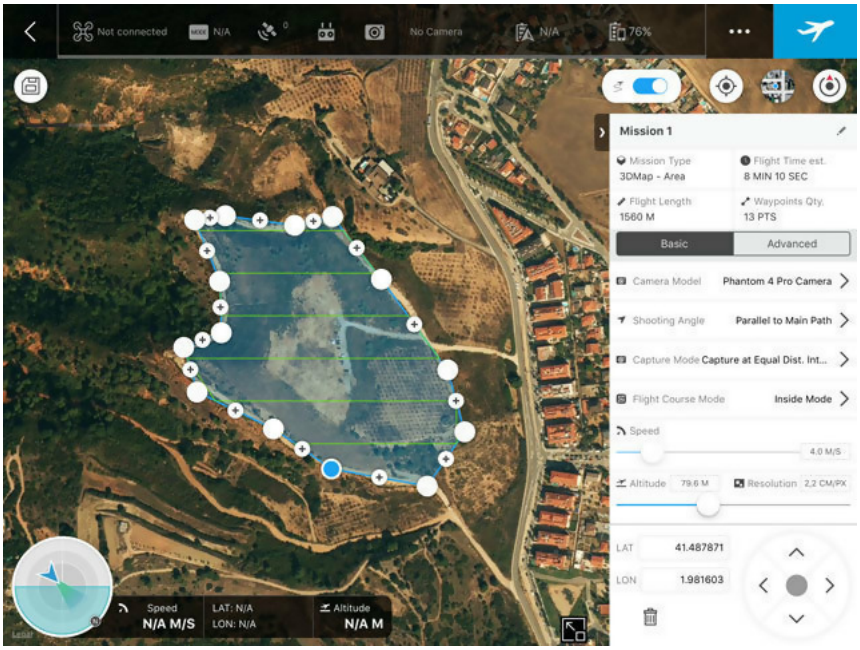

Figure 5-6 Photogrammetric flight plan in DJI GS pro

This software enables different imaging geometry (nadiral, nadiral sloped, circular, free flight) and permits to consider the morphology of the land with the use of a DTM internally accessed by the software, for which no metadata or accuracy figures are provided. Finally, it doesn't estimate the expected precision and its use is "limited" to the drones produced by DJI.

5.2 The Aim of the U.Ph.O. Project

This brief overview on software packages available at the current time in which the work has been written as GCS is not exhaustive. However it is clear that the market is offering tools for the use of UAV which are easy-to-use and compatible with portable devices (tablet and smartphone). However, all available software underestimates the problem of the a-priori evaluation of reachable precisions, generally considering only the Ground Sample Distance. Sometimes the morphology of the territory is taken into account by means of DTM, but generally it is not possible to use one supplied by the users. Obstacles and occlusions that you can find during the survey, are never considered (as far as the author is aware).

This simplification can be still a valid option for a lot of applications related to documentation, rebuilding of virtual environment with recreational purposes, for visualization in the real-estate field and big video-inspections. However, in the case of metric surveys with a complex morphology, the metric issue and the right estimation of the reachable precisions are relevant aspects which cannot be ignored. We need only think of structure monitoring applications in the civil field, of architectonic documentation for cultural heritage, of territory surveys in morphologically complex environments (landslides in mountain regions, glaciers, etc.) and, finally, at the survey in urban areas, where buildings are elements of complexity and obstacle.

In all these cases the complexity of architecture, the protuberances of rock or buildings are obstacles that hide the view of a part of the scenario lowering the calculated redundancy, if these elements are not taken into account.

To this aim it has been planned a “container” of tools, which is able to plan a survey and to verify the data collected after a survey. The development of this “Office suite”, called U.Ph.O. (Unmanned Photogrammetric Office), is realized in Matlab environment by MathWorks®. The basic idea is providing flight planning tools considering the required metric precisions, giving a priori information about expected precisions, ground pixel dimensions (Ground Sample Distance, GSD) and number of observations (number of rays per object point). The developed suite has been structured into two modules: PLAN and ANALYSIS.

The PLAN module allows to design a flight plan with different cameras, providing not only standard solution, but also a forecast of the expected precisions, taking into account the imaging geometry, the effective cover of the images on the object surface and their overlap percentage in respect of threshold users customize, any obstructions due to the DTM supplied by users, the accuracy and position of the GCPs to be placed on the ground and the number of frames where the generic point appears.

The ANALYSIS module permits, given the approximate position of the projection centers, which are known thanks to telemetry or a first quick elaboration of images, to produce in a short time after a flight a compliance test of what was planned and expected with the same capabilities of the plan module.

Thanks to these tools the U.Ph.O. project is aimed to favor the planning of photogrammetric surveys by UAV, paying the maximum attention to the metric quality of results.

The inspiring principle of the project U.Ph.O. is providing the users with an easy-to-use device, with a simple graphic interface offering the same functionalities of a less user-friendly scientific software, which can be often used only by CLI (Command-line Interface) with rigid format of input and output data.

At the moment these tools are available in Matlab code only but, in the near future, they could be available as web services accessible to those people willing to plan survey in geomatic field. The following chapters will deal with tools and their functionalities in details.

5.3 The Planning Module

The planning module allows the planning of a photogrammetric survey by UAV; it outputs the flight parameters, which are essential to plan an autonomous mission for a navigation software. The knowledge of the attainable precisions over the object surface can be very useful to modify the initial survey design with particular attention in the respect of the metric quality.

According to chapter 4, it is well known and clear that further is the approach to the observed object, higher is the precision in photogrammetric surveys. However, an excessive approach to the object could cause collision dangers, increase the time needed for the survey, the consumption of batteries and the number of shot images to assure the exact covering. All these aspects make the process of photogrammetric elaboration of the same images much more onerous.

In fact, it is important to know that a tool to obtain a realistic planning for UAV photogrammetric survey could be particularly useful where it is important evaluate the correct equilibrium between the expected

accuracy and the distance from the object to navigate in safety and in efficiency. Several are the occasions where the geomatics surveyor and the UAV pilot have to evaluate this crucial point. The U.Ph.O tools may contribute in this direction.

The workflow in Figure 5-7 shows the processes leading the planning/of the survey.

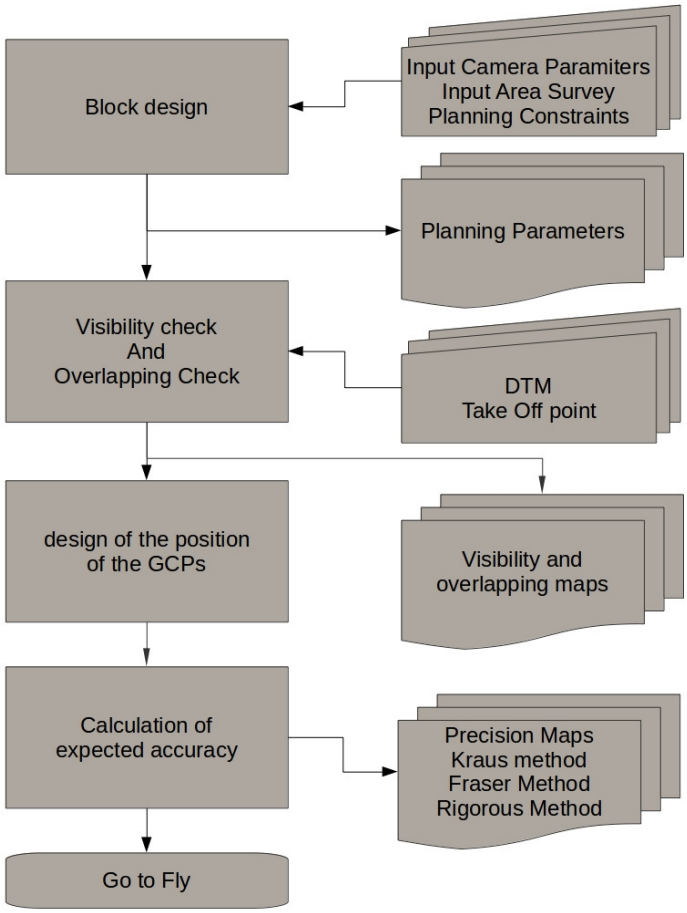

Figure 5-7 Workflow of U.Ph.O. planning module

At the beginning the module requires a “classical” design of the photogrammetric survey. The parameters of internal orientation of the camera are requested as input data (principal point PP, focal distance c and sensor format size). Then, through the graphic interface the user has the possibility to identify directly on the map the area of interest, establishing the limit with a generic polygon. The tool allows different imaging geometries for the planning and the choice of the direction of strips.

Once set up the limits of the project: type of camera used Internal Orientation (IO), overlap (longitudinal and transversal), flight altitude (the flight is planned with a reference plane and the strips are designed at constant altitude); the choice of these aspects is usual in most planning software, because it is the most conservative one for the consumption of batteries and, therefore, for the security of the flight.

In this way all the projection centers positions and attitudes are defined for all the images planned in the survey. The figure 5-8 shows an example of it.

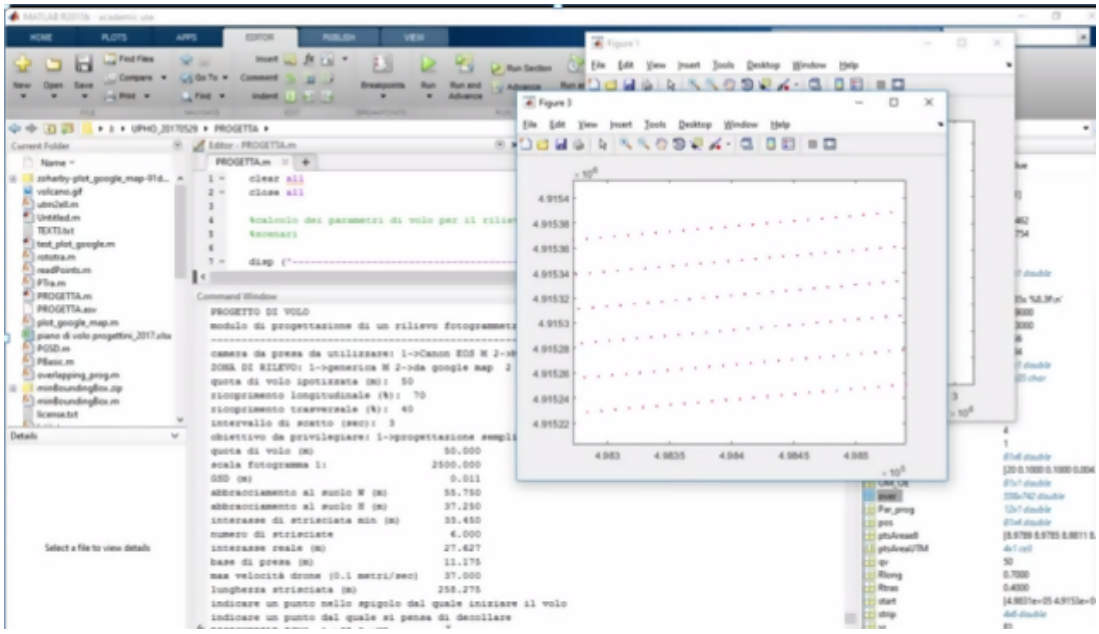

Figure 5-8 interface of the tool that reports the estimated flight parameters

To better describe the functionalities of the tool, it is here presented the planning of a flight on a semi-flat area surrounded by buildings with a height of about 10 meters on the north and by breakwater barriers on the south, with a significant change of its orography.

For this area a flight at altitude of 30 meters has been planned, with 70% longitudinal and 40% transversal coverings with the use of a not-metric camera Canon EOS M.

After defining the flight parameters, the tool proposes to control if these parameters will satisfy the precision requirements of the survey. To do this, the user needs to load a DTM. The presence of a DTM in the area is necessary, in order to be able to estimate the expected precisions. Actually, as a DTM describes the ground surface only, it would be better to have a DSM (Digital Surface Model), which describes the ground and all the obstacles due to anthropization and the vegetation present in the area.

As it will be widely explained in the next pages, this planning tool considers the effective visibility of the points. That's why it is better to use a DSM able to report also the objects that could obstruct the view in a photogrammetric flight, that is vegetation and buildings. The use of a DTM makes the analysis of the effective visibility less useful and incisive. The use of a DSM, on the contrary, allows to estimate the overlapping in a more realistic way and, therefore, to better estimate the expected precision.

In most cases in Italy, and in Europe in general, there are available DTM and/or DSM databases, which are almost adequately detailed for the planning (regions usually produce DTM with a grid resolution generally not bigger than 4 meters). For a lot of Italian and European territories LIDAR flights with enough density (more than one point per meter) to generate both DTM and DSM suitable to the planning with this

tool are also available. There is also another possibility to have a DSM available for this scope and it consists in performing an exploratory survey at much higher altitude before the official survey (to avoid obstacles, cover the territory with few images and speed the operations) and generate from this exploratory survey a DSM for the planning. Thanks to photogrammetry software implementing largely automated and efficient image orientation and surface reconstruction algorithms from Computer Vision, this operation can be performed also in the days or even hours preceding the survey.

Through the DSM every projection center acquires its altitude related to the ground, that is, the real distance of UAV from the ground at the moment of the photograph shot.

The grid resolution of the DSM will be the resolution used for all the following checks and for the maps of produced precisions. In fact, visibility, overlap (i.e. the number of frames where the generic point appears) and $\sigma_{x,y,z}$ are computed cell by cell starting from the DSM discretization at the original resolution of DSM.

Once imported the DSM, the tool makes firstly the check of visibility. This means that, from every expected projection center of the survey, it checks the DSM cells that can be seen and the cells that cannot be seen for the obstacle's presence. The development of such a procedure has been made through the evolution of the algorithm "*line of sight*", called "LOS2", present in the Matlab libraries. This algorithm has been planned to verify the visibility among selected points on ground (as shown in Figure 5-9).

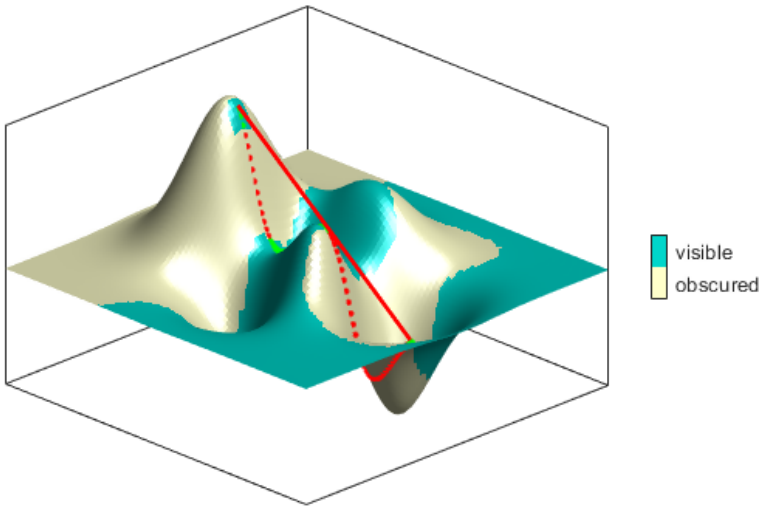

Figure 5-9 Line of sight algorithm

This algorithm has been modified to make it able to show the visible points from a flight over a reference surface. No commercial software performs this kind of control, but it is important to get an estimation of the number of rays per object point and of the real overlap between images and the adjacent strips (longitudinal and transversal overlaps respectively). Obviously in case of a survey of a wide territory without obstacles, this control is not so relevant, but in case of a survey of a mountain territory, a structure or an urban environment, its results may point out deficiencies of the initial plan and suggest changes. The

effects of the visibility control for a survey of a structure are shown in Figure 5-10, with three different visibility situations of the ground points (visible points are in yellow and the non-visible points are in blue) in response to the flight altitude changes.

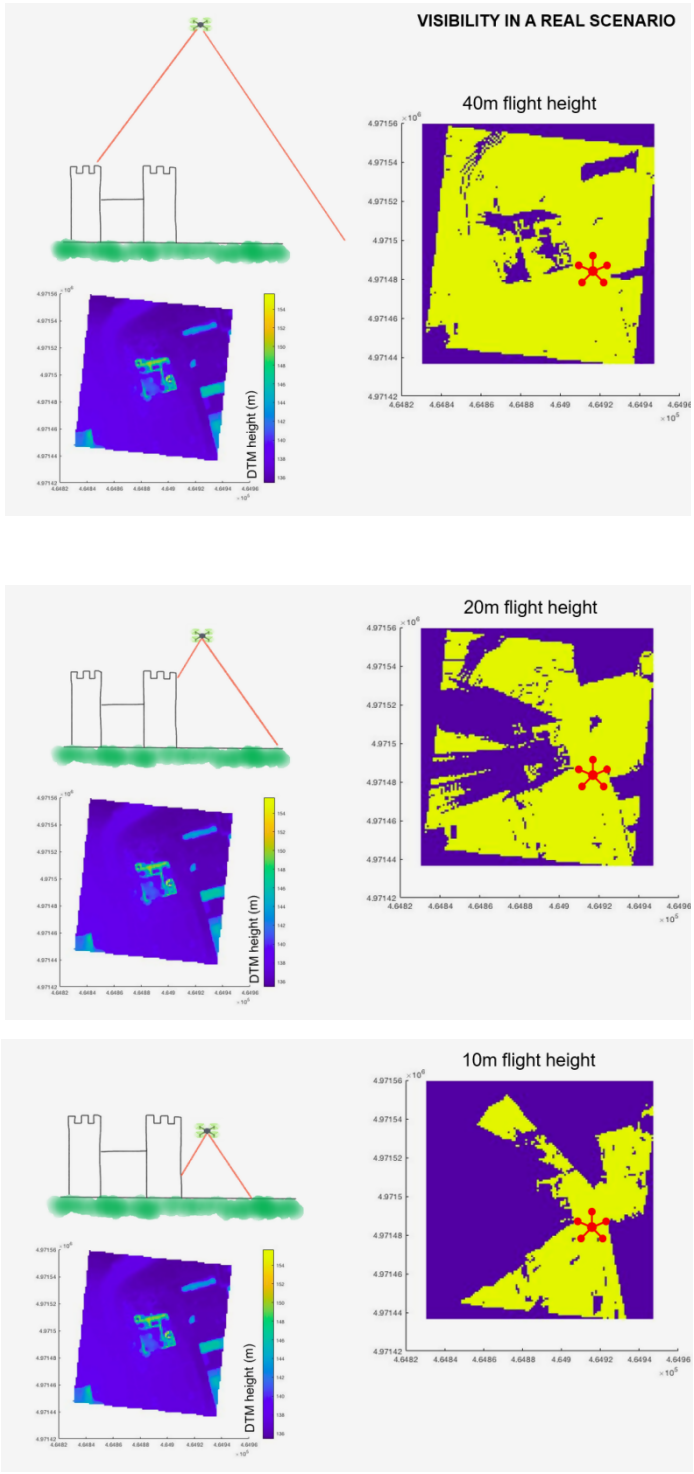

Figure 5-10 Visibility map changes as a function of camera height above ground

After the classification of ground in visible and occluded areas, the tool counts how many times a DSM cell appears on the images. To count how many images see a ground point, the collinearity principle is used. The collinearity equations back-project to the ground an image point, but they can be used in inverse way too. When the equation of the straight line connecting the object point with the projection center of an image is solved w.r.t. the image coordinates, we can observe if this straight line intersects the plane of the image within the limits of the sensor dimension (in this case the point is seen) or intersects outside it (in this case the point is not seen). Obviously, for this operation the analysis of visibility, previously described, will be taken into account. At the end of this processthe produced map (called the overlap map in the following) is exported in GeoTiff format, which is easily readable by Geographic Information System (GIS) software, and a preview of the same image is displayed on the screen. An example of this image is shown in Figure 5-11. The overlap percentages of every couple of photos and of the adjacent strips, instead, are saved in a text format file in order to be imported in table format on a spreadsheet.

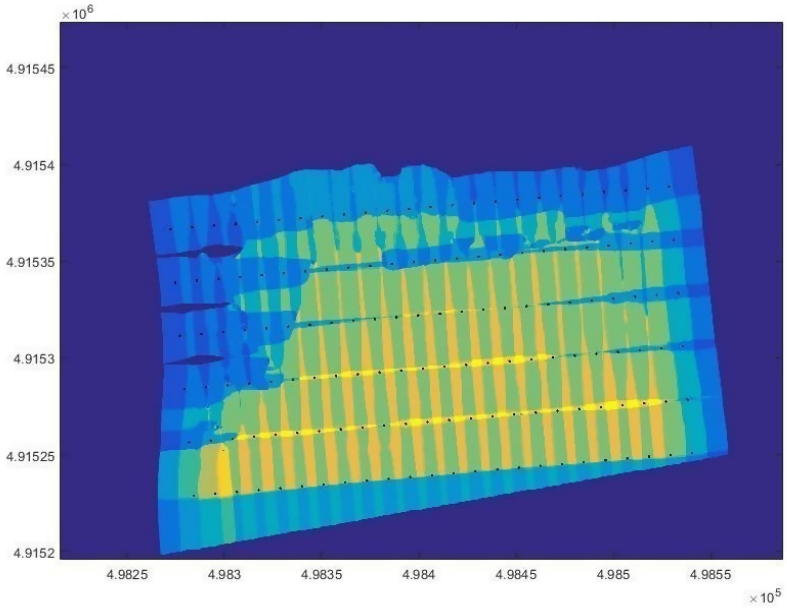

Figure 5-11 Overlap map and terrain expected coverage

These elements are all the information needed for the calculation of expected precisions according both to Kraus' and Fraser's methods (see paragraphs 4.2.1 and 4.2.2). Therefore, for every DSM cell the expected precision is calculated according to Kraus formula. The map of precisions is displayed on the screen and exported in GeoTiff format. The same procedure applies to Fraser's method, however in this case, the appropriate value of the form factor "q" must be specified. In this case a value equal to 3.5 has been assigned to "q", as suggested by Fraser for surveys with nadiral shot geometry. For the estimate of precisions through the rigorous method, it is necessary to previously identify the number and the position of GCPs that will be materialized and measured on the ground at the moment of the flight. This operation is made through an interface with the direct indication of the position of the project GCPs on the DEM. A precision of 3 cm is attributed to the measurement of GCPs on the ground supposing a survey with GPS instruments in RTK mode, but this precision can be modified in case of more or less precise surveys on the ground. The precision of the measurements on the images ($\sigma_{p\xi}$) is fixed equal to half pixel. All of this information, as already explained in chapter 4.2.3, are able to define the limits of the system.

The Figure 5-12 shows a comparison between the three precision maps exported, which have been estimated in a case of nadiral planning on a plane territory of Vernazzola beach in Genoa (Italy), which has been previously described. The general view of the three results shows how the formula proposed by the classical aerial photogrammetry is affected by the flight altitude and the orography of the territory, while the formula suggested by Fraser depends mainly on how many times the ground point is seen on photograms. However, it is clear that these two approaches are based only on a propagation of the variance of measurement precision on the images of the object points. The rigorous method, instead, takes into account the whole uncertainty of the compensation of the photogrammetric block that is concentrated on EO parameters and allows the test of solidity and correctness of the geometry of planned GCPs.

DEM of the test area

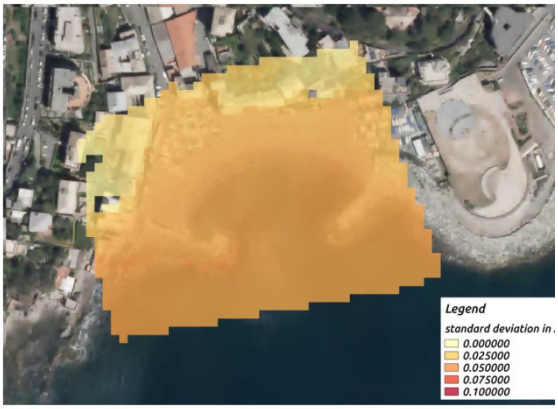

Map of standard deviations along Z computed with Kraus approach

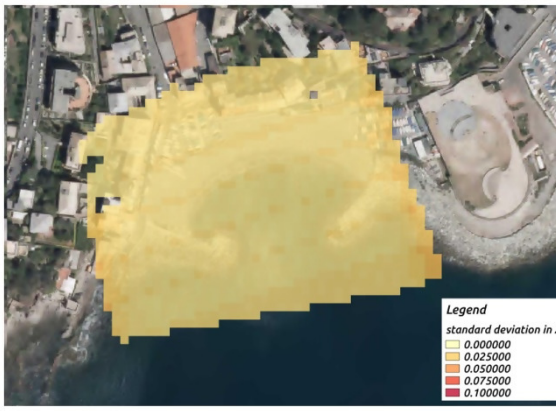

Map of standard deviations along Z computed with Fraser approach

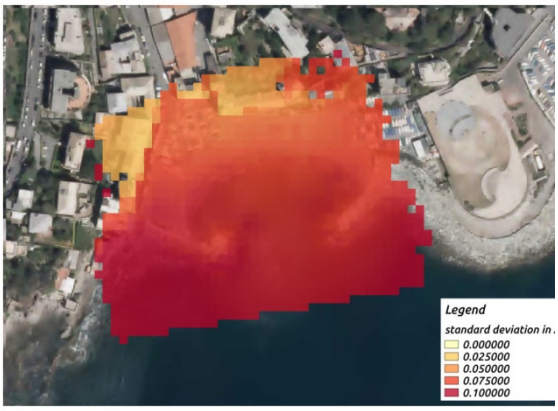

Map of standard deviations along Z computed with rigorous approach

Figure 5-12 Maps of DEM and standard deviations along Z computed with different approaches [m]

This procedure has to be meant as an iterative one. In fact, if the expected precisions are not sufficient anywhere or the overlap is not satisfying or some points cannot be observed due to the obstructions, it is possible to modify the planning parameters (flight altitude, overlap percentage, number and position of GCPs) and to process the whole project again. It should be also considered that the performance of the flight can not exactly coincide with what has been planned, for example, because of winds, that make the

layout variable and not perfectly nadiral. A possible future development in this field could be the introduction of accidental mistakes, generated through the MonteCarlo method, to compromise EO parameters, as suggested by the works of Santise and Robson (2015).

5.4 The Analysis Module

U.Ph.O. has also a module for the analysis of an already performed flight. It often happens that a flight hasn't exactly followed the project indications because of environmental conditions (for example a strong wind) or instrumental errors of the navigation system (for example a wrong positioning of GNSS on board). To know if these aspects have compromised the reachable precisions or the visibility of all points on ground, it is necessary to quickly analyze the data, before their long photogrammetric elaboration. The tool has been designed to be used directly on site just after the landing of UAV, to have the possibility to repeat the survey, if needed. As shown in the workflow of Figure 5-13, the structure of the analysis tool is very similar to that of the design tool, but its philosophy of use is rather different.

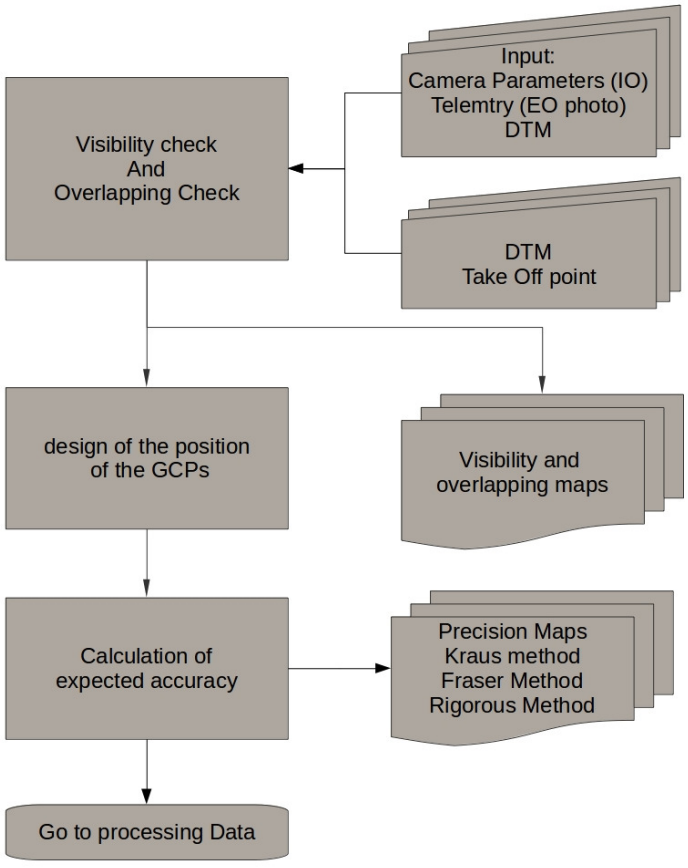

Figure 5-13 Workflow of the U.Ph.O. module of analysis

In fact, the project parameters are not estimated but acquired from the telemetry of UAV or from the position data saved in the images (Geotag written in the EXIF).

The calculation of precision maps through the stereo normal case (Krauss) and Fraser's formulas could appear as simple theoretical exercises, but they actually represent whatever a validation tool of what has been shown by the precision estimation with the rigorous method. Although these estimation methods do not consider all possible variables and only give an estimate of the precision of restitution, they provide values of orders of magnitude comparable to the accuracies estimated with the rigorous method.

6. APPLICATION TO A CASE STUDY AND VALIDATION

In this chapter we want to test the functionality of the planning and analysis tools with the application to real and illustrative case studies. We will present some examples of typical applications, that a generic user willing to plan and analyze photogrammetric flight by UAV can normally face.

The case study of Belvedere Glacier in Piedmont (Italy) is suitable to the planning and the comparison among different scenarios of the project. The case study of the Castle of Casalbagliano in Alessandria (Italy) presented in this chapter will encompass the analysis of the UAV photogrammetric block. An independent check will be provided through the comparison between the results achieved with a survey in loco and completed with a scientific software.

6.1 Case Study "Belvedere Glacier"

The Belvedere Glacier (shown in Figure 6-1) is an alpine glacier located in the territory of Macugnaga (Piedmont, Italy). The glacier arises on the east side of Monte Rosa and pushes toward north till a quote of about 1800 m. It is one of the few alpine glaciers moving forward and this phenomenon is supposed to be caused by the rise of ice temperature in the upper areas of the East side. That's why the Belvedere Glacier is of great scientific interest and it is monitored with seasonal surveys. The ending part of the glacier is characterized by a moving orography, but not by great declivities and presents steep moraines on both sides. All these features make of it a perfect zone to test the planning tool. The selected area has therefore an extension of 400 m x 400 m and is located in the central part of the ending strip.

Figure 6-1 the Belvedere Glacier

6.2 Planning of the Survey for the Case Study

The planning of the survey of the test area should guarantee that: every ground point is seen at least three times; the expected precision should be always better than 5 cm

We proceed selecting the area to be detected. Varying the overlapping and flight altitude parameters, with the selected camera (Canon EOS M) and its objective (principal distance 22mm), it is possible to suppose different scenarios till the achievement of the best result.

According to the scheme presented in paragraph 5.3, we start with the manual selection of the survey area using an orthophoto provided by Web Map Service (WMS) as background map, as shown in Figure 6-2:

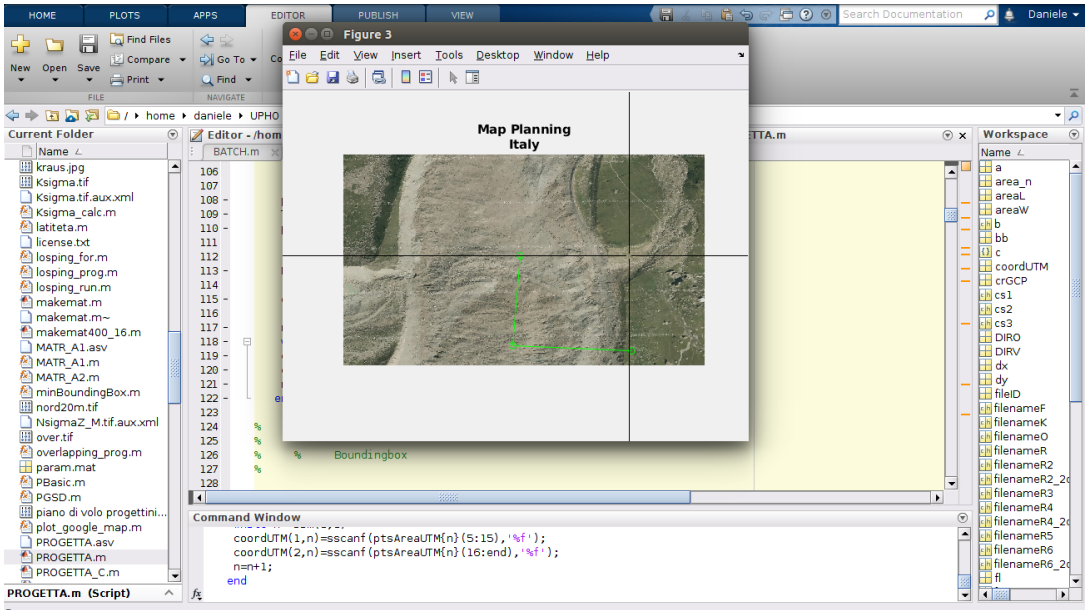

Figure 6-2 Selection of the survey area

Considering the related restrictions to the planning:

The initial project parameters:

- Flight altitude (m): 150 (above ground)
- Longitudinal overlapping (%): 60
- Lateral overlapping (%): 30

and defining the direction of the strips, we obtain the first planning parameters:

Scale frame 1:	7500
GSD (m)	0.032
Ground projection W (m)	167.25
Ground projection H (m)	111.75
Distance between flight lines (m)	94.31
Number of strips	4
Base length (m)	44.70
Strip length (m)	401

and the position of the planned projection centres both in numerical way and graphically (as shown in Figure 6-3).

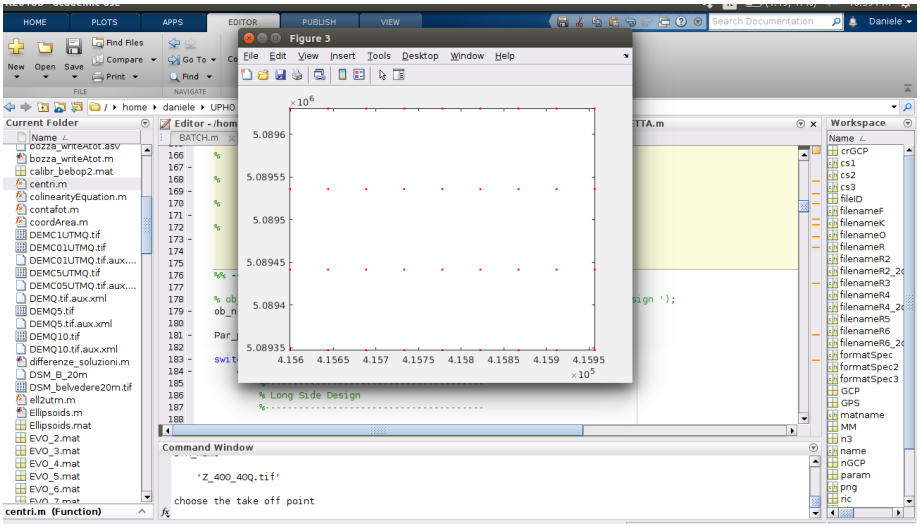

Figure 6-3 Calculated projection centers

Terminated the design of the strips, it is possible to start with the check process, that dictates the use of a DSM provided by the user to validate the estimated parameters, to prove that the project parameters are verified and to make an estimate the reachable precisions.

In this case study we have used a DSM with a resolution of 40 meters coming from a previous survey of the same portion of the Glacier performed one year before.

The visibility analysis and the image overlap on the ground are shown in the map of Figure 6-4, where the number of frames imaging that DSM pixel is shown. In this case the image overlapping is up to 8 frames for points in the inner part of the area, while it is evident that along the borders there are few images and less still in the corners. The presence of rocks and depressions makes the visibility map uneven.

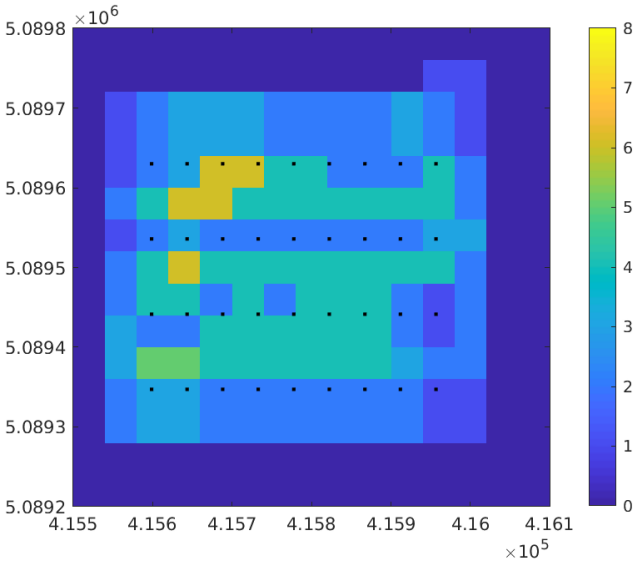

Figure 6-4 Map of visibility and overlapping
(Est and North coordinate in UTM/ETRF2000-2008.0 in meters)

To complete this group of information, the tool writes all the overlapping values on file (in percentage) between consecutive images and also between adjacent strips. Thanks to these data the user can easily create statistics and verify that all territory portions appear in the required number of frames.

Finally, through the methodology presented in chapter 5, the maps of the expected precisions are generated. The most reliable map is the one calculated with the rigorous method.

For this flight it has been planned the materialization of 16 support points situated on the ground according to a regular scheme, as shown in Figure 6-5.

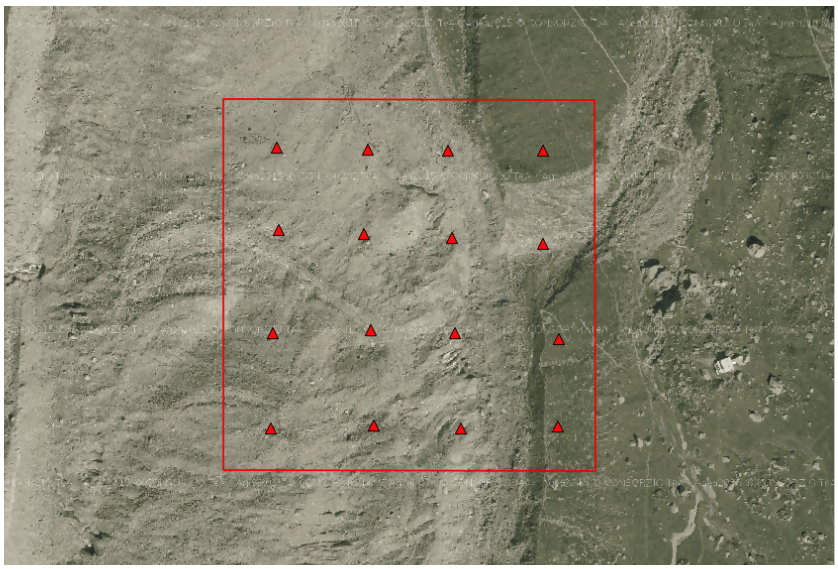

Figure 6-5 Designed GCPs

It is supposed that the positions of the projection centers are known with metric precision (coordinates of the projection centers registered with GPS code solution). Given these flight parameters and the so planned support points, we get the estimates of expected precisions shown in Figure 6-6, where the black points represent the positions of the projection centers and the chromatic scale represents the values of σ_x, σ_y and σ_z.

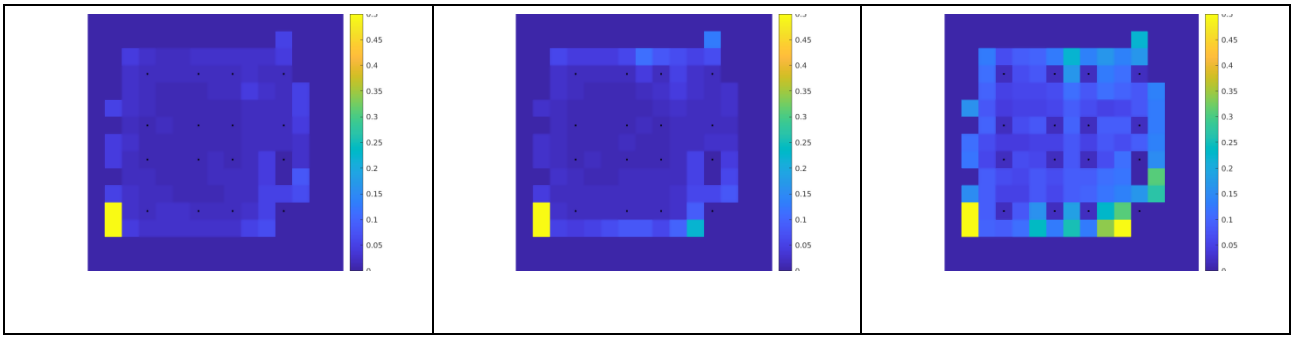

Figure 6-6 Map of the expected precisions [m] for the x-coordinate (figure on the left), for the y-coordinate (figure in the center) and for the z-coordinate (figure on the right) calculated using the rigorous method

One wonders whether with the diminution of the number of support points, to avoid to walk on dangerous zones of the glacier, it is possible to keep the expected precisions through the increase of the project coverings. A possible alternative to make the photogrammetric block more rigid with the reduction of support points could be the use of a more precise on-board GPS, able to register the position of the projection centers with a centimetric precision (3 cm per GPS RTK solution). Limiting the position of the projection centers it is possible to reduce the number of support points, as proved by several publications, like Pinto et al. (2002) or Heipke et al. (2002).

The suggested tool allows to plan a flight varying the overlapping, the position and the number of GCPs and the precision of EO parameters. Taking advantage of this flexibility in this case study, different combinations of parameters are tested, in order to observe their effects on the planning parameters. Some solutions with varying overlapping and a variable number of GCPs are supposed. The variation of GCPs goes maximum to 16 with regular spacing, 4 rows made up of 4 points at the same spacing, with the result of a GCP every 3 photograms in the case of a minimum overlapping 60/30 until a GCP every 5 photograms in the maximum overlapping of 80/80. Finally, it is considered the possibility to know EO parameters with metric precision (10 m with GPS code solution) or centimetric precision (3 cm with GPS RTK solution).

For each combination of “overlapping – number of GCPs – EO precision” shown in Table 6-1, we will present the final results of the related flight plannings.

Table 6-1 Analyzed Combinations

OVERLAPPING	NUMBER OF GCPs	PRECISION OF THE POSITION OF THE PROJECTION CENTERS
60% longitudinal and 30% lateral	16	Known projection centers with metric accuracy
60% longitudinal and 30% lateral	16	Known projection centers with centimetric accuracy
60% longitudinal and 30% lateral	8	Known projection centers with metric accuracy
60% longitudinal and 30% lateral	8	Known projection centers with centimetric accuracy
60% longitudinal and 30% lateral	4	Known projection centers with metric accuracy
60% longitudinal and 30% lateral	4	Known projection centers with centimetric accuracy
60% longitudinal and 60% lateral	16	Known projection centers with metric accuracy
60% longitudinal and 60% lateral	16	Known projection centers with centimetric accuracy
60% longitudinal and 60% lateral	8	Known projection centers with metric accuracy
60% longitudinal and 60% lateral	8	Known projection centers with centimetric accuracy
60% longitudinal and 60% lateral	4	Known projection centers with metric accuracy
60% longitudinal and 60% lateral	4	Known projection centers with centimetric accuracy
80% longitudinal and 60% lateral	16	Known projection centers with metric accuracy
80% longitudinal and 60% lateral	16	Known projection centers with centimetric accuracy
80% longitudinal and 60% lateral	8	Known projection centers with metric accuracy
80% longitudinal and 60% lateral	8	Known projection centers with centimetric accuracy
80% longitudinal and 60% lateral	4	Known projection centers with metric accuracy

80% longitudinal and 60% lateral	4	Known projection centers with centimetric accuracy
80% longitudinal and 80% lateral	16	Known projection centers with metric accuracy
80% longitudinal and 80% lateral	16	Known projection centers with centimetric accuracy
80% longitudinal and 80% lateral	8	Known projection centers with metric accuracy
80% longitudinal and 80% lateral	8	Known projection centers with centimetric accuracy
80% longitudinal and 80% lateral	4	Known projection centers with metric accuracy
80% longitudinal and 80% lateral	4	Known projection centers with centimetric accuracy

For each one of these combinations it has been evaluated the number of photograms observing the single ground points, defined with regular spacing of 40 m in X and Y. The visibility of the generic point by the photograms is appraised taking into consideration the possible obstructions; that's why it is said "realistic". For each point the standard deviations of the positions on the ground for each one of the three components (X, Y, Z) have been observed through the rigorous method treated in this work. The results are shown in the following Figures, from 6-7 to 6-18.

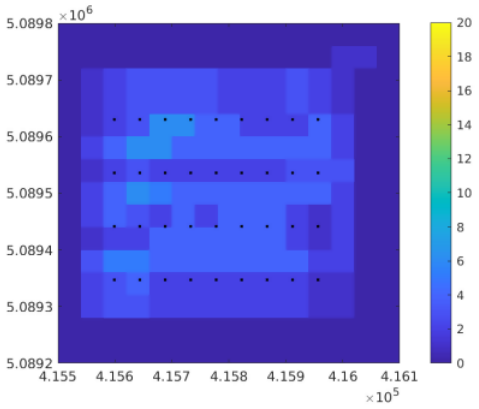		Cases with longitudinal overlapping equal to 60% and transversal overlapping equal to 30% (the real overlapping taking into account the DTM and obstructions is shown in the figure on the left), but with different configurations of GCPs and different precision of the positions of the projection centers.
	Known projection centers with metric accuracy	Known projection centers with centimetric accuracy
16 GCPs	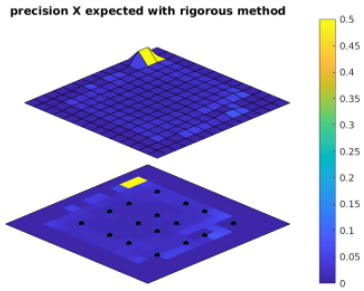	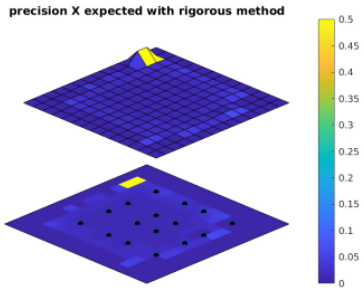
8 GCPs	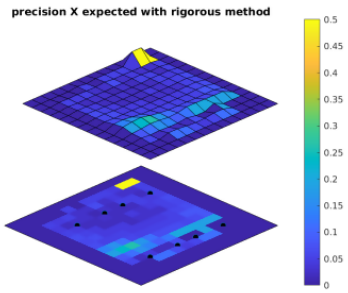	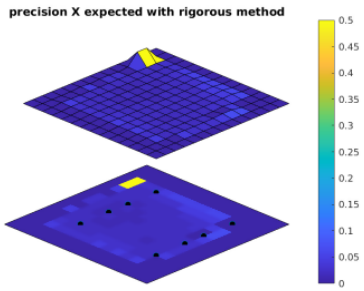
4 GCPs	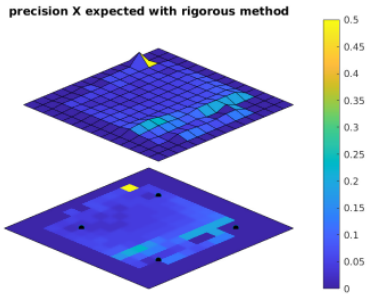	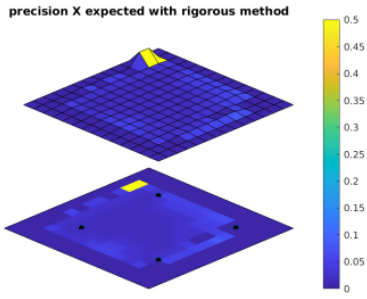

Figure 6-7 Precision X expected with rigorous method and overlapping 60%-30%: 2D and 3D representations with GCPs in different configurations - scale bar from 0m to 0.5m

<table>
<tr><td> 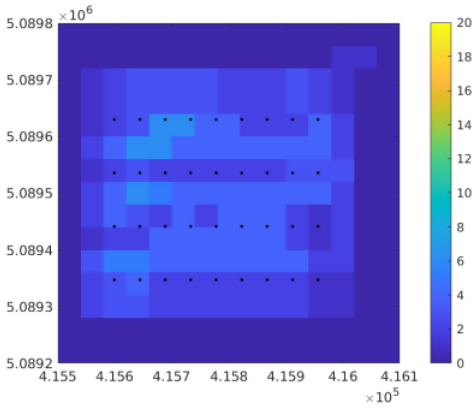
</td><td colspan="2">Cases with longitudinal overlapping equal to 60% and transversal overlapping equal to 60% (the real overlapping taking into account the DTM and obstructions is shown in the figure on the left), but with different configurations of GCPs and different precision of the positions of the projection centers.</td></tr>
<tr><td></td><td>Known projection centers with metric accuracy</td><td>Known projection centers with centimetric accuracy</td></tr>
<tr><td>16 GCPs</td><td> 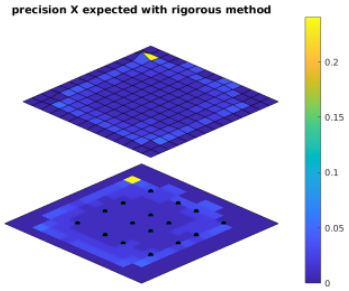
</td><td> 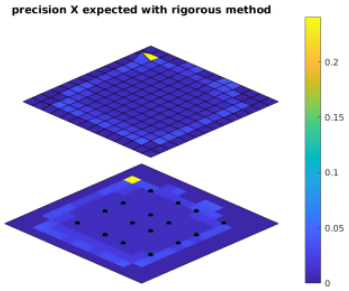
</td></tr>
<tr><td>8 GCPs</td><td> 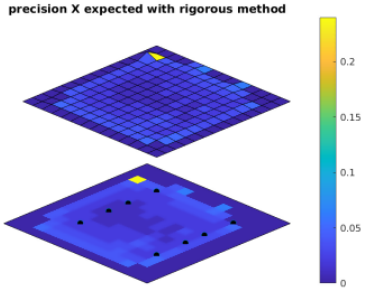
</td><td> 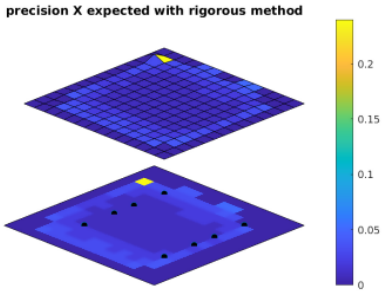
</td></tr>
<tr><td>4 GCPs</td><td> 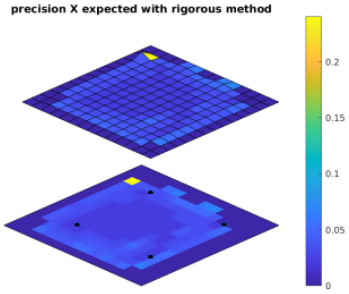
</td><td> 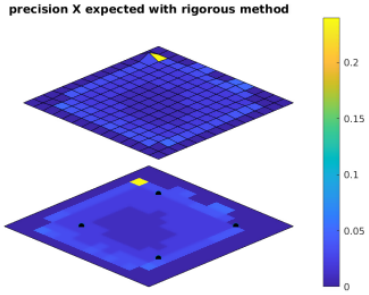
</td></tr>
</table>

Figure 6-8 Precision X expected with rigorous method and overlapping 60%-60%: 2D and 3D representations with GCPs in different configurations - scale bar from 0m to 0.25m

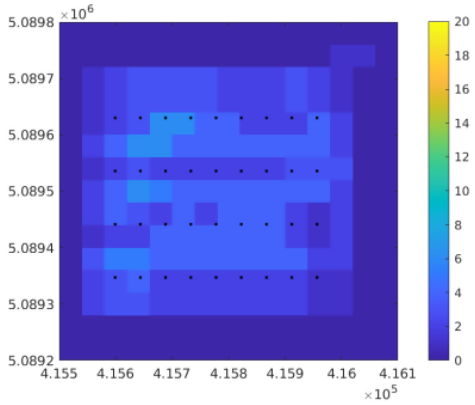		Cases with longitudinal overlapping equal to 80% and transversal overlapping equal to 60% (the real overlapping taking into account the DTM and obstructions is shown in the figure on the left), but with different configurations of GCPs and different precision of the positions of the projection centers.
	Known projection centers with metric accuracy	Known projection centers with centimetric accuracy
16 GCPs	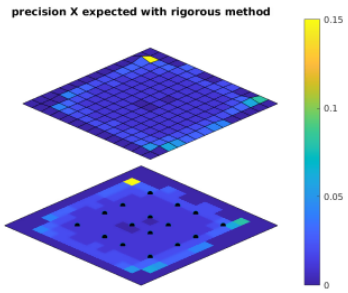	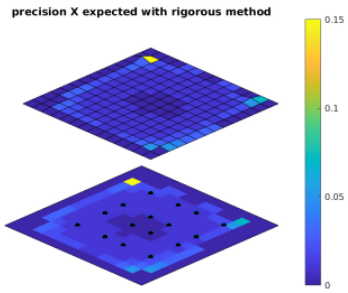
8 GCPs	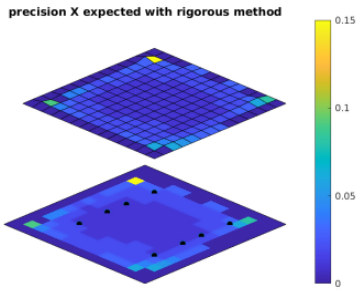	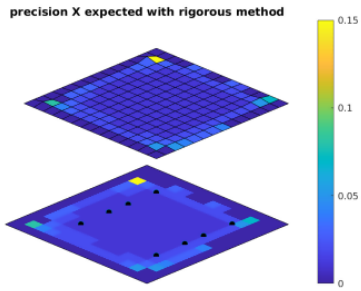
4 GCPs	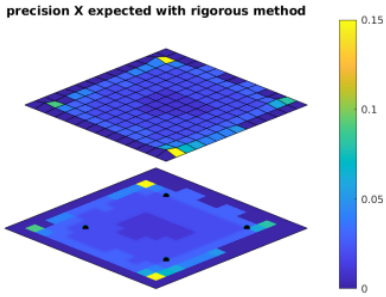	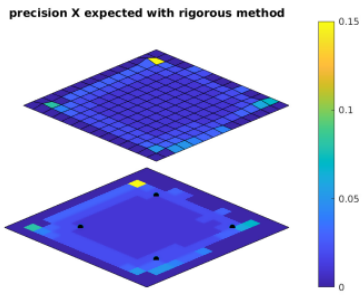

Figure 6-9 Precision X expected with rigorous method and overlapping 80%-60%: 2D and 3D representations with GCPs in different configurations - scale bar from 0m to 0.15m

<table>
<tr><td colspan="2"> 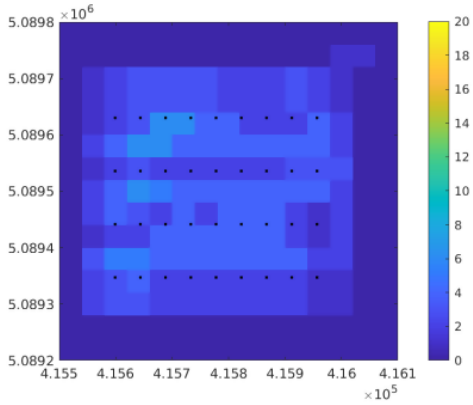
</td><td>Cases with longitudinal overlapping equal to 80% and transversal overlapping equal to 80% (the real overlapping taking into account the DTM and obstructions is shown in the figure on the left), but with different configurations of GCPs and different precision of the positions of the projection centers.</td></tr>
<tr><td></td><td>Known projection centers with metric accuracy</td><td>Known projection centers with centimetric accuracy</td></tr>
<tr><td>16 GCPs</td><td> 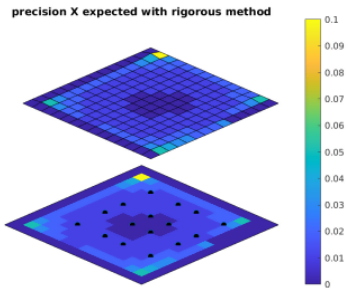
</td><td> 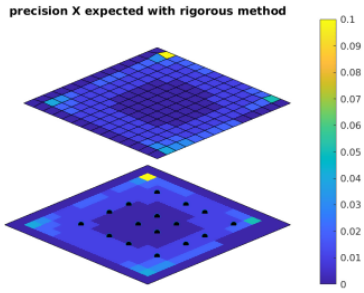
</td></tr>
<tr><td>8 GCPs</td><td> 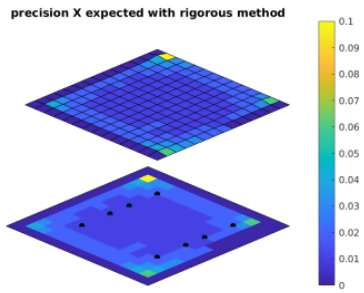
</td><td> 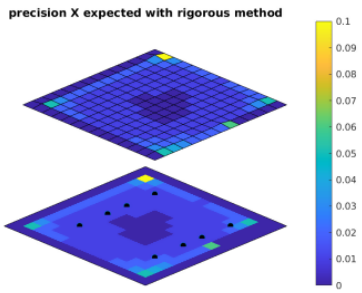
</td></tr>
<tr><td>4 GCPs</td><td> 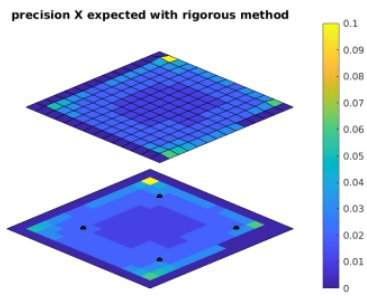
</td><td> 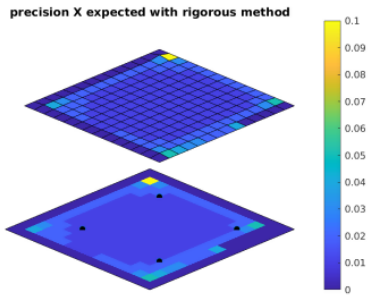
</td></tr>
</table>

Figure 6-10 Precision X expected with rigorous method and overlapping 80%-80%: 2D and 3D representations with GCPs in different configurations - scale bar from 0m to 0.10m

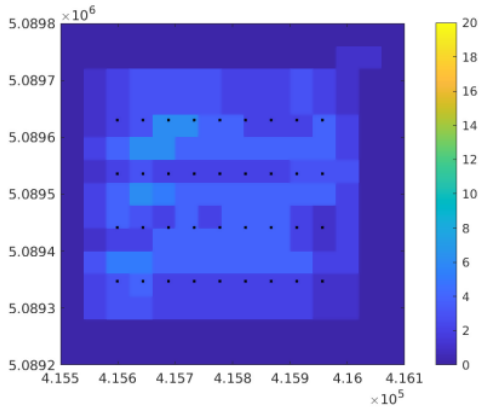		Cases with longitudinal overlapping equal to 60% and transversal overlapping equal to 30% (the real overlapping taking into account the DTM and obstructions is shown in the figure on the left), but with different configurations of GCPs and different precision of the positions of the projection centers.
	Known projection centers with metric accuracy	Known projection centers with centimetric accuracy
16 GCPs	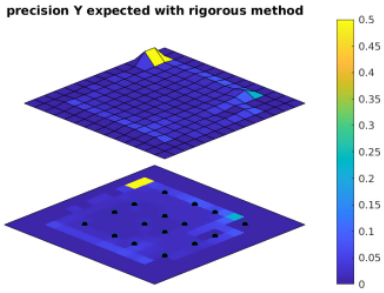	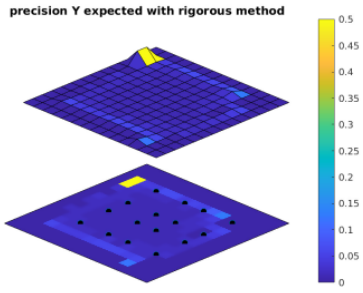
8 GCPs	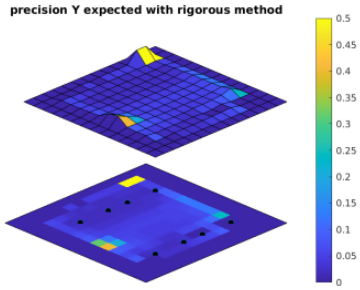	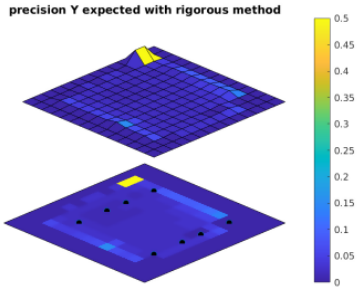
4 GCPs	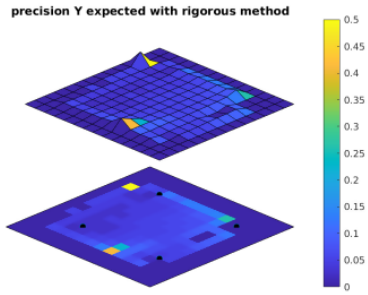	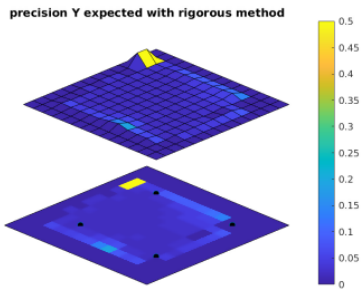

Figure 6-11 Precision Y expected with rigorous method and overlapping 60%-30%: 2D and 3D representations with GCPs in different configurations - scale bar from 0m to 0.5m

<table>
<tr><td colspan="2"> 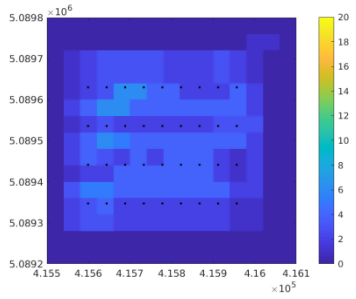
</td><td>Cases with longitudinal overlapping equal to 60% and transversal overlapping equal to 60% (the real overlapping taking into account the DTM and obstructions is shown in the figure on the left), but with different configurations of GCPs and different precision of the positions of the projection centers.</td></tr>
<tr><td></td><td>Known projection centers with metric accuracy</td><td>Known projection centers with centimetric accuracy</td></tr>
<tr><td>16 GCPs</td><td> 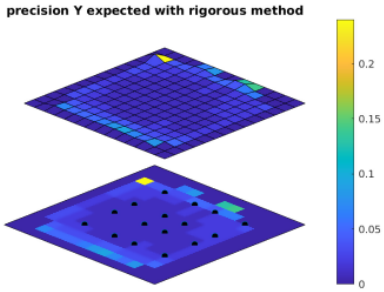
</td><td> 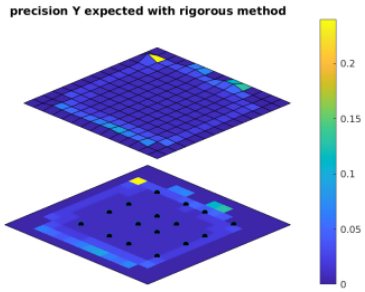
</td></tr>
<tr><td>8 GCPs</td><td> 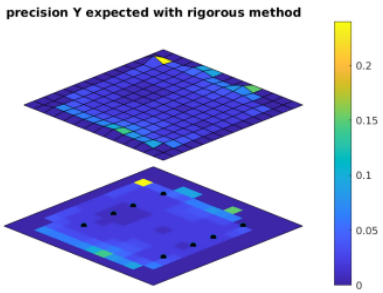
</td><td> 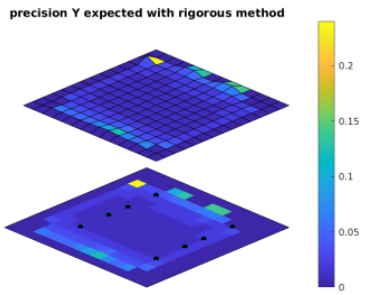
</td></tr>
<tr><td>4 GCPs</td><td> 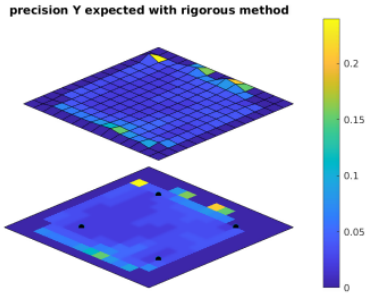
</td><td> 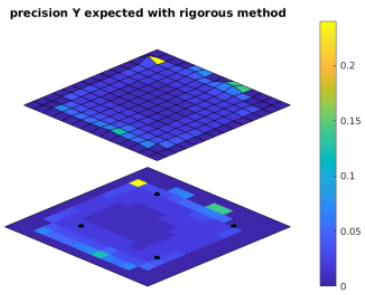
</td></tr>
</table>

Figure 6-12 Precision Y expected with rigorous method and overlapping 60%-60%: 2D and 3D representations with GCPs in different configurations - scale bar from 0m to 0.25m

<table>
<tr><td> 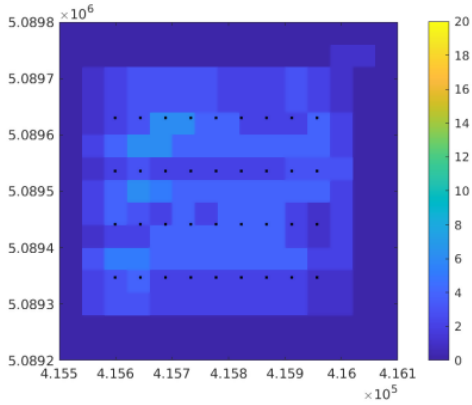
</td><td colspan="2">Cases with longitudinal overlapping equal to 80% and transversal overlapping equal to 60% (the real overlapping taking into account the DTM and obstructions is shown in the figure on the left), but with different configurations of GCPs and different precision of the positions of the projection centers.</td></tr>
<tr><td></td><td>Known projection centers with metric accuracy</td><td>Known projection centers with centimetric accuracy</td></tr>
<tr><td>16 GCPs</td><td> 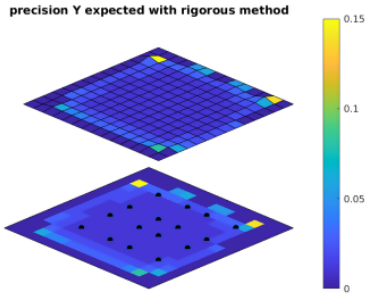
</td><td> 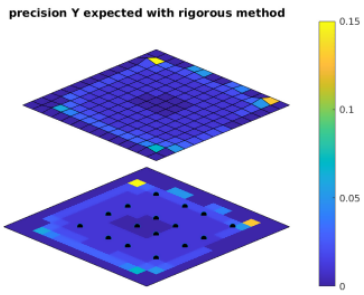
</td></tr>
<tr><td>8 GCPs</td><td> 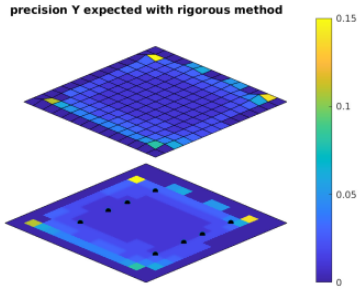
</td><td> 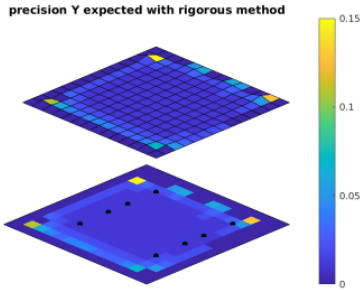
</td></tr>
<tr><td>4 GCPs</td><td> 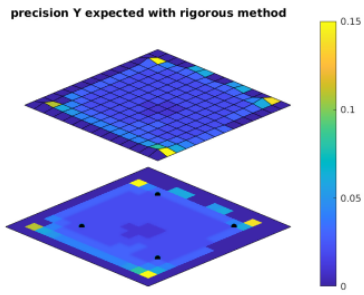
</td><td> 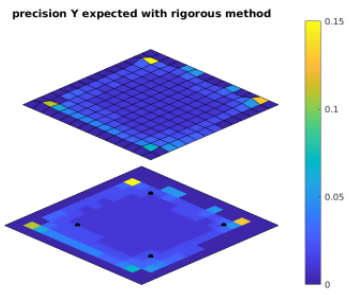
</td></tr>
</table>

Figure 6-13 Precision Y expected with rigorous method and overlapping 80%-60%: 2D and 3D representations with GCPs in different configurations - scale bar from 0m to 0.15m

<table>
<tr><td colspan="2"> 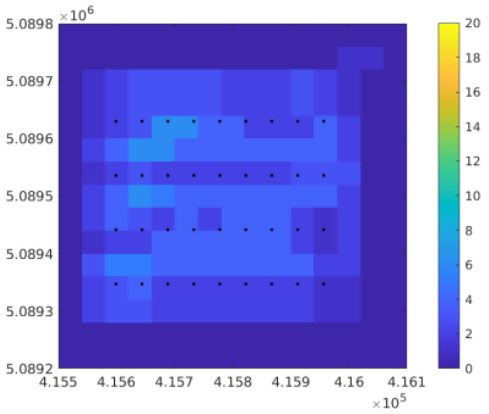
</td><td>Cases with longitudinal overlapping equal to 80% and transversal overlapping equal to 80% (the real overlapping taking into account the DTM and obstructions is shown in the figure on the left), but with different configurations of GCPs and different precision of the positions of the projection centers.</td></tr>
<tr><td></td><td>Known projection centers with metric accuracy</td><td>Known projection centers with centimetric accuracy</td></tr>
<tr><td>16 GCPs</td><td> 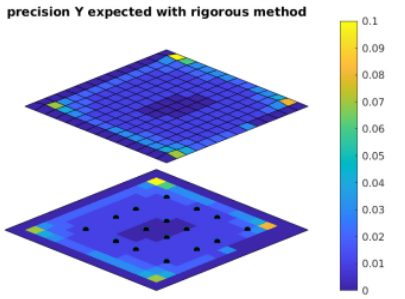
</td><td> 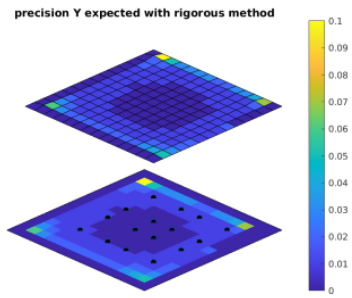
</td></tr>
<tr><td>8 GCPs</td><td> 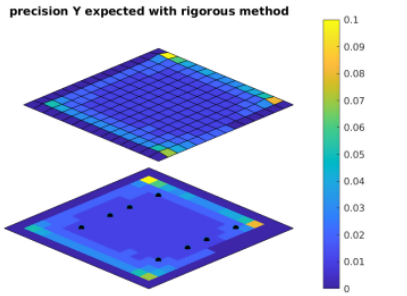
</td><td> 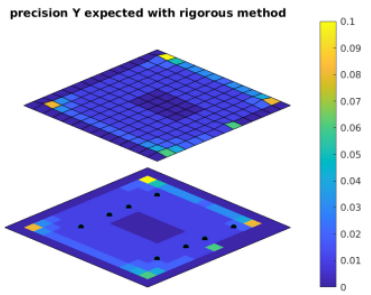
</td></tr>
<tr><td>4 GCPs</td><td> 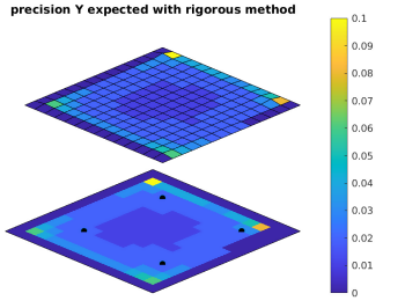
</td><td> 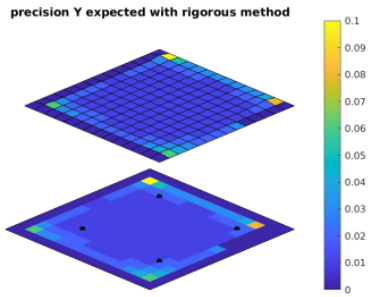
</td></tr>
</table>

Figure 6-14 Precision Y expected with rigorous method and overlapping 80%-80%: 2D and 3D representations with GCPs in different configurations - scale bar from 0m to 0.10m

<table>
<tr><td> 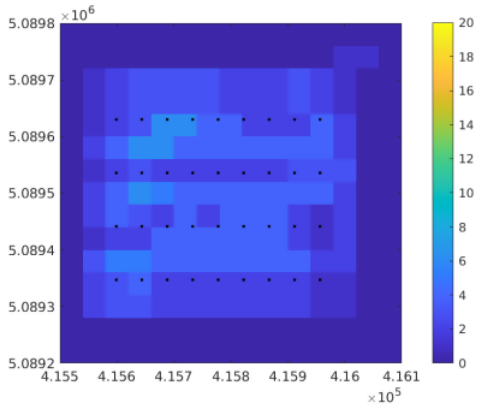
</td><td colspan="2">Cases with longitudinal overlapping equal to 60% and transversal overlapping equal to 30% (the real overlapping taking into account the DTM and obstructions is shown in the figure on the left), but with different configurations of GCPs and different precision of the positions of the projection centers.</td></tr>
<tr><td></td><td>Known projection centers with metric accuracy</td><td>Known projection centers with centimetric accuracy</td></tr>
<tr><td>16 GCPs</td><td> 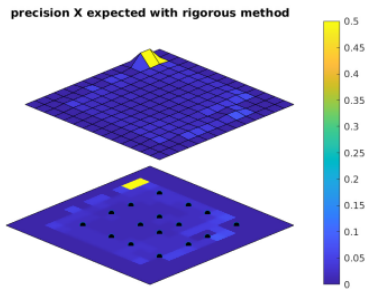
</td><td> 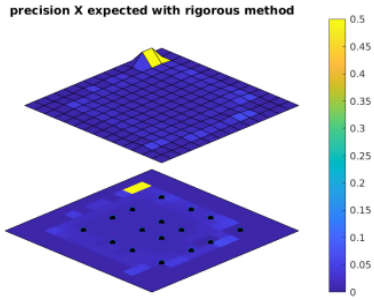
</td></tr>
<tr><td>8 GCPs</td><td> 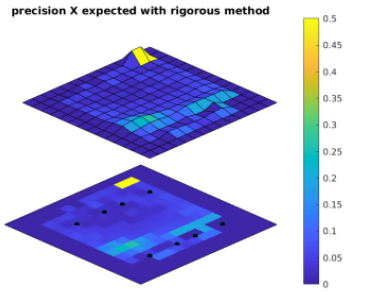
</td><td> 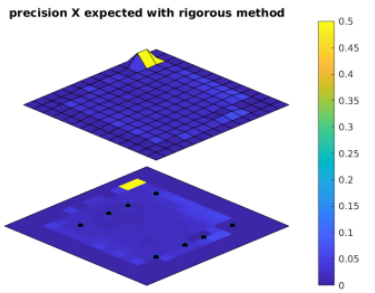
</td></tr>
<tr><td>4 GCPs</td><td> 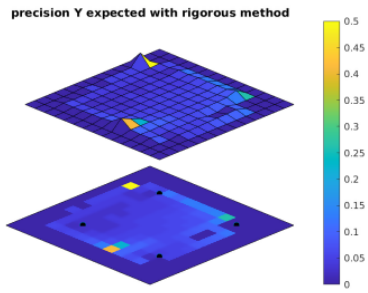
</td><td> 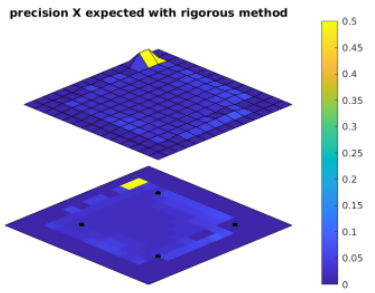
</td></tr>
</table>

Figure 6-15 Precision Z expected with rigorous method and overlapping 60%-30%: 2D and 3D representations with GCPs in different configurations - scale bar from 0m to 0.5m

<table>
<tr><td> 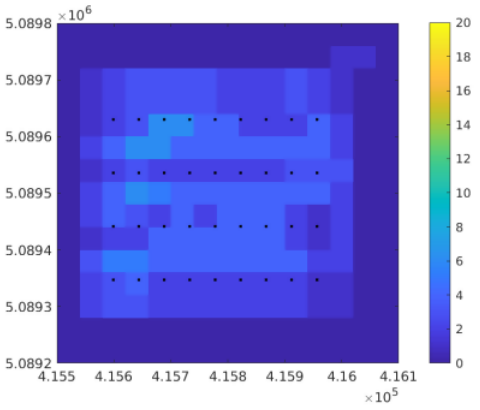
</td><td colspan="2">Cases with longitudinal overlapping equal to 60% and transversal overlapping equal to 60% (the real overlapping taking into account the DTM and obstructions is shown in the figure on the left), but with different configurations of GCPs and different precision of the positions of the projection centers.</td></tr>
<tr><td></td><td>Known projection centers with metric accuracy</td><td>Known projection centers with centimetric accuracy</td></tr>
<tr><td>16 GCPs</td><td> 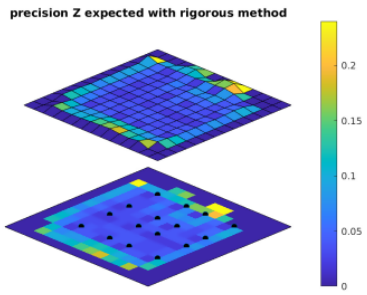
</td><td> 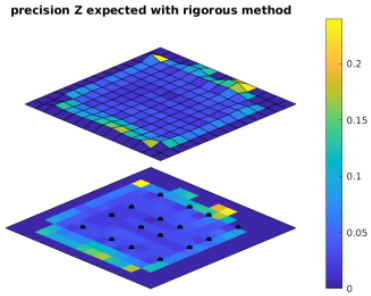
</td></tr>
<tr><td>8 GCPs</td><td> 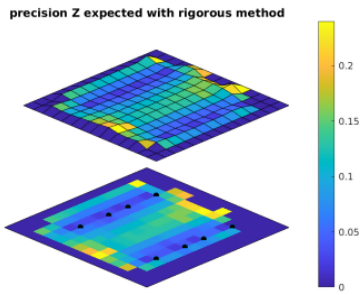
</td><td> 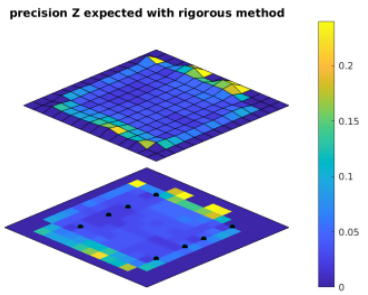
</td></tr>
<tr><td>4 GCPs</td><td> 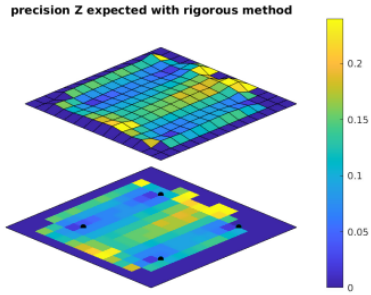
</td><td> 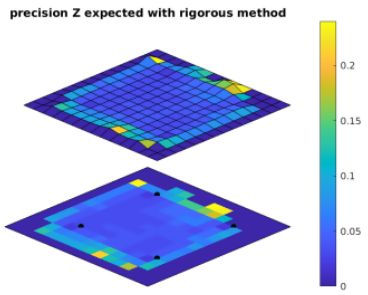
</td></tr>
</table>

Figure 6-16 Precision Z expected with rigorous method and overlapping 60%-60%: 2D and 3D representations with GCPs in different configurations - scale bar from 0m to 0.25m

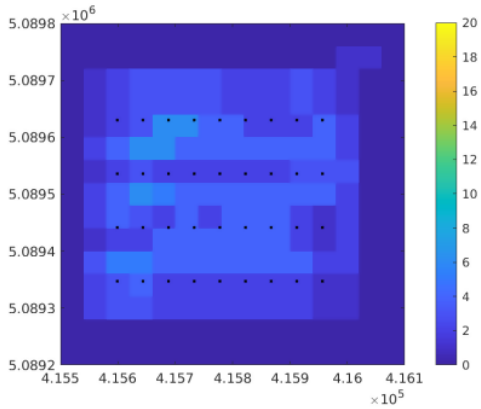	Cases with longitudinal overlapping equal to 80% and transversal overlapping equal to 60% (the real overlapping taking into account the DTM and obstructions is shown in the figure on the left), but with different configurations of GCPs and different precision of the positions of the projection centers.	
	Known projection centers with metric accuracy	Known projection centers with centimetric accuracy
16 GCPs	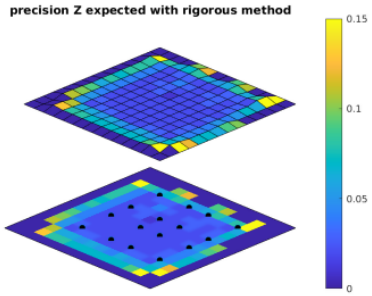	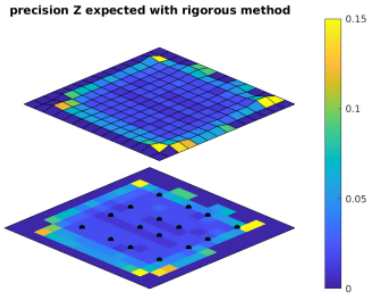
8 GCPs	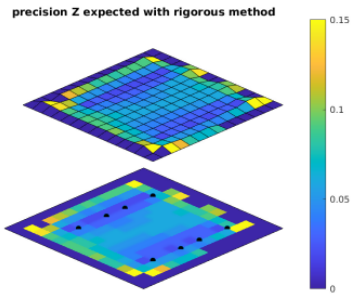	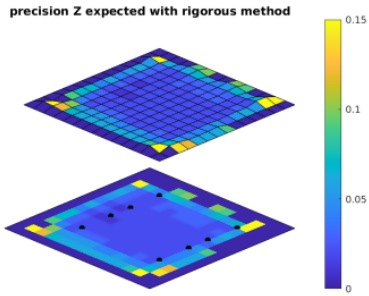
4 GCPs	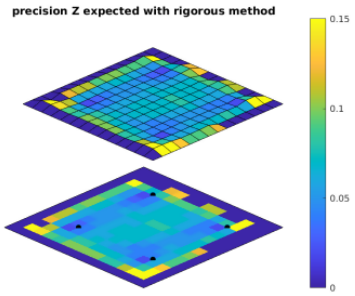	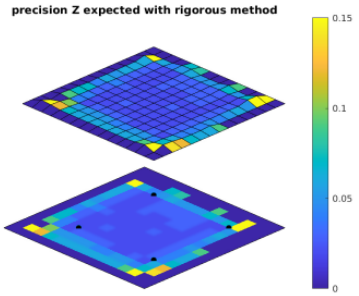

Figure 6-17 Precision Z expected with rigorous method and overlapping 80%-60%: 2D and 3D representations with GCPs in different configurations - scale bar from 0m to 0.15m

<table>
<tr><td colspan="2"> 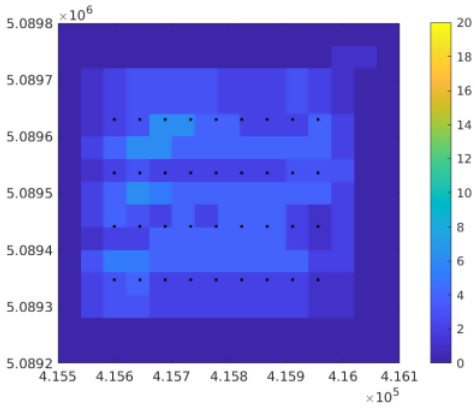
</td><td>Cases with longitudinal overlapping equal to 80% and transversal overlapping equal to 80% (the real overlapping taking into account the DTM and obstructions is shown in the figure on the left), but with different configurations of GCPs and different precision of the positions of the projection centers.</td></tr>
<tr><td></td><td>Known projection centers with metric accuracy</td><td>Known projection centers with centimetric accuracy</td></tr>
<tr><td>16 GCPs</td><td> 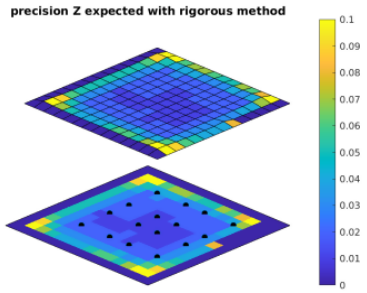
</td><td> 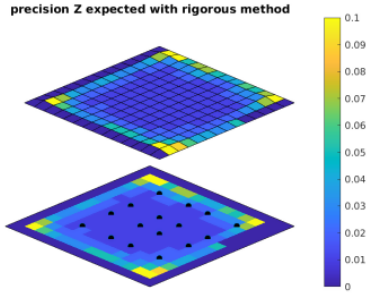
</td></tr>
<tr><td>8 GCPs</td><td> 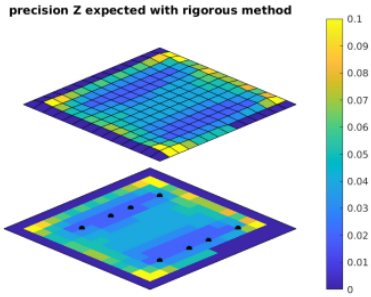
</td><td> 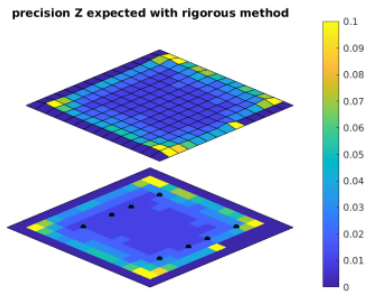
</td></tr>
<tr><td>4 GCPs</td><td> 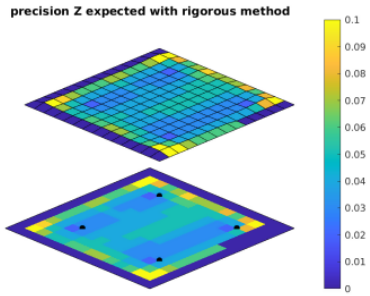
</td><td> 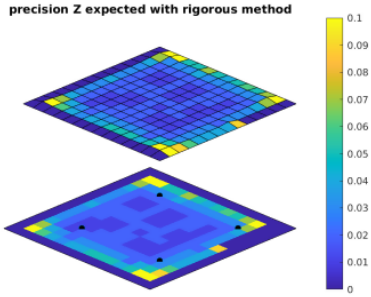
</td></tr>
</table>

Figure 6-18: Precision Z expected with rigorous method and overlapping 80%-80%: 2D and 3D representations with GCPs in different configurations - scale bar from 0m to 0.10m

The images show the expected precisions both in the 2D representation with chromatic scale and in the 3D representation, where to the chromatic scale corresponds the height of the surface. The position of GCPs is pointed out by the black points. The images of the standard deviations for the different components X, Y, Z, in the different cases organized by the overlappings, the number of GCPs and the quality of positioning of the shot centers, highlight how the areas with minor standard deviation expand from the central area of the photogrammetric block with the increase of the number of GCP and, GCP being equal, with the increase of the precision of UAV positioning. It is important to note the difference of scales (for all the components X, Y, Z) when going from a block with an overlapping of 60/30 with maximum values lower than 50 cm to a block with an overlapping of 60/60 with values lower than 25 cm, to a block with an overlapping of 80/60 with values equal to 15 cm and, finally, to a block with an overlapping of 80/80 with values lower than 10 cm.

The case with an overlapping of 60/30 and position of known shot centers with metric precision does not seem to improve with the increase of GCPs from 4 to 8, while the standard deviations considerably reduce with 16 GCPs. The improvement of standard deviations in the component Z is, instead, more regular passing from 4 to 8 and to 16 GCPs in the solutions with GPS positioning of centimetric precision (GPS RTK solution).

The case with an overlapping of 60/60 and position of known shot centers with metric precision considerably changes the entity of precisions compared to the case with an overlapping of 60/30 and position of known shot centers with metric precision. The same occurs in the case with an overlapping of 60/60 and position of known shot centers with centimetric precision compared to the case with an overlapping of 60/30 and position of known shot centers with centimetric precision.

It is worth to notice that the effect due to the higher precision in the knowledge of the coordinates of projection centers (overlapping being equal) is lower than the effect of the increase in the overlapping (precision in the knowledge of the coordinates of projection centers being equal).

In the case with an overlapping of 60/60 and position of known shot centers with metric precision, the precision improves with the use of 16 GCPs instead of 4 GCPs. If we consider the presence of 16 GCPs, the values of the expected precision for the case with an overlapping of 60/60 and position of known shot centers with metric precision and those for the case with an overlapping of 60/60 and position of known shot centers with centimetric precision are comparable. The effect due to the knowledge of the coordinates of the shot centers with centimetric precision is therefore comparable to the effect due to the increase of GCPs from 4 to 16.

The trends are considerably different in the cases where the position of the projection centers is known with centimetric or metric precision (overlapping, number and geometry of GCPs being equal). In the analyzed case study it seems that the knowledge of the shot centers with centimetric precision tends to make the precision in Z area more uniform (except on sides), save whether the knowledge of coordinates of projection centers with metric precision is reached with a high number of GCPs. The bigger overlapping seems to compensate for the number of GCPs, allowing to increase the precisions where it is not possible to get a high number of GCPs.

The tables 6-2, 6-3, and 6-4 report the numerical results, that have been presented till now in a graphic form, showing the summarizing statistics of all the different cases for the components X, Y and Z. In these tables we find the values of the main statistics organized by the different performed tests in relation to the overlapping, the number of GCPs and the level of knowledge of the shot centers. The minimum and maximum values are reported, with the corresponding average and median of the standard deviations, evaluated by the rigorous method previously described.

Table 6-2 statistics of precision X expected with rigorous method

CASE	MIN (m)	MAX (m)	AVERAGE (m)	MEDIAN (m)
Overlapping 60%-30% 16 GCPs GPS code	0.01	0.50	0.04	0.02
Overlapping 60%-30% 16 GCPs GPS RTK	0.01	0.50	0.03	0.02
Overlapping 60%-30% 8 GCPs GPS code	0.01	0.50	0.08	0.05
Overlapping 60%-30% 8 GCPs GPS RTK	0.01	0.50	0.04	0.02
Overlapping 60%-30% 4 GCPs GPS code	0.02	0.50	0.08	0.05
Overlapping 60%-30% 4 GCPs GPS RTK	0.02	0.50	0.05	0.03
Overlapping 60%-60% 16 GCPs GPS code	0.01	0.24	0.02	0.02
Overlapping 60%-60% 16 GCPs GPS RTK	0.01	0.24	0.02	0.01
Overlapping 60%-60% 8 GCPs GPS code	0.01	0.24	0.03	0.02
Overlapping 60%-60% 8 GCPs GPS RTK	0.01	0.24	0.02	0.02
Overlapping 60%-60% 4 GCPs GPS code	0.02	0.24	0.03	0.03
Overlapping 60%-60% 4 GCPs GPS RTK	0.01	0.24	0.03	0.02
Overlapping 80%-60% 16 GCPs GPS code	0.00	0.15	0.02	0.01
Overlapping 80%-60% 16 GCPs GPS RTK	0.00	0.15	0.02	0.01
Overlapping 80%-60% 8 GCPs GPS code	0.01	0.15	0.02	0.02
Overlapping 80%-60% 8 GCPs GPS RTK	0.01	0.15	0.02	0.01
Overlapping 80%-60% 4 GCPs GPS code	0.01	0.15	0.03	0.02
Overlapping 80%-60% 4 GCPs GPS RTK	0.01	0.15	0.02	0.01
Overlapping 80%-80% 16 GCPs GPS code	0.00	0.10	0.02	0.01
Overlapping 80%-80% 16 GCPs GPS RTK	0.00	0.10	0.01	0.01
Overlapping 80%-80% 8 GCPs GPS code	0.01	0.10	0.02	0.01
Overlapping 80%-80% 8 GCPs GPS RTK	0.00	0.10	0.01	0.01
Overlapping 80%-80% 4 GCPs GPS code	0.01	0.10	0.02	0.02
Overlapping 80%-80% 4 GCPs GPS RTK	0.01	0.10	0.02	0.01

Table 6-3 statistics of precision Y expected with rigorous method

CASE	MIN (m)	MAX (m)	AVERAGE (m)	MEDIAN (m)
Overlapping 60%-30% 16 GCPs GPS code	0.01	0.50	0.04	0.02
Overlapping 60%-30% 16 GCPs GPS RTK	0.01	0.50	0.04	0.02
Overlapping 60%-30% 8 GCPs GPS code	0.02	0.50	0.06	0.04
Overlapping 60%-30% 8 GCPs GPS RTK	0.01	0.50	0.05	0.02
Overlapping 60%-30% 4 GCPs GPS code	0.02	0.50	0.07	0.05
Overlapping 60%-30% 4 GCPs GPS RTK	0.02	0.50	0.05	0.03
Overlapping 60%-60% 16 GCPs GPS code	0.01	0.24	0.03	0.02
Overlapping 60%-60% 16 GCPs GPS RTK	0.01	0.24	0.02	0.01
Overlapping 60%-60% 8 GCPs GPS code	0.01	0.24	0.03	0.02
Overlapping 60%-60% 8 GCPs GPS RTK	0.01	0.24	0.03	0.02
Overlapping 60%-60% 4 GCPs GPS code	0.02	0.24	0.04	0.03
Overlapping 60%-60% 4 GCPs GPS RTK	0.01	0.24	0.03	0.02
Overlapping 80%-60% 16 GCPs GPS code	0.01	0.15	0.02	0.01
Overlapping 80%-60% 16 GCPs GPS RTK	0.00	0.15	0.02	0.01
Overlapping 80%-60% 8 GCPs GPS code	0.01	0.15	0.02	0.02
Overlapping 80%-60% 8 GCPs GPS RTK	0.01	0.15	0.02	0.01
Overlapping 80%-60% 4 GCPs GPS code	0.01	0.15	0.03	0.02
Overlapping 80%-60% 4 GCPs GPS RTK	0.01	0.15	0.02	0.01
Overlapping 80%-80% 16 GCPs GPS code	0.00	0.10	0.02	0.01
Overlapping 80%-80% 16 GCPs GPS RTK	0.00	0.10	0.01	0.01
Overlapping 80%-80% 8 GCPs GPS code	0.01	0.10	0.02	0.01
Overlapping 80%-80% 8 GCPs GPS RTK	0.00	0.10	0.02	0.01
Overlapping 80%-80% 4 GCPs GPS code	0.01	0.10	0.02	0.02
Overlapping 80%-80% 4 GCPs GPS RTK	0.01	0.10	0.02	0.01

The behavior of the precisions of the coordinates X and Y shows a similar trend. As expected, there is a reduction of the median with the increase of GCP (inside each block with the same overlapping) and passing from a case with known projection centers with metric precision to a case with known projection centers with centimetric precision, the variations of the median are soft inside the block with homogenous overlapping and vary in the passage from an overlapping block to another, with a decreasing trend at the increase of overlapping. The median of the blocks considerably decreases with the increase of overlapping.

Table 6-4 Statistics of precision Z expected with rigorous method

CASE	MIN (m)	MAX (m)	AVERAGE (m)	MEDIAN (m)
Overlapping 60%-30% 16 GCPs GPS code	0.02	0.50	0.11	0.09
Overlapping 60%-30% 16 GCPs GPS RTK	0.02	0.50	0.08	0.06
Overlapping 60%-30% 8 GCPs GPS code	0.02	0.50	0.30	0.27
Overlapping 60%-30% 8 GCPs GPS RTK	0.02	0.50	0.09	0.07
Overlapping 60%-30% 4 GCPs GPS code	0.02	0.50	0.30	0.29
Overlapping 60%-30% 4 GCPs GPS RTK	0.02	0.50	0.11	0.08
Overlapping 60%-60% 16 GCPs GPS code	0.02	0.24	0.07	0.05
Overlapping 60%-60% 16 GCPs GPS RTK	0.01	0.24	0.06	0.04
Overlapping 60%-60% 8 GCPs GPS code	0.02	0.24	0.10	0.09
Overlapping 60%-60% 8 GCPs GPS RTK	0.02	0.24	0.06	0.04
Overlapping 60%-60% 4 GCPs GPS code	0.02	0.24	0.12	0.12
Overlapping 60%-60% 4 GCPs GPS RTK	0.02	0.24	0.06	0.04
Overlapping 80%-60% 16 GCPs GPS code	0.01	0.15	0.05	0.03
Overlapping 80%-60% 16 GCPs GPS RTK	0.01	0.15	0.04	0.02
Overlapping 80%-60% 8 GCPs GPS code	0.02	0.15	0.06	0.06
Overlapping 80%-60% 8 GCPs GPS RTK	0.01	0.15	0.04	0.02
Overlapping 80%-60% 4 GCPs GPS code	0.02	0.15	0.07	0.06
Overlapping 80%-60% 4 GCPs GPS RTK	0.02	0.15	0.05	0.03
Overlapping 80%-80% 16 GCPs GPS code	0.01	0.10	0.04	0.02
Overlapping 80%-80% 16 GCPs GPS RTK	0.01	0.10	0.03	0.01
Overlapping 80%-80% 8 GCPs GPS code	0.02	0.10	0.04	0.04
Overlapping 80%-80% 8 GCPs GPS RTK	0.01	0.10	0.03	0.02
Overlapping 80%-80% 4 GCPs GPS code	0.02	0.10	0.05	0.04
Overlapping 80%-80% 4 GCPs GPS RTK	0.01	0.10	0.03	0.02

As for the planimetric components, also for the altimetric component Z the extent of deviation (Max - Min) mainly depends on the overlapping, then on the number of GCPs and finally on the precision of the coordinates of the projection centers.

The median values, as expected, are homogenous inside the blocks with equal overlapping, but a little bit higher than the median of the planimetric components X and Y. Conversely to the analyzed cases in the components X and Y, the altimetric component Z presents some median values (marked in yellow) different from the values of the belonging block, with higher values with the reduction of overlapping. This effect could be caused by the bigger weakness of the configuration with limited overlapping or with limited GCPs, especially in relation to the component Z of the survey. We can notice that the particularly high median values (marked in yellow) correspond to the solutions with known projection centers with metric precision, which are, in fact, the weakest configurations of the whole case study.

The Average values have almost the same behavior as the Median ones, even with generally higher values, because they are affected, contrary to the Median estimator, by the lack of stability of the Average estimator.

6.3 Case Study "Castle of Casalbagliano"

The Castle of Casalbagliano is located in the countryside of Alessandria (Piedmont, Italy). The building is characterized by a square layout, typical of medieval fortifications, about 20 m x 20 m wide, with the tower height of about 25 m. It was originally built using bricks, then restored several times; currently the building is abandoned and unsafe (Figure 6-19).

Figure 6-19 The Castle of Casalbagliano in its 3D reconstruction

A survey has been performed in the test area and a complete dataset of nadiral and oblique images has been acquired by UAS. The Total Station (Leica Nova MS60 Multistation) and the GNSS (Topcon Hyper SR) in Network Real Time Kinematic survey have been used to georeference the Ground Control Points (GCPs). Eighteen GCPs have been materialized on the ground using 30 cm x 30 cm black and white targets spread out all around the castle, to which the access is forbidden. GCPs survey is taken as reference to validate the reliability of the precisions which come from the planning and analysis suite.

The Check Points (CP) were selected from the 18 points measured, of which 6 were used as GCP and 12 as CP (Figure 6-20).

Figure 6-20 The position of GCPs and Check Points (CPs)

For the photogrammetric survey, the images have been acquired using a Canon EOS-M camera, with a fixed focal length equal to 22 mm. The camera intrinsic, extrinsic and lens distortion parameters were estimated with the Camera Calibrator application of Matlab®. The camera has been put on a Mikrokopter Hexacopter, equipped with a gimbal stabilized platform.

The survey campaign has involved several degree students in one day. The elaboration of the several survey methodologies for the different adopted instruments and, in particular, the elaboration of the photogrammetric UAV survey will be not approach in the present thesis work because it is not about to the research field.

The average flight height for the dataset with nadiral geometry was approximately of 40 m. A high overlap has been guaranteed (80% along flight direction and 70% across flight direction). The resulting average GSD was about 9 mm. The nadiral flight was designed and realized with 4 strips, as shown in Figure 6-21. The strong overlapping is used to ensure the visibility of all points of the object even when the tower or the walls of the castle are an obstacle to the view of the points on the ground. Figure 6-21 clearly shows the obstructions to sight caused by the tower and walls.

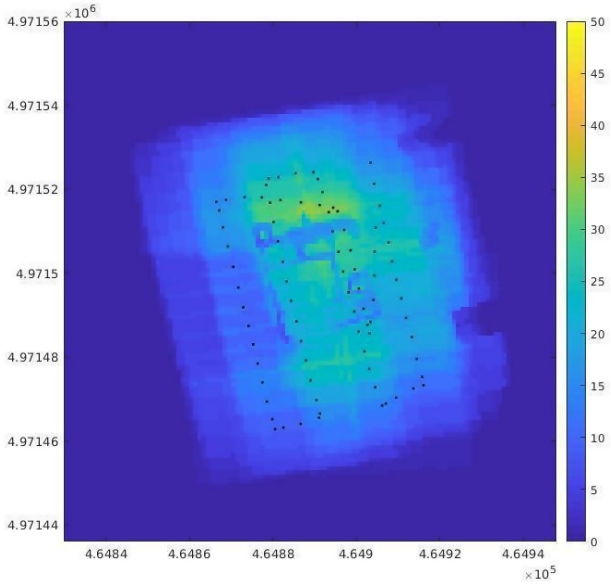

Figure 6-21 Camera location of the nadiral survey (black dots) and image overlap (colour bar)
(Est and North coordinate in UTM/ETRF2000-2008.0 in meters)

All the acquired images have been processed using the commercial software Agisoft Photoscan - version 1.2.6 (http://www.agisoft.com/), that provides the External Orientation (EO) parameters and performs the camera self-calibration (for both the considered datasets). In fact, in case of blocks acquired from UAS, it is quite important to refine the Internal Orientation (IO) parameters, eventually changed after the estimation during a standard calibration procedure because of the impacts suffered by the lens during take-off and landing. This software was chosen because it has a remarkable reliability in the orientation phase of the aerial triangulation. Together with the solution of Agisoft Photoscan (which is opinion of the author that today it is one of the best software for photogrammetry combined with Computer Vision surely with a great distribuition), the scientific program Calge, developed at Milan Polytechnic (Forlani, 1986) performing the rigorous compensation of an Aerial Triangulation has been used.

6.4 Analysis of the results and validation

In the previous chapter it has been described that the analysis module is needed to analyze the telemetry of the flight of the survey in order to have indications about the metric quality of the products realizable with this flight, also before the complete processing of the images.

The advantage of this process is that it is realizable in few minutes in situ. If anomalies are identified (for example, parts of territory not seen for a sufficient number of times) or if the achievable precision is not satisfying, it is possible to plan again and repeat the flight.

A comparison is performed between the simulation results and the real case study survey, that involves obviously a series of random errors that cannot be foreseen a priori (for example images not perfectly focused, like due to a gust of wind, or rolling shutter effect). For this reason, it is interesting to verify if the

expected accuracies, computed during the design phase, are comparable to the observed root mean square. The aim is to verify the reliability of the estimate precisions comparing them with the precisions reached at the end of the survey. The measured precisions on the images and constraints have been defined in empirical way, as said in chapter 4, and for validation purposes it is important that these values are set equally for both methods to be compared. It is also interesting to check if the simulation and the real case study have the same critical zones, i.e. areas where the precision drastically decreases. In fact, the aim of a network simulation is, on the one hand, to predict the magnitude of the achievable precisions and, on the other hand, to highlight the eventual weaknesses of the designed flight plan. The identification of these weaknesses also provides a guidance on how to redesign the flight to improve the survey.

After using the commercial software Agisoft Photoscan to get the automatic measure of “tie points” through matching algorithms, an analysis of the covariance matrix of the unknown parameters of the bundle block adjustment can be performed by exporting the image block and analyzing it with a “scientific” photogrammetric software. In this way, the theoretical accuracy of the object point coordinates can be estimated.

For this purpose, the scientific software Calge has been used. It is designed to compute the Least Squares adjustment of a general topographic network with Total Stations o spirit levels or a photogrammetric block. The photogrammetric observations, obtained through automatic matching in Agisoft Photoscan, have been exported and reformatted for processing in Calge. The positions of the projection centres (of which only approximate values are required) have been also exported from Photoscan.

Calge outputs the adjusted coordinates of the projection centers, the GCP and the Check Points with the corresponding estimated precisions. In this case study, if we want to a priori estimate the precisions of a photogrammetric survey, it is very interesting to consider the estimated precisions expected for the 12 mentioned Check Points. In particular, the estimated precisions of the variables provided by Calge are compared with the estimated precisions calculated with the rigorous method developed inside the tools of U.Ph.O. As already mentioned, the estimated precisions are deduced from the main diagonal of the matrix C_{xx} for both methods. The scientific software CALGE provides the output of the matrix Cxx with the precision of each unknown or x, y, z components of each point observed. U.Ph.O. instead provides as output a raster of the entire territory to be detected with cells equal in size to the DSM provided in input (in this case the size of the cells is 5m). What is compared here is then the precise value provided by the software CALGE and the value contained in the cell of the raster provided by U.Ph.O. in which the position of the point considered falls. Also for this reason the values proposed by the two software are different. U.Ph.O. certainly provides a more approximate estimate but it guarantees to know this estimate on the whole territory to be detected with homogeneous distribution.

In order to compare the estimation of the accuracies of the measured block with Calge and the analysis tool for both methods, the same boundary conditions were set. The accuracy of the measurements was fixed at half pixel (about 2 microns) and the position of the frames was constrained with a precision of 10 meters (known projection centers with GPS code solution). Finally, the GCPs (corresponding with the same GCPs selected in the planning phase) have been constrained with a precision of 3 cm (typical of GPS RTK measures). Figure 6-22 shows this comparison for the nadiral block. There is an interesting coherence

between the results of the “a priori” expected accuracies made with the Office suite here presented and the “a posteriori” estimates accuracy obtained with Calge for the X, Y and Z component.

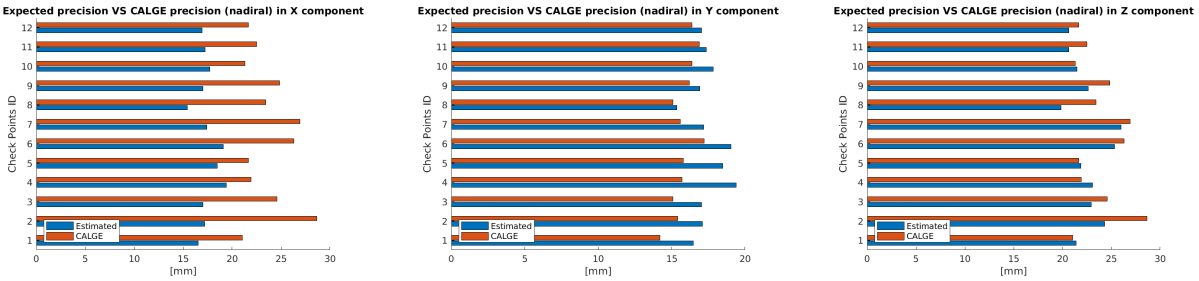

Figure 6-22 Comparison between estimation accuracies in the nadiral case

Although the results obtained are not exactly coincident, they are comparable and of the same order of magnitude.

However, the analysis of this case study opens the way to the development of the tools of the U.Ph.O. project showing the potential both in the design phase and in the analysis of the data immediately after the execution of the survey.

CONCLUSIONS AND PERSPECTIVE

The development of UAV surveys is rapidly increasing in several fields. The initial objective of this work was to focus on surveys that require high metric accuracy. From the technological point of view there has been a very rapid and effective growth of the hardware. Manufacturers have been steadily producing drones more and more agile, safe and able to move independently along precise routes. The new UAVs implement anti-collision safety systems and very accurate positioning sensors (GNSS - Global Navigation Satellite System - also in RTK mode and very sophisticated barometers and accelerometers). It can be said that the world of UAVs is going more and more "Citius!, Altius!, Fortius!" driven by a competition between manufacturers. The geomatic research in the field of UAV surveys requires, instead, an alternative concept, which could be summarized in the expression "lentius!, profundius!", slower and deeper, seeking the best result of a survey deepening its characteristics and potentialities. For this reason, we need new software tools that can support the metric use of this new hardware. Nowadays there is no photogrammetric software on the market that pays specific attention to the metric planning of the surveys. A photogrammetric survey, that is aimed to maintain high metric characteristics, requires a project as accurate as any other engineering work. The method proposed in this work moves in this direction.

The project called U.Ph.O. (Unmanned Photogrammetric Office) aims to provide tools for the design of photogrammetric surveys that can take into account the complexity of reality. It is made up two modules, the first for the planning phase and the second one for the analysis phase of the survey campaigns. The design tool uses a Digital Surface Model (DSM) to verify the projection of the frames on the ground, evaluate the Ground Sample Distances (GSD), verifies the visibility of the points on the ground taking into account the presence of obstructions to the view and estimates the expected precision on each object pixel, taking into account the real visibility by the frames.

The analysis tool, on the other hand, provides a quick check of the measurements made just before their processing. The analysis tool verifies the coverings with the supplied DSM, checks the absence of holes and estimates the accuracy achievable with the survey. The analysis tool uses the telemetry recorded by the drone during the flight or the External Orientation parameters obtained from expeditious processing of the images as its starting data. However, the tools developed are suitable only for users with geomatic knowledge, in order to provide the geometric parameters of the cameras used and calibrate the parameters necessary for estimating the expected accuracy, such as the accuracy of measurement on the images.

The proposed tools (chapter 5) have solid roots in the planning of aerial and close-range surveys and lead to proposal that better suits the needs of UAV flights. Significantly different case study has been treated: Castle of Casalbagliano and Belvedere glacier (chapter 6). The analysis coming from the obtained results in tested procedures with several configurations of these case studies opens the way to the development of the tools of the U.Ph.O. project. In fact, the main problem, to obtain a good survey, is know the realistic visibility of the generic object point in the images. To obtain this, it is important taking into account the obstructions induced by the DSM itself. Realistic overlapping of the frames (projected on DSM), number and distribution of GCPs and known quality of the shot points complete the analysis applied to the two different case studies.

In the present work, in order to obtain an agile and operational system with rapid computational times, the problem has been simplified with the use of a DSM with a resolution limited to cells of a dimension between 5 and 50 meters according to the survey scale, not to get calculation matrix with bigger dimensions than 100 cells x 100 cells. In the future it would be interesting and advantageous to be able to represent the territory with a DSM of bigger resolution (also sub metrical). To make it possible without having computational problems it will be necessary to apply techniques of mathematical calculation that make the matrix product more efficient, for example, by reorganizing the matrix (with reference to the design matrix). This tool gives the possibility of simulating different possible scenarios according to the variation of the constraints on the ground (GCPs) and of the constraints to the external orientations, in addition to the classic variations of shot geometry (flight altitude, overlapping …).

The development of what has been presented in this thesis rose from several survey application cases performed in the recent years. Surveys related to "monitoring of structures", like the "Castle of Casalbagliano" in March 2016, have raised the need to know a priori the expected precisions. Surveys in emergency conditions, like that of "the Belfry of Norcia" and that of "the Church of San Salvatore in Campi di Norcia" in November 2016 have been interesting tests to validate the procedures. Surveys in case of emergency in rapid evolution, like that of "Morandi bridge in Genoa" in August 2018, have favored the development of analysis tools and highlighted the importance of computational times. Finally, environmental surveys, like those on "Belvedere Glacier" in July 2018, have requested a multi-scenario analysis with the possibility of varying the system constraints in a simple and fast way.

To check the quality of the estimated precision coming from the rigorous method developed inside the tools of U.Ph.O., has been used the scientific program Calge, developed at Milan Polytechnic, performing the rigorous compensation of an Aerial Triangulation. The comparison of the standard deviations provided by Calge and by U.Ph.O. have been obtained in the Castle of Casalbagliano case study.

The case studies presented a good consistency of the standard deviation estimation by U.Ph.O. with the reference solution. Thus, the potentiality both in the design phase and in the analysis of the data immediately after the execution of the survey is showed.

The present work suggests some operative good practice criteria, coming from the analysis of different configurations simulated in two real scenarios, that may be useful to improve the experience of the operator (like number and distribution of Ground Control Points, related to the positioning quality of the shot centers).

Nowadays, the use of DSM as starting point for all the precision calculations does not permit to analyze cases with vertical faces with a sufficient level of details. In monitoring and Cultural Heritage fields there is a great interest in the possibility to estimate the expected precisions in the surveys of vertical faces, the development of this prospect will be therefore sure investigated, also increasing the possibilities of planning flights with oblique camera. This means that it is necessary to know well the geometric characteristics of the camera used, taking into account the possible deformations due to perspective distortions. In any case the suite tools are useful also in this case considering to compare different UAV plans.

Tools to obtain a realistic planning for UAV photogrammetric surveys could be particularly useful where it is important to evaluate the correct equilibrium between the expected accuracy and the distance from the

object to survey. This tool aims to find solutions that allow you to keep a safe distance and minimize the number of images and the number of GCPs of the survey, without losing accuracy. Several are the occasions where the surveyor and the UAV pilot have to evaluate this crucial point. The proposed tools are also very useful whenever the surveys require predefined metric accuracies and would not allow the repetition of the survey in the event that the images taken are not adequate to achieve the desired results.

The proposed and developed tools can certainly find application in the daily work of planning metric surveys for those willing to do it through the use of UAVs. In order not to let this job remain exclusively a theoretical one, it is necessary to make these tools available with a web service, that could be accessible to people willing to plan surveys according to geomatics basics. Its diffusion may also build a collection of case studies, that will promote improvements and new functions.

REFERENCES

Accardo, D., Fasano, G., Forlenza, L., Moccia, A., & Rispoli, A. (2013). Flight test of a radar-based tracking system for UAS sense and avoid. IEEE Transactions on Aerospace and Electronic Systems, 49(2), 1139-1160.33

Achille, C., Adami, A., Chiarini, S., Cremonesi, S., Fassi, F., Fregonese, L., Taffurelli, L. (2015). UAV-based photogrammetry and integrated technologies for architectural applications—Methodological strategies for the after-quake survey of vertical structures in Mantua (Italy). Sensors 15(7), pp. 15520-15539.

Adams, S.M., Friedland, C.J. (2011). A survey of Unmanned Aerial Vehicle (UAV) usage for imagery collection in disaster research and management. Proceedings of the Ninth International Workshop on Remote Sensing for Disaster Response, 15-16 September, Stanford, CA, USA.

Agüera, F., Carvajal, F., Pérez, M. (2011). Measuring sunflower nitrogen status from an unmanned aerial vehicle-based system and an on the ground device. ISPRS Archives, UAV-g 2011, 14-16 September, Zurich, Switzerland, Vol. 38(1)/C22, pp. 33-37. DOI: 10.5194/isprsarchives-XXXVIII-1-C22-33-2011.

Aicardi, I. (2016). UAVs for spatial data acquisition, Sensors evaluation, flight design and planning, multi-temporal solutions, Doctoral Dissertation, Doctoral Program in Environmental Engineering (29 th cycle), Politecnico di Torino

Alberda, J. E. (1980). A review of analysis techniques for Engineering control schemes, Proceedings of the Industrial and Engineering Survey Conference, London.

Ballarin, M., Buttolo, V., Guerra, F., Vernier, P. (2013). Integrated surveying techniques for sensitive areas: San Felice sul Panaro. ISPRS Annals of the Photogrammetry, Remote Sensing and Spatial Information Sciences 5, W1.

Bareth, G., Bendig, J., Tilly, N., Hoffmeister, D., Aasen, H., Bolten, A. (2016). A comparison of UAV-and TLS-derived plant height for crop monitoring: using polygon grids for the analysis of crop surface models (CSMs). Photogrammetrie-Fernerkundung-Geoinformation, 2016(2), 85-94.

Berni, J. A., Zarco-Tejada, P. J., Suárez Barranco, M. D., & Fereres Castiel, E. (2009). Thermal and narrow-band multispectral remote sensing for vegetation monitoring from an unmanned aerial vehicle. Institute of Electrical and Electronics Engineers.

Briechle, S., Sizov, A., Tretyak, O., Antropov, V., Molitor, N., & Krzystek, P. (2018). UAV-Based detection of unknown radioactive biomass deposits in Chernobyl's exclusion zone. International Archives of the Photogrammetry, Remote Sensing & Spatial Information Sciences, 42(2).

Cannarozzo, R., Cucchiarini, L. and Meschieri, W. (2012). Misure, rilievo, progetto - modulo T: Fotogrammetria, Zanichelli, Bologna, Italy.

Charisiadis, P., Andra, S. S., Makris, K. C., & Christophi, C., Skarlatos, D., Vamvakousis, V., Kargaki, S. and Stephanou, E.G. (2015). Spatial and seasonal variability of tap water disinfection by-products within distribution pipe networks. Sci. Total Environ, 506(507), 26-35.

Chiabrando, F., Lingua, A., & Piras, M. (2013). Direct photogrammetry using UAV: tests and first results. *Int. Arch. Photogramm. Remote Sens. Spat. Inf. Sci*, *1*, 81-86.

Colomina, I., Molina, P. (2014). Unmanned Aerial Systems for Photogrammetry and Remote Sensing: a review. ISPRS Journal of Photogrammetry and Remote Sensing, Vol. 92, pp. 79-97. DOI: 10.1016/j.isprsjprs.2014.02.013.

Dunford, R., Michel, K., Gagnage, M., Piegay, H., Trémelo, M.L. (2009). Potential and constraints of Unmanned Aerial Vehicle technology for the characterization of Mediterranean riparian forest. International Journal of Remote Sensing, Vol. 30(19), pp. 4915-4935. DOI: 10.1080/01431160903023025.

Eisenbeiss, H. (2004). A mini Unmanned Aerial Vehicle (UAV): system overview and image acquisition. International Workshop on "Processing and visualization using high-resolution imagery", 18-20 November, Pitsanulok, Thailand, Vol. 36(5)/W1, pp. 1-7.

Eisenbeiss, H. (2008). UAV Photogrammetry in plant sciences and geology. 6th ARIDA Workshop on "Innovations in 3D Measurement, Modeling and Visualization", 25-26 February, Povo (Trento), Italy.

Eisenbeiß, H. (2009). UAV Photogrammetry, Ph.D. dissertation, Institute of Geodesy and Photogrammetry, ETH, Zurich, Switzerland.

Eisenbeiss, H. (2009). UAV Photogrammetry. Ph. D. thesis - Institute of Geodesy and Photogrammetry, ETH Zürich, Zurich, Switzerland.

ENAC (2018). Remote Control Aircraft Regulations, Issue No. 2 dated 16 July 2015, Revision 3 dated May 2018

European Commission (2007). Study Analysing the Current Activities in the Field of UAV. Technical Report. ENTR/2007/065, Second Element: Way Forward.

Everaerts, J. (2008). The use of Unmanned Aerial Vehicles (UAVs) for Remote Sensing and mapping. ISPRS Archives, XXI ISPRS Congress, 3-11 July, Beijing, China, Vol. 37/B1, pp. 1187-1192.

Fagandini, R., Federici, B., Ferrando, I., Gagliolo, S., Pagliari, D., Passoni, D. & Sguerso, D. (2017). Evaluation of the laser response of Leica Nova multistation MS60 for 3D modelling and structural monitoring. In *International Conference on Computational Science and Its Applications* (pp. 93-104). Springer, Cham.

Forlani, G. (1986). Sperimentazione del nuovo programma CALGE dell'ITM. Bollettino SIFET 1986, 2, 63–72.

Fraser, C. S. (1984). Network design considerations for non-topographic photogrammetry. Photogrammetric Engineering and Remote Sensing, vol. 50, no. 4, pp. 561-570, 1984.

Fraser, C. S. (1992). Photogrammetric measurement to one part in a million. Photogrammetric engineering and remote sensing, 58, 305-310.

Gagliolo, S., Fagandini, R., Federici, B., Ferrando, I., Passoni, D., Pagliari, D., Pinto, L., Sguerso, D. (2017). Use of UAS for the conservation of historical buildings in case of emergencies. International Archives of the Photogrammetry, Remote Sensing and Spatial Information Sciences, Vol. XLII-5/W1, p. 81-88.

Gagliolo, S., Fagandini, R., Passoni, D., Federici, B., Ferrando, I., Pagliari, D., Pinto, L., Sguerso, D. (2018). Parameter optimization for creating reliable photogrammetric models in emergency scenarios. Applied Geomatics, 10:501–514, p. 501-514.

Gini, R. (2010). Processing of high resolution and multispectral aerial images for forest DSM production and tree classification. Master thesis, DIIAR, Politecnico di Milano, Italy.

Gini, R., Passoni, D., Pinto, L., & Sona, G. (2014). Use of unmanned aerial systems for multispectral survey and tree classification: A test in a park area of northern Italy. European Journal of Remote Sensing, 47(1), 251-269.

Grafarend, E. W. (1974). Optimization of geodetic networks. Bolletino di Geodesia a Science Affini, 33(4), 351-406.

Grün, A. (1978). Progress in photogrammetric point determination by compensation of systematic errors and detection of gross errors. Inform. Relative to Cartography and Geodesy. Ser. 2: Transl. p 113-140(SEE N 80-12455 03-43).

Grün, A. (1980). Precision and reliability aspects in Close-Range photogrammetry. Invited paper, XIV Congress of ISP, Comm. V., Hamburg.

Heipke C., Jacobsen K., Wegmann H. (2002). Analysis of the results of the OEEPE Test Integrated Sensor Orientation, OEEPE Official Publication n° 43, pp. 31-49.

Hunt, E.R., Cavigelli, M., Daugherty, C.S.T., McMurtrey, J.E., Walthall, C.L. (2005). Evaluation of digital photography from model aircraft for Remote Sensing of crop biomass and nitrogen status. Precision Agriculture, Vol. 6, pp. 359-378. DOI: 10.1007/s11119-005-2324-5.

Kennert, A., & Torlegard, I. (1980). An Introduction to Close Range Photogrammetry. 1996). Development in Close Range Photogrammetry-1, London: Applied Science Publishers.

Klette, R. (2014). Concise computer vision. Springer, London.

Kraus, K. (1993). Photogrammetry Vol. I., Fundamentals and Standard Processes, Der. Dümmler Verlag, Bonn, Germany, ISBN 3-427-78684-6

Laliberte, A. S., Goforth, M.A., Steele, C.M., Rango, A. (2011). Multispectral Remote Sensing from Unmanned Aircraft: image processing workflows and applications for rangeland environment. Remote Sensing, Vol. 3(11), pp. 2529-2551. DOI: 10.3390/rs3112529.

Malinowski, R., Höfle, B., Koenig, K., Groom, G., Schwanghart, W., Heckrath, G. (2016). Local-scale flood mapping on vegetated floodplains from radiometrically calibrated airborne LiDAR data. ISPRS Journal of Photogrammetry and Remote Sensing,119, 267-279.

Merino, L., Caballero, F., Martínez-de-Dios, J.R., Maza, I., Ollero, A. (2010). Automatic forest fire monitoring and measurement using Unmanned Aerial Vehicles. D. X. Viegas (Ed.), VI International Conference on Forest Fire Research, 15-18 November, Coimbra, Central Portugal.

Meyer, D., Hess, M., Lo, E., Wittich, C. E., Hutchinson, T. C., Kuester, F. (2015). UAV-based post disaster assessment of cultural heritage sites following the 2014 South Napa Earthquake. Digital Heritage, Vol. 2, pp. 421-424.

Nebiker, S., Annen, A., Scherrer, M., Oesch, D. (2008). A light-weight multispectral sensor for micro UAV - Opportunities for very high resolution airborne Remote Sensing. ISPRS Archives, ISPRS Congress, 3-11 July, Beijing, China, Vol. 37/B1. pp. 1193-1199.

Nebiker, S., Lack, N., Abächerli, M., Läderach, S. (2016). Light-Weight Multispectral UAV Sensors and Their Capabilities for Predicting Grain Yield and Detecting Plant Diseases. ISPRS-International Archives of the Photogrammetry, Remote Sensing and Spatial Information Sciences, 963-970.

Niemeier, W. (1982). Design, diagnosis and optimization of monitoring networks in engineering surveying. In Invited Paper, Centennial Convention of CIS, Ottawa.

Nocerino, E., Menna, F., Remondino, F., & Saleri, R. (2013). Accuracy and block deformation analysis in automatic UAV and terrestrial photogrammetry-Lesson learnt. ISPRS Annals of the Photogrammetry, Remote Sensing and Spatial Information Sciences, 2(5/W1), 203-208.

Pagliari, D., Rossi, L., Passoni, D., Pinto, L., De Michele, C., & Avanzi, F. (2017). Measuring the volume of flushed sediments in a reservoir using multi-temporal images acquired with UAS. Geomatics, Natural Hazards and Risk, 8(1), 150-166.

Pinto. L., Forlani G. (2002). Integrated INS/DGPS Systems: Calibration and Combined Block Adjustment. Heipke C., Jacobsen K., Wegmann H. (Eds). Frankfurt am Main Germany. OEEPE Official Pubblication n. 43, pp. 85-96.

Pratt, K., Murphy, R., Stover S. (2006). Overview of requirements for semi-autonomous flight in miniature UAVs for structural inspection. AUVSI's Unmanned Systems North America, Orlando, Florida, Association for Unmanned Vehicle Systems International.

Reavis, B., Hem, B. (2011). Honeywell T-Hawk Aids Fukushima Daiichi Disaster Recovery: Unmanned Micro Air Vehicle Provides Video Feed to Remote Monitors. Honeywell Aerospace Media Center. Honeywell International Inc., 19 April.

Roberts, M.R. (2014). Five drone technologies for fire fighting. Fire Chief Magazine, 20 March.

Schwidefsky, K., & Ackermann, F. (1976). Photogrammetrie: Grundlagen, Verfahren, Anwendungen. Vieweg Teubner Verlag.

Torlegård, K. (1980). On accuracy improvement in Close-Range photogrammetry, Proceedings of the Industrial and Engineering Survey Conference, London.

van Blyenburgh, P. (2011). UAS Yearbook: Remotely Piloted Aircraft Systems-The Global Perspective. 9th Edition, Technical Report. UVS International, Paris, France.

van Blyenburgh, P. (2013). RPAS Yearbook: Remotely Piloted Aircraft Systems-The Global Perspective. 11th Edition, Technical Report. UVS International, Paris, France.

van Blyenburgh, P. (2014). RPAS Yearbook: Remotely Piloted Aircraft Systems-The Global Perspective. 12th Edition, Technical Report. UVS International, Paris, France.

Wallace, L., Lucieer, A., Watson, C. S. (2014). Evaluating tree detection and segmentation routines on very high resolution UAV LiDAR data. IEEE Transactions on Geoscience and Remote Sensing,52(12), 7619-7628.

Wang, Q., Wu, L., Chen, S., Shu, D., Xu, Z., Li, F., Wang, R. (2014). Accuracy evaluation of 3D geometry from low-attitude UAV images: a case study at Zijin mine. ISPRS Archives, ISPRS Technical Commission IV Symposium, 14-16 May, Suzhou, China. Vol. 40(4), pp. 297-300. DOI: 10.5194/isprsarchives-XL-4-297-2014.